PROGRESS REPORT

by

Prof. Dr. C. Ruhi Kaykayoglu

Istanbul University
Faculty of Engineering
Mechanical Engineering Department
Avcilar Kampusu, Avcilar, Istanbul,TURKEY

UNSTEADY SUBSONIC AERODYNAMICS FOR MANEUVERING WING/FUSELAGE/PYLON/STORE CONFIGURATION AND STORE SEPARATION INCLUDING WAKE EFFECTS

April 23, 1993

REPORT DOCUMENTATION PAGE

Form Approved OMB No. 0704-0188

1. AGENCY USE ONLY (Leave blank)	2. REPORT DATE	3. REPORT TYPE AND DATES COVERED
	21 April 1993	Final Report

4. TITLE AND SUBTITLE

Unsteady Subsonic Aerodynamics for Maneuvering Wing/Fuselage/Pylon/Store Configuration and Store Separation Including Wake Effects

5. FUNDING NUMBERS

F6170892W0238

6. AUTHOR(S)

Prof Dr C.Ruhi Kaykayoglu

7. PERFORMING ORGANIZATION NAME(S) AND ADDRESS(ES)

Instanbul Technical University
Dept of Space Sciences and Technology
Faculty of Aeronautics and Astronautics

8. PERFORMING ORGANIZATION REPORT NUMBER

SPC-92-4006

9. SPONSORING/MONITORING AGENCY NAME(S) AND ADDRESS(ES)

EOARD
PSC 802 BOX 14
FPO AE 09499-0200

10. SPONSORING/MONITORING AGENCY REPORT NUMBER

SPC-92-4006

11. SUPPLEMENTARY NOTES

12a. DISTRIBUTION/AVAILABILITY STATEMENT

Unlimited

12b. DISTRIBUTION CODE

13. ABSTRACT (Maximum 200 words)

The goal of the present investigation is to characterize the instantaneous flow field and force characteristics for a wing/fuselage/pylon/external store system during steady and unsteady flight. Emphasis is placed on practical, cost-effective engineering solution for the short-term treatment of the problem rather than an elegant mathematical modeling for the longer terms. Application of a Nonlinear Vortex Lattice Method (NVLM) Computational Fluid Dynamics (CFD) system with unsteady free wake formulation to obtaining flow field predictions about a maneuvering wing/pylon/store configuration is the primary objective of the current investigation. Separation the external store under the influence of unsteady wake roll up behind wing will be modeled by considering the full mutual interactions between the store and wing/pylon system in the second phase of the project. In this report, preliminary results were presented regarding the unsteady flow field below the wing about the external store and the unsteady aerodynamic forces on the external store before the separation during flight maneuvers. The validation of the computer modeling approach for the maneuvering wing/pylon/store combination needs experimental data. Unfortunately, the comparison experimental data were not available for the current research configuration and conditions. The experimental unsteady wing flow field and stability derivatives literature data was considered as the basis to test the accuracy and effectiveness of the computer code.

14. SUBJECT TERMS

15. NUMBER OF PAGES

126

16. PRICE CODE

17. SECURITY CLASSIFICATION OF REPORT	18. SECURITY CLASSIFICATION OF THIS PAGE	19. SECURITY CLASSIFICATION OF ABSTRACT	20. LIMITATION OF ABSTRACT
UNCLASSIFIED	UNCLASSIFIED	UNCLASSIFIED	UL

TABLE OF CONTENTS

ABSTRACT

The goal of the present investigation is to characterize the instantaneous flow field and force characteristics for a wing/fuselage/pylon/external store system during steady and unsteady flight. Emphasis is placed on practical, cost-effective engineering solution for the shortterm treatment of the problem rather than an elegant mathematical modelling for the longer terms. Application of a Nonlinear Vortex Lattice Method (NVLM) Computational Fluid Dynamics (CFD) system with unsteady free wake formulation to obtaining flow field predictions about a maneuvering wing/pylon/store configuration is the primary objective of the current investigation. Separation of the external store under the influence of unsteady wake roll up behind wing will be modeled by considering the full mutual interactions between the store and wing/pylon system in the second phase of the project.

The modeling of the unsteady wake roll up behind wing/pylon/store combination on external store carriage and release requires advanced computational techniques. A grid based approach seems to be computationally expensive requiring a grid update during the history of the flow field. The NVLM approach is still the most efficient tool for complex geometries as it uses only a surface grid which is relatively easy to generate. The NVLM model of the three dimensional flow field was used to treat arbitrary maneuvers of a trapezoidal wing with and without underwing external store. A time dependent wing following and wake shedding procedure provides transient wake shapes and wing loadings without utilizing the iterative wake relaxation procedure. A Vortex Lattice Method based computer code **TRNVLM** enables the user to orchestrate the input motions of a variety of steady flight conditions through unsteady maneuvers.

In this report, preliminary results were presented regarding the unsteady flow field below the wing about the external store and the unsteady aerodynamic forces on the external store before the separation during flight maneuvers.

The validication of the computer modeling approach for the maneuvering wing/pylon/store combination needs experimental data. Unfortunately, the comparison experimental data were not available for the current research configuration and conditions. The experimental unsteady wing flow field and stability derivatives literature data was considered as the basis to test the accuracy and effectiveness of the computer code.

The presence of the external store affect both the trailing edge wake dynamics and the unsteady lift characteristics of the wing. During the early stages of the input maneuver motion, the unsteady loading on the store shows a novel character and set the initial conditions for the store release process. The influence of unsteady wing induced perturbation velocities and the induced unsteady wake velocities will modify the early trajectory of the external store after the release.

NOMENCLATURE

AR	wing aspect ratio
b(x)	wing local span
c(y)	wing chord
Δc_{ij}	chordwise length of the ij th subsurface
Δb_{ij}	spanwise length of the ij th subsurface
CR	wing root chord
CT	wing tip chord
C_L	lift coefficient
C_D	drag coefficient
C_M	pitching moment coefficient
C_R	rolling moment coefficients
C_p	pressure coefficient
F_{cx} ,F_{cy},F_{cz}	store force coefficients
n	normal vector
r	position vector
p,q,r	angular velocity about x,y,z axes respectively
S	span of the wing
u,v,w	cartesian components of perturbation velocity
U,V	velocity vector
U(t), V(t).	time dependent wing forward velocity
x,y,z	Cartesian coordinates
t	time
T	nondimensional time (Ut/CR)
α	angle of attack
Γ	strength of ring vortices

Φ	perturbation velocity potential
Λ	sweep angle
ρ	density
$\vec{z}_i, \vec{z}_j$	panel tangential vectors in the i and j directions

LIST OF FIGURES

Figure 7.3 Comparison of different computation methods for the prediction of the steady state lift coefficient.

Figure 7.4 Comparison of the results of TRNVLM with the computational results of Fang[61] and the experimental results of Lamar [60]. (-■- Present Results, -▲- Fang's Computational Results, -●- Lamar's Experimental Results)

Figure 7.5 Transient lift coefficient variation with time for the thin rectangular wings of different Aspect Ratio that were suddenly set into a constant speed forward flight.

Figure 7.6 Comparison of the predictions of the Katz's [30] Vortex Lattice Computer code with the Predictions of TRNVLM.(● Katz's results, ▲ Present results).

Figure 7.7 Lift coefficient variation as a function of angle of incidence: effect of pylon/store configurations on the lift coefficient.

Figure 7.8 a) Simulation of wake evolution by releasing vortex sheets from the wing's trailing edge. b) Properties of the vortex wake. c) Transient lift coefficient variation.

Figure 7.9 Effect of vortex ring density on the computed steady lift coefficient.

Figure 7.10 Computed lift curves for the wing/ fuselage configuration with and without external store.

Figure 7.11a Comparison of the transient lift coefficient variation with time for the research geometries that were suddenly set into a constant speed forward flight.

Figure 7.11b Simulation of the wake evolution by releasing vortex sheets from separation edges i) wing /fuselage combination ii) wing/ fuselage/ store combination

Figure 7.12 Computed shapes of separated trailing edge vortex wake structures behind the research configuration:effect of angle of incidence.

Figure 7.13

Computed shape of a vortex wake structure behind the wing/ fuselage/ pylon/ store a) wire diagram representation b) representation with hidden surfaces and lines c) side view of the wake roll-up d) rear view of the wake with hidden surfaces e) rear view of the wake with wire diagram.

Figure 7.14

Computed shape of a vortex wake structure behind the wing/ fuselage/ pylon/ store a) perspective hidden surface view of the vortex wake evolution b) representation of the wake with vortex filaments c) side view of the wake roll-up d) details of the near wake from different point of visualization e) side view of the near wake and deformation of the wake structure.

Figure 7.15

Computed shape of a vortex wake structure behind the wing/ fuselage/ pylon/ store a) perspective view of the vortex wake evolution formation of secondary roll-up with the influence of external store b) side view of the wake roll-up c) details of the near wake from different point of visualization:deformation of the wake structure.

Figure 7.16

Computed shape of a vortex wake structure behind the wing/ fuselage/ pylon/ store a) perspective view of the vortex wake evolution formation of secondary roll-up with the influence of external store b) top view of the vortex wake c) side view of the wake roll-up.

Figure 7.17

Computed shape of a vortex wake structure behind the wing/ fuselage/ pylon/ store a) top view of the wake b) perspective view of the vortex wake evolution formation of secondary roll-up with the influence of external store c) side view of the wake roll-up d) details of the near wake deformation.

CHAPTER I

INTRODUCTION AND LITERATURE SURVEY

1. Background

An underwing installations affect the performance characteristics of the wing. They are frequently a source of considerable adverse aerodynamic interference giving large increases in drag, variations in aerodynamic stability derivatives and change in flutter boundaries [1, 2, 3, 4]. Flutter characteristics of the aircraft are substantially influenced by the pitch and yaw oscillations of the underwing pylon/store combination. An understanding of the wing-store interaction is central to determining the unsteady airloads , the safe store release and the sound generation.

To aim an underwing external store (weapon, guided missile, etc.) so that it will hit a target, a knowledge of the flight characteristics of the store as it travels to the target is required. It is necessary to perform testing to obtain the data necessary to establish or verify the stores's drag, event times, and other factors that effect the store's flight characteristics. Although there exist data on steady flight conditions, the prediction of the characteristic behavior of the stores during unsteady maneuvers is still a challenge. Some of these characteristics depend on aircraft presence, the aircraft flight history and mode of delivery during 1 to 3 seconds after release from the underwing pylon.

Separation effects occur when a store is released from an aircraft and its motion is temporarily influenced by the interaction of the non-uniform flow of air between the aircraft and the store. Separation-effects testing

involves releasing stores from an aircraft, one at a time, under controlled test conditions. A scenario which shows negligible separation effects under one set of delivery conditions may show large separation at different delivery conditions (different airspeed, altitude, normal acceleration, dive angle and climb angle).

To calculate a store delivery and to deliver that store on a target accurately and effectively requires the data consisting aircraft accelerations, velocities, altitudes, positions, and heading data. Furthermore, the information on normal acceleration values (g's) are necessary for use in separation effect calculations. It has been shown that g's have a definite effect on the flow field that influences the store trajectory during release [5].

Store separation effects are highly dependent on the aircraft loadout. The separation effects are different for each store station under the wing. Each station should be modeled to characterize store trajectories. The detailed discussion on weapon delivery systems were presented by Arnold and Knight [5].

The flight conditions at which the store will properly work as designed is the store functioning envelope. The nature of the envelope depends on the type of store and also on the type of testing to be performed. The total number of external stores needed for store freestream testing requires certain amount of store release experiments. This amount reaches upto a three digits store amount for complete characterization.

On the other hand, computer aided experiments will help the designer to cut certain amount of possibilities before doing the full set of scheduled experiments. This study also aims at providing a new computer aided analysis procedure to be use to reduce the number of experiments.

CHAPTER II

NUMERICAL SIMULATION METHODS

There are various theoretical and experimental methods to study the nonlinear aerodynamic characteristics of the wing and other aircraft components. The prediction of the aerodynamic characteristics of complex configurations is essential for the aeronautical industry as a tool for the preliminary and final design state. However, the complexity of the flow require approximate models with reasonable engineering accuracy. Recent advances in techniques for exact solutions of the Euler equations and the full Navier Stokes equations require expensive computation time [6, 7, 8, 9]. The grid generation procedure require very large programming efforts.

In this section a brief description of the approximate methods with practical engineering value and reasonably accurate mathematical basis will be described. The discussion of the methods based on Navier Stokes equations will not be presented.

2.1 Slender Body Modeling

This group of models uses slender body and conical flow assumptions. The model works very well in the vicinity of the apex of the wing due to its assumptions. Legendre [10], Brown and Michael [11], Mangler and Smith [12], Gersten [13], Cohen and Nimri [14] have applied slender body models in various analysis. Brown and Michael introduced the first model for the simulation of a roll-up vortex sheet. Their model does not include the real roll up due to its straight planar surface feeding sheet model for the primary vortex

representation. Later, Mangler and Smith introduced the first realistic model for the primary vortex and its feeding sheet. Both of these models have predicted the pressure distributions near the apex. Due to slender body assumptions, models are unable to simulate the pressure distribution near the trailing edge. Furthermore, the unsteady trailing edge Kutta condition is not satisfied during the application of these methods.

On the other hand, the slender wing theory retains the appealing feature that the instantaneous 3-D flow about the wing can be studied by the superposition of 2-D time dependent flows in successive cross flow planes. Recently, Tavares [15] has developed a method for calculating the response of wings to large amplitude imposed motion. It was concluded that the Tavares's technique which is based on the Munk-Jones slender wing theory [16,17] can complement CFD calculations and provide a powerful practical tool.

2.2 Vortex Lift Analogy

The vortex lift analogy of Polhamus [18] has been used frequently for the calculation of the aerodynamic characteristics of wings with vortex separation from swept leading edges. Lamar [19] extended the method to study streamwise side-edge separations. Bartlett and Vidal [20] studied the effect of leading edge shapes on the aerodynamic lift and drag values. Shepshelovich [21] extended the method to study the aerodynamic characteristics of cambered wings.

Although this method and its extensions were good to study the effect of vortex separation, it was not ready to be implemented to new problems such as strake/wing flow or canard/wing combinations.

2.3 Panel Methods

Panel methods have been proven to be a remarkably versatile and useful tool for analyzing subsonic and supersonic flow by several researchers [22, 23, 24, 25]. The theoretical, numerical and practical aspects of the method were surveyed by Morino [26]. Panel Methods are in wide spread use through out the aerospace industry. A panel method solves a linear partial differential equation so called Prandtl-Glauert numerically by approximating the complex configuration surface by a panel network. The panel network consists of source or doublet distributions. The strength of sources and doublets are determined by an appropriate set of boundary conditions [26].

Panel Method market is full of various codes for studying different applications. Among the products PAN AIR code is one of the well known higher order panel method code which has emerged during the last decade [27].

Kaykayoglu [28] have utilized the method to study the aerodynamic flow characteristics of various complex configurations. Figures 2.1 and 2.2 illustrate several cases studied by using a doublet panel method based computer code developed by Kaykayoglu.

The doublet panel method was extended by Hoeijmakers and Bennekers [29] to include the effect of primary vortex core formation over a delta wing.

The other important practical method so called Vortex Lattice Method (VLM) will be presented separately in Chapter III.

CHAPTER III

NONLINEAR VORTEX LATTICE METHOD

3.1 Computational Challenges

The combined fluid dynamic problem of external store carriage/release and three dimensional wing leading edge and trailing edge separation is highly complex and nonlinear. In this research investigation, a computer method based on a vortex ring element representation of the body surfaces was used to solve three dimensional unsteady flow field. This method is based on the general Nonlinear Vortex Lattice Method (NVLM) [30].

The Vortex Lattice Method approach was proven to be accurate and effective in various aerodynamic simulations. The ability of the method to enable predictions with leading edge separation at high angle of attack, excluding cases in which vortex breakdown occurs is demonstrated in the literature [31]. The principal of modelling wakes and leading edge vortices shed from highly swept wings is presented in details in references [32,33]. Recently Katz and Kern [34] used a simplified vortex lattice model to simulate the effect if vertical ejector jet on the aerodynamics of delta wings.

High angle of attack regime requirements imposed on aircraft performance results in nonlinearities and unsteadiness due to large regions of three dimensional separated flows and concentrated vortex flows. For a maneuvering aircraft , the instantaneous state of the flow field depends on the time history of the aircraft motion. Detailed solution of the complete nonlinear fluid dynamics equations (Navier Stokes Equations)

along time dependent flight paths requires the computational grid to cover large wake histories. Furthermore, during store release modeling, the grid update procedure at new store stations need extensive time and efforts. Unfortunately, these require large storage capabilities and computing times which are still unacceptable with today's computer technology. On the other hand, the use of simplified fluid dynamic equations while retaining the three dimensional nature of the aircraft geometry and its flight path is a realistic alternative approach for the simulation.

In the course of developing computational aerodynamic method to analyze aircraft maneuvers, the simulation of unsteady aerodynamics and the resulting wake dynamics is still a challenge. In addition, the presence of external stores complicates the overall flow field. Models of vortex wake motion can contribute to the investigation of leading edge flow separation from swept wings, as would occur during angle of attack, landing or maneuvering. Moreover, due to the separated flow during complex maneuvering phase of the wings, the external store loading can be modified considerably.

Interest in supermaneuvreability has also stimulated research into unsteady flows past wings. Several recent investigations have studied the effects of pitching maneuvers at high angle of attack. Flow visualization studies such as those, Magness, Robinson and Rockwell [35] and Gad-el-Hak [36] have provided information about the complex field during transient maneuvers.

When the wing is maneuvering at high angle of attack, flow separates near the leading edges and the separated flow rolls up above and behind the wing to form concen

trated vortices. The structure of the wake vortices depends on the type of wing motion history. A wing which is executing a roll motion about the midspan axis, one side of the wake is always above the wing and the other side is always below the wing thus modifying the flow field above and below the wing [35]. On the other hand, the wing which is pitching about the axis parallel to the trailing edge exhibits variety of new flow topologies at low Reynolds numbers [35].

The lifting characteristics and wake structure of highly swept wings with sharp leading edge were lately attracted increasing interest. A study of the unsteady aerodynamic loads with allowance for leading edge separation was reported by Atta et al. [37] and Kandil et al. [38]. The nonsteady wake roll up was calculated by a complex iterative method. The major disadvantage of these style codes is the large amount of computer time required for complex wake geometries, since the final bound vorticity and wake roll up is obtained by an iterative procedure. Moreover, the first assumed vortex wake shape which starts the iterative procedure should be close to the final solution to eliminate a possible convergence to an undesired solution.

Katz [31] formulated the unsymmetric motion of a slender delta wing via vortex lattice method including tip and leading edge separation in an incompressible flow. Katz performed calculations of the aerodynamic forces and time dependent wake roll up with a non iterative technique. A time dependent wing following wake shedding procedure provided both transient and asymptotic wake shapes and wing loadings without utilizing the iterative method. Similar methods were also developed by Summa [39] and Widnall [40].

3.2 Nature of the Vortex Lattice Method

This section gives a brief description of the Vortex Lattice Method (VLM). A detailed presentation of the method is done by Katz [30]. The wing bound vortex sheet and the wake free vortex sheets are approximated by a system of concentrated vortex lines. The bound vortex sheet is replaced by a bound ring vortex lattice. The lifting body surface is considered as a vortex sheet and the strength of the vortices are calculated by satisfying the impermeability condition over the surface. As opposed to the other methods based on source distributions, vortex lattice methods predicts the aerodynamic lift directly since the vortices generate circulation which is related to the lift.

Among the vast applications of the Vortex Lattice Method to various aerodynamic related problems, research work at Technion-Israel Institute of Technology has been deserving a special attention over the last two decades. Zorea and Rom [41] presented a method for the combined calculation of both the lift distribution on the wing planform and the trailing vortex flow field behind a wing. This study has shown that for the high aspect ratio wings, the primary vortex formation from the leading edges has small effect on nonlinear lift variation with angle of attack. Hence the computed results were almost identical to those obtained when the vortices stayed on the planform and were shed from the trailing edge only. Rom, Portney and Zorea [42] later carried out a more detailed investigation for the understanding of the development of the vortex flow field near the wing tips and trailing edges in more detail.

The longitudinal aerodynamic characteristics of various planar shapes including multiple lifting surface configurations in subsonic flow at a high angle of attack was presented by Almosnino,Zorea and Rom [43] by utilizing the Vortex Lattice Method computer code. This code was able to handle complex configurations such as close-coupled canard-wing combinations, wing-tail combinations, various flaps, elevators and dihedral angles, as well as ground effect problems.

A Vortex Lattice Method applications for general unsteady aerodynamic problems have been proven to be powerful in various applications by the Virginia Polytechnic Institute and State University researchers at Blacksburg, Virginia [44, 45, 46]. The numerical study of wings in steady and unsteady ground effects were successfully carried out by Nuhait and Mook [46]. Konstainopoulos and et. al. have also shown that the results of vortex lattice method is accurate enough to be used for preliminary design purposes.

The Vortex Lattice Method has not been developed yet to become a full surface panel method for thick wings. However, wide applications cited in the literature makes the method an effective and practical engineering alternative to classical panel methods. For this reason, the Nonlinear Vortex Lattice Method (NVLM) was chosen to be a candidate method so as to model the present problem. Author and his research team has aimed at developing an industrial code based on the Vortex Lattice Method ready to be used for practical applications. This code is named as **TRNVLM** (Turkey Nonlinear Vortex Lattice Method).

CHAPTER IV

RESEARCH GEOMETRY AND WAKE MODELING

4.1 Geometry and Vortex Lattice Formation

4.1.1 Research Geometry

In the present investigation, incompressible, unsteady Nonlinear Vortex Lattice Method CFD scheme was prepared to investigate 3-D unsteady flow field about wing/fuselage/pylon/store configuration. Figure 4.1 shows the research configuration featuring wing/ pylon/ fuselage/ store setup. The research wing has an Aspect Ratio, AR, of AR=3 and zero thickness (The case of wings with thickness is under investigation by Bayar [47]). The geometry of several classes of wing systems can also be defined by parameters like sweep, camber and twist by the geometry module of the computer code prepared. Present investigation considers a trapezoidal wing with the relevant dimensions of CR/CT=3.28, S/CR=2 and Λ =35°. There is no twist and camber over the wing system. Figure 4.2 shows the properties of the research configuration at different view planes.

The external store (see Fig. 4.3) has an ellipsoidal geometry. The Store Aspect Ratio (SAR= Total length of the store, L_s/ Maximum Thickness, R_s) is SAR = 12. The location of the generic store installation under the wing is chosen with respect to the geometric center of the store measured from the origin of the geometric reference axis. The Store Spanwise Location, SSL/CR=-0.434, the Store Transverse Location, STL/CR=-0.163, and the Store Chordwise Location, SCL/CR=0.652 are chosen as typical study parameters during this investigation.

The pylon has a rectangular geometry (See Fig. 4.3). The geometry of the pylon can be defined by parameters like used in the wing system.

A simplified wing-body model is chosen in the present study. Similar research geometry was investigated by Baxendale [6] at Aircraft Research Association Ltd., Bedford, UK. Figure 4.4 depicts the experimental and numerical research configuration.

In actual airplane and missile configurations, the contribution of the body to the aerodynamic properties was proven to be very significant. The estimation of the nonlinear wing-body interference by a superposition of solutions for isolated wings and isolated bodies is unsatisfactory [48]. There exist only a few methods for the computation of the nonlinear aerodynamics of wing-body configurations at high angle of attack. Uchiyama et al. [49] has suggested combining a nonlinear vortex lattice method for the lifting surfaces with concentrated source type singularities to simulate the body. Hence the combined iterative solution of the singularity strengths has provided the mutual interaction. Later Atta and Nayfeh [50] extended the method of Kandil et al. [51] to treat wing-body combinations. Their method used a potential flow model consisting of constant strength quadrilateral vortices distributed over the body and wing surfaces. Atta and Nayfeh have considered only the central-wing-body combination without body nose effects. Their results showed good agreement with experimental data. Rusak, Wasserstrom and Seginer [52] developed a method which was based on a combination of the linear source panel method for the body and the Nonlinear Vortex Lattice Method for the lifting surfaces and their separated wakes. Rusak et al. [52] extended the vortex cells of the wing adjacent

to the body through the body up to the plane of symmetry. Hence a vortex along the wing-body intersection line is thus completely avoided.

In the present study the whole configuration is modeled by using vortex cells (See Figure 4.5) similar to the work of Atta and Nayfeh [50]. This modeling procedure eliminates the problem of a discontinuity in the vorticity distribution at the wing-body intersection line. Hence, the shedding of a strong vortex along the intersection line is avoided. The wake vortex originating near the wing-fuselage juncture, whose circulation is opposite in direction to the wing tip vortex were allowed to deform freely along the streamwise and transverse directions while it is assumed to be attached to the fuselage surface until it leaves the extension of the fuselage aft of the wing.

4.1.2 Division of the research geometry into vortex lattices

The first step of the Vortex Lattice Method is the creation of the mesh system. Although the finite difference or finite elements methods solutions heavily depend on grid refinement , the VLM does not show such character. Each vortex-grid setup provide unique solutions. Rusak, Seginer and Wasserstrom [53] have provided an extensive study on the parameters effecting the character of the solution. Their study involves an iterative procedure of estimating the final wake shape. The iterative NVLM has two independent length scales. One is the length of the free vortex segments in the wake used in the integration of the wake shape. Second is the length of the vortex panel length. This last scale is defined as $x_p = CR/N_c$, where CR is the root chord length and N_c is the chordwise number of vortex

panels along the wing's root chord. The present investigation uses a time marching technique for the modeling of the wake geometry. Hence, the first scale is not a relevant scale for the technique used in this study. However the second scale is a very important parameter for this study.

Rusak et al. [53] discusses various paneling schemes for delta wings. In the present investigation, the chord plane of zero-thickness wing of trapezoidal shape was divided by a set of rows and lines and then a quadrilateral vortex ring is placed on each panel. Figure 4.6 shows the research configuration with subsurfaces defined automatically by the computer code.

The configuration panelling will require careful modeling. In order to assess the requirements for the number of panels to adequately represent the configuration, fine and sparse panel configurations will be tested against known standard solutions. Effect of panelling density on transient aerodynamic interference and forces will be investigated by computer experiments.

4.2 Vortex Wake Model

Wake evolution was simulated by shedding ring vortices from the sharp edges of the wing satisfying Kutta condition at each time step. The separation of the flow about the store was neglected and attached flow conditions was considered in this investigation. However, for the future research activities, a separation model similar to the work of Rom and Alsomino [54] will be recommended.

This study presents two wake models. Model A considers a steady rigid trailing edge wake which extends in the

direction of angle of attack and it carries the effect of the external store presence through steady Kutta condition requirements at the wing trailing edge. Second Model B is an unsteady wake model which involves unsteady wake progress development (See Figure 4.7). The details of the wake models are given by Katz [30].

The simple case of steady interference between the wing and the store is followed by the computation of dynamic interference of the store and the wing at various flight maneuvers.

The evaluation of aerodynamic loads on the external store during carriage and release requires complicated aerodynamic task. In the present work this task involves the following sources of effects;

a) steady interference of the wing on the airflow around the store.

b) the disturbance on the store caused by the unsteady wake roll up.

c) unsteady effects including store and wing rotations during release and maneuvering.

To evaluate the above interference effects, two computation tasks were carried out simultaneously,

1) The continues mutual interference evaluated by unsteady aerodynamics including wakes,

2) The resulting store motion by flight mechanics.

The perturbed flowfield induced by the wing wake, wing and store wake will have a significant effect on the store separation trajectory.

The steps of the formulation and analysis will be presented in the next section.

CHAPTER V

NUMERICAL MODEL

5.1. Previous Related Progress

Today, aircraft companies and several university departments often make use of the computational aerodynamic methods based on Panel Method [22]. For this reason a group of researchers in the Faculty of Aeronautics and Astronautics of Istanbul Technical University have been considering to develop aerodynamic codes ready to be used for simulating the aerodynamics of military aircraft/store carriage and release [28]. Three of these resulted codes are **TRAERO** [55], **TRESSP** [56] and **TWAERO** [57]. **TRAERO** (Turkey **AERO**dynamics) is a first generation type panel code which computes velocity and pressure distributions, forces and moments in 3-D complex configuration in linearized subsonic flow. **TRESSP** (Turkey External Store Separation Program) is the code designed for analyzing store separation and unsteady trajectory prediction. **TWAERO** (Turkey Wake **AERO**dynamics) is the code designed for unsteady wing wake analysis. Pre- and Post- computer graphic softwares have been prepared to visualize the aerodynamic performance and support main source programs. Figure 5.1 shows a sample output of the above computer codes where a simulation of the store separation from F-4 under steady flight conditions were performed.

Methods such as doublet-lattice or vortex-lattice methods are widely used for calculating the pressure distribution about lifting surfaces in steady and oscillatory potential flows along a straight flight path. These methods can be modified further to solve the time dependent lift variations on the wings of a

maneuvering aircraft. The calculation of nonsteady flight of wing/pylon/store combination along a curved path needs modifications in the steady state surface singularity method CFD code. These modifications will include,

a) Correction of the downwash distribution on wing surface.

b) A modification in the pressure distributions including nonsteady effects.

c) A nonsteady wake model construction.

Below author presents the formulation philosophy of the Nonlinear Vortex Lattice Method (NVLM) which covers the above modifications.

5.2. Present Numerical Method

5.2.1 Nonlinear Vortex Lattice Method (NVLM) Formulation

The flow is incompressible and inviscid. The whole flow field is regarded as a potential flow with regions of viscous domination confined to infinitely thin shear layers separating only along the trailing edges and wing tips. The disturbance velocity potential, ϕ ,due to the presence of the bodies and also wake vortices is governed by the Laplace equation

$$\nabla^2 \phi = 0 \qquad \text{.....(1)}$$

The boundary conditions require that the geometry induced disturbances will decay far from the wing;

$$\nabla \phi \rightarrow 0 \quad r \rightarrow \infty \qquad \text{.....(2)}$$

and there will be no flow through the geometry surface. In a wing attached coordinate system this condition gives [30, 31] ,

$$(\vec{V} - \vec{V}_p) \cdot \vec{n} = 0 \qquad \ldots\ldots\ldots (3)$$

where Vp is the local boundary surface velocity.

Due to angular momentum conservation, the overall circulation Γ generated in the fluid must be zero. Hence;

$$\frac{d\Gamma}{dt} = 0 \qquad \ldots\ldots\ldots\ldots (4)$$

Although the Laplace equation (Eq. 1) is linear the problem poses nonlinearity due to the separating free vortex rings from the prescribed edges. Since the unsteady trajectories of the rings is going to be determined as part of the solution from the supplementary conditions, this brings nonlinearity to the current problem.

According to the Green's theorem [58] , the general solution of Eqs. (1-4) consists of a doublet and source distribution over the wing surface. For lifting problem solutions, the vortex distribution which is derived from the doublets, is sufficient. In the present investigation all surfaces are considered to be lifting surfaces and are described by a distribution of bound vortices that is equivalent to the appropriate dipole distribution and that describes the tangential velocity and potential jump across the body.

The zero thickness wing lifting surface is divided into N x M (N x M = N_w) vortex rings with streamwise paneling. Each vortex ring of unknown strength $\Gamma_{w,j}$ (j=1, N_w)is bound to the 1/4 of the panel chord thus satisfying the Kutta condition [30]. Thus control point is located at 3/4 panel chord. Similar to the wing surface paneling, fuselage is divided into NN x MM (NN x MM = N_f) with $\Gamma_{f,j}$, (j=1, N_f) vortex strengths, pylon is divided into NNN x MMM (NNN x MMM = N_p) vortex rings with $\Gamma_{p,j}$, (j=1, N_p) vortex strengths . Finally, the external store surface is divided into NNNN x MMMM (NNNN x MMMM = N_s) with $\Gamma_{s,j}$, (j=1, N_s) vortex strengths. Nxxx and Mxxx values represent the number of panels in the spanwise and chordwise directions respectively.

The complete solution of the problem in terms of unknown bound vortices, $\Gamma_{w,j}$, $\Gamma_{f,j}$, $\Gamma_{p,j}$, $\Gamma_{s,j}$ is carried out by satisfying Eq. 3. The induced velocity $(\partial\phi/\partial z)_{ij}$ due to body (wing+fuselage+store+pylon) vortices, trailing edge wake and tip wake elements is given at each control point by

$$\left(\frac{\partial\phi}{\partial z}\right)_{ij} = [WFPS]_{ij} \begin{bmatrix} \Gamma_{w,1} \\ \vdots \\ \Gamma_{f,1} \\ \vdots \\ \Gamma_{p,1} \\ \vdots \\ \Gamma_{s,1} \\ \vdots \\ \Gamma_{s,j} \end{bmatrix} + [TEWI] \begin{bmatrix} \Gamma_{tew,1} \\ \vdots \\ \Gamma_{tew,j} \\ \vdots \\ \Gamma_{tew,n} \end{bmatrix} + [TIPI] \begin{bmatrix} \Gamma_{tip,1} \\ \vdots \\ \Gamma_{tip,j} \\ \vdots \\ \Gamma_{tip,n} \end{bmatrix}$$

The influence matrix coefficients [WFPS], [TEWI] and [TIPI] are obtained by using Biot Savart Law [30]. Since the number of wake elements increase with the time step, the matrices [TEWI] and [TIPI] are computed at each time step while the matrix [WFPS] is computed once.

The normal kinematic velocities at each control point due to the unsteady maneuver of the whole system can be written as [30, 31],

$$w_{ij} = -[\ (U-ry)(\frac{\partial h}{\partial x} - \sin\alpha\ ) - qx + py + \frac{\partial h}{\partial t}) \qquad ...(6)$$

Then the final condition that fulfill Eq. 3 becomes

$$w_{ij} + \left(\frac{\partial \phi}{\partial z}\right)_{ij} = 0 \qquad .... (7)$$

Rewritten in matrix form, Eq. 4 becomes

$$[WFPS][F] + [V]_t = 0 \qquad ....(8)$$

where [WFPS] is defined as

$$[WFPS] = \begin{bmatrix} WOW & FOW & POW & SOW \\ WOF & FOF & POF & SOF \\ WOP & FOP & POP & SOP \\ WOS & POF & POS & SOS \end{bmatrix}$$

with the submatrices,

WOW, the influence coefficients of the wing vortices on the wing cells

FOW, the influence coefficients of the fuselage vortices on the wing cells

POW, the influence coefficients of the pylon vortices on the wing cells

SOW, the influence coefficients of the store vortices on the wing cells

WOF, the influence coefficients of the wing vortices on the fuselage cells

FOF, the influence coefficients of the fuselage vortices on the fuselage cells

POF, the influence coefficients of the pylon vortices on the fuselage cells

SOF, the influence coefficients of the store vortices on the fuselage cells

WOP, the influence coefficients of the wing vortices on the pylon cells

FOP, the influence coefficients of the fuselage vortices on the pylon cells

POP, the influence coefficients of the pylon vortices on the pylon cells

SOP, the influence coefficients of the store vortices on the pylon cells

WOS, the influence coefficients of the wing vortices on the store cells

FOS, the influence coefficients of the fuselage vortices on the store cells

POS, the influence coefficients of the pylon vortices on the store cells

SOS, the influence coefficients of the store vortices on the store cells

[F] is the vector of vortex singularity intensities and, [V] is the normal velocities at control points due to external velocities and the kinematic velocities due to unsteady maneuvering.

Equation (8) is solved for the intensities of the singular elements. An iterative method, Gauss Seidel Iterative method was preferred to a Gaussian elimination due to the nature of the influence coefficient matrix.

5.2.2 Vortex Wake Modeling

The modeling of the unsteady wake roll up behind a maneuvering wing system requires advanced computational techniques. Although several methods are available to compute the flow over a stationary wing, there is still a need for simple but accurate computational methods able to predict the basic properties of a wing under maneuvering conditions. The Vortex Lattice Method (VLM) approach is one of the most efficient tools among the typical and widespread "singularity methods" for the representation of the wake roll-up.

The Vortex Lattice approach was proven to be accurate and effective in various aerodynamic simulations. The ability of the method to enable predictions with leading edge separation at high angle of attack, excluding cases in which vortex breakdown occurs is demonstrated in the literature [37]. The principal of modelling wakes and leading edge vortices shed from highly swept wings is presented in details in references [30,32].

The nonsteady wake roll up may be calculated by a complex iterative method. The major disadvantage of these style codes is the large amount of computer time required for complex wake geometries, since the final bound vorticity and wake roll up is obtained by an iterative procedure. Moreover, the first assumed vortex wake shape which starts the iterative procedure should be close to the final solution to eliminate a possible convergence to an undesired solution.

A time dependent wing following and wake shedding procedure will provide transient wake shapes and wing loadings without utilizing the iterative wake relaxation procedure. A computer algorithm will enable the user to orchestrate the input motions of a variety of steady flight conditions through unsteady maneuvers.

The modeling of the vortex wake which is shed at the wing tip and trailing edges requires time marching scheme. Since the initial estimate of the geometry of the wake is uncertain during unsteady flight conditions, rigid and/or free models fail to simulate the unsteady wake formation. Free wake models which relies on first guess and successive iterations will be very costly and difficult to apply for the research configuration. Hence, lagrangian type, time dependent wing following and wake shedding procedure model under complex solid boundaries and unsteady flow boundary conditions are chosen in this investigation. The vortex ring segments released at each time step at the trailing and tip edges build the continuous wake structure. Fig. 4.7 illustrates the important aspects of the unsteady vortex wake model.

Application of the research configuration to simulate unsteady maneuvering will be limited to small displacements and rotations. Hence the vortex breakdown over the wing surface won't be considered.

5.2.3 Computation of the Pressure Coefficient Distribution and the Aerodynamic Coefficients

Following the method outlined by Katz [30], the pressure difference equation results in

$$\Delta p_{ij} = \rho\{[U(t)+ u_w,\ V(t)+v_w,\ W(t)+w_w]_{ij}\cdot \tau_{ij}\frac{\Gamma_{ij}-\Gamma_{i-1,j}}{\Delta c_{ij}} \qquad \ldots (10)$$

$$+ [U(t)+ u_w,\ V(t)+v_w,\ W(t)+w_w]_{ij}\cdot \tau_{ij}\frac{\Gamma_{ij}-\Gamma_{i,j-1}}{\Delta b_{ij}} + \frac{\partial}{\partial t}\Gamma_{ij}\}$$

for a single vortex ring lattice.

The contribution of this panel to the loads, resolved along the three body axes, is then

$$\Delta F_{ij} = -(\Delta p\ \Delta S)_{ij} n_{ij} \qquad \ldots\ldots\ldots\ldots (11)$$

The resulting lift,drag, pitching moment, and rolling moment coefficients are obtained by integrating each panel normal force Fij along the body surface. Hence,

$$C_L = \sum_{\substack{i=1\\ j=1}}^{n,m} \Delta F_{ij}\cos\alpha_i \Big/ \tfrac{1}{2}\rho V^2 S$$

$$C_D = \sum_{\substack{i=1\\ j=1}}^{n,m} \Delta F_{ij}\sin\alpha_i \Big/ \tfrac{1}{2}\rho V^2 S$$

$$C_M = \sum_{\substack{i=1\\ j=1}}^{n,m} \Delta F_{ij} x_i \Big/ \tfrac{1}{2}\rho V^2 S.CR \qquad \ldots\ldots\ldots (12)$$

$$C_R = \sum_{\substack{i=1\\ j=1}}^{n,m} \Delta F_{ij} y_i \Big/ \tfrac{1}{2}\rho V^2 S.CR$$

CHAPTER VI

" TRNVLM " COMPUTER CODE

This section presents the properties of the computer program based on the Nonlinear Vortex Lattice Method. The program, called **TRNVLM** (**TuRkey Nonlinear Vortex Lattice Method**) consists of several subroutines. The brief outline of the important subroutines are given below.

The **TRNVLM** computer code is written in FORTRAN language and it is open to structural modifications. Currently it is running on a 80486 type PC computer with a minimum required 8 Mb Ram total memory. A run time depends on the number of vortex ring subsurfaces used during body modeling. Approximately a computer run time of 60 minutes is needed for the flight path of 10 wing's root chord distance.

Below, the main functions of the important code subroutines are presented.

Subroutine INPUTDATA

This subroutine asks the main geometrical characteristics of the wing. The wing is defined with respect to an origin on the leading edge, at midspan. Figure 6.1 demonstrates the wing geometry and the reference axis of the wing. The geometry of the wing is defined by parameters like; CR, the root chord, CT, the tip chord, S, total span, PHI, the sweep angle.

The total number of vortex rings to be used on wing, fuselage, pylon and external store geometries are given as a second set of data.

Subroutine GEOMETRY

The main surface of the wing is divided into subsurfaces with streamwise panelling method. The panels (vortex cells) are numbered from the leading edge to the trailing edge and from the negative to the positive Y. All necessary parameters of these subsurfaces are stored in arrays.

The control points are computed and stored for latter use. The surface normal vector components are calculated by using the side vectors of the panels. The unit subsurface normal vectors are also stored in a different array.

Subroutine GEO1

The panelling of the fuselage geometry is carried out in this subroutine. The fuselage is represented by a symmetric curved wall attached to the wing at the symmetry plane. The streamwise extension of the fuselage at the aft and fro of the wing platform is adaptable to a certain desired finite size.

All necessary relevant parameters (control points, normal vectors, etc..) are computed and stored in different arrays.

Subroutine GEO2

The panelling of the external store is carried out in this subroutine. The functional parameters of the ellipsoidal geometry are used to compute subsurface data. The external store is attached to the pylon at a

desired location given which is given as an input data point. The streamwise, spanwise and transverse location of the store is prescribed with respect to the geometric center of the ellipsoidal store geometry. The size of the store is given by two parameters; the length and the thickness of the store at the symmetry plane (i.e. at the midchord).

All necessary relevant parameters (control points, normal vectors, etc..) are computed and stored in different arrays.

Subroutine GEO3

The panelling of the pylon geometry is carried out in this subroutine. The pylon is attached to the wing at a desired location which is given as an input data point. The streamwise, spanwise and transverse location of the pylon is prescribed with respect to the leading edge. The geometry of the pylon is adjustable to various shapes varying from rectangular to swept planforms. The size of the pylon is given by three parameters; the root chord (chord at the attachment line to the wing surface) , the tip chord (chord at the attachment line to the store surface) and the sweep angle with respect to the approaching flow direction.

All necessary relevant parameters (control points, normal vectors, etc..) are computed and stored in different arrays.

Subroutine MATRIX

This subroutine computes influence coefficients for finite and semi infinite vortex lattice rings. The

influence of a unit strength bound vortex of a given body ring on all other body rings are computed by using the 3-D Biot Savart Law. The influence coefficient matrix is prepared by considering the mutual interaction between bodies.

Subroutine STERM

This subroutine computes the components of the normal velocity across the body surfaces due to the free stream velocity. A column matrix with total number of subsurfaces as the row size is prepared.

Subroutine TTERM

This subroutine computes the components of the normal velocity across the body surfaces due to both the trailing edge and the tip vortex rings shed into the flow field. A column matrix with total number of subsurfaces as the row size is prepared.

Subroutine FTERM

This subroutine computes the components of the normal velocity across the body surfaces due to unsteady maneuver of the body components. A column matrix with total number of subsurfaces as the row size is prepared.

Subroutine SOLVE

The linear system given by AX=R (where A is a matrix, X and R are column vectors are solved by using a Gauss

Seidel iterative linear equation solver. This subroutine is supported by the basic elements of artificial intelligence of problem formulation so as to accelerate the convergence of the solution.

Subroutine GEOM2

This subroutine prepares the geometric data of the shed vortices from the trailing edge of the wing at each time step.

All necessary relevant parameters (control points, four corner points, normal vectors, etc..) are computed and stored in different arrays.

Subroutine GEOM3

This subroutine prepares the geometric data of the shed vortices from the tip of the wing at each time step.

All necessary relevant parameters (control points, four corner points, normal vectors, etc..) are computed and stored in different arrays.

Subroutine MOVELE1

This subroutine advances the shed and nascent vortex rings shed from the tip of the wing. The induced velocities at four corner points of the ring vortices by other shed rings and stationary surface panels are considered for the next position of the tip wake.

Subroutine MOVETE

This subroutine advances both the already shed and nascent vortex rings from the trailing edge of the wing. The induced velocities at four corner points of the ring vortices by other shed rings and stationary surface panels are considered for the next position of the trailing edge wake.

Subroutine CPRESSWING

This subroutine computes the pressure jump at each control point of the subsurfaces of the wing geometry. The unsteady pressure coefficients are stored in an array.

Subroutine CPRESSTRORE

This subroutine computes the pressure jump at each control point of the subsurfaces of the external store geometry. The unsteady pressure coefficients are stored in an array.

Subroutine FORCEWING

This subroutine presents the normal force data by integrating the pressure coefficients over the surface of the wing. The normal of the each subsurface is then used to compute the 3-D force field including the lift coefficient.

Subroutine FORCESTORE

This subroutine presents the normal force data by integrating the pressure coefficients over the surface of the wing. The normal of the each subsurface is then used to compute the 3-D force field including the lift coefficient.

Subroutine UVW

The velocity components induced by both the stationary body surface vortex rings and the wake vortex rings at a given field point is calculated by this subroutine.

GRAPHICS

Post processing of the output data were handled by using the AUTOCAD and GRAPHER commercial graphic software packages. The interface computer programs to AUTOCAD were written and used interactively with it.

CHAPTER VII

RESULTS AND DISCUSSION

7.1 Validation of the " TRNVLM " Computer Code

As means of establishing the credibility of the Vortex Lattice technique, some applications of the steady and unsteady Nonlinear Vortex Lattice scheme will be presented in this section for validation purpose before investigating the characteristics of the research geometry. Hence, by these exercises the TRNVLM computer code results will be compared with the other code results and the experimental predictions.

An understanding of the steady and unsteady flow field characteristics due to sudden acceleration of an uncambered rectangular wing into a constant-speed forward flight was chosen as a relevant case since there exist extensive data in the literature. This task was accomplished in two separate steps; i) Wing/ No wake {steady} and ii) Wing / Wake {unsteady}.

i) Wing / No Wake {steady}

A preliminary results of the applications with the early versions of the TRNVLM code is presented by Kaykayoglu and Bozkurt[59]. The overall symmetry of the vortex strengths over a rectangular wing surface is shown by the pressure jump distribution. The spanwise and chordwise steady state pressure coefficient topology is depicted in Figure 7.1. Three dimensional features obviously become evident in the flow past a rectangular wing of lower Aspect Ratio. As expected pressure coefficient is maximum near the leading edge

and drops to zero near at the trailing edge. A spanwise distribution shows an elliptic character. The wing tip separation is not considered during this simulation.

Computer experiments have been performed to predict the lift coefficient value as a function of angle of incidence for various rectangular wings having different Aspect Ratios. The variation of the lift coefficient slope with the Aspect Ratio, AR is presented in Fig. 7.2. The theoretical results of Graham [60] is also shown on the same Figure. The computed results agree well with the theoretical values. The deviation from the theoretical results are expected since the leading edge vortex lattices also contribute to the overall lift coefficient value in the computation routine.

The effect of angle of attack on the value of steady state lift coefficient for an unit Aspect Ratio (AR), AR=1, rectangular wing system, is shown in Fig. 7.3. Comparisons with Thin Airfoil Theory [61] for an uncambered wing were carried out by using two different pressure coefficient calculation procedures. First, after representing the trailing edge wake vorticity with horseshoe vortices, thus simulating the vorticity shed behind the wing, the horseshoe vortex strengths are computed by satisfying the steady Kutta condition. The lift for the whole wing is then computed by using Kutta-Jukowski Law [61]. Secondly, the pressure jump coefficient distribution on the wing surface was computed by using the force vector data acting on a single vortex element. Then the pressure distribution was integrated so as to obtain the lift coefficient value. Both methods yields almost the same values with slight deviation at high angles of incidence.

The curves shown in Figure 7.4 are the predictions of the transverse loads on a rectangular wing having Aspect Ratio equal to 1. In the figure,the experimental results of Lamar [62] and the computational results of Fang and Luo [63] are also plotted. computational results of Fang and Luo were also based on a Vortex Lattice type of modeling. The predictions with TRNVLM computer code are near to both results.

Above comparisons show that the steady state lift values computed by the Nonlinear Vortex Lattice Method through utilization of the TRNVLM computer code agree well with the experimental and theoretical results available in the literature.

ii) Wing / Wake {Unsteady}

The transient lift coefficient variation with time for various Aspect Ratio rectangular wings which are suddenly set into forward flight is depicted in Figure 7.5. A time dependent development of a typical wake is also shown at an angle of attack of 5 degrees. A correct roll-up of the wake is obtained despite of the limited number of panels used in this example [59]. A starting vortex forms first along trailing edge during the impulsive start and is then convected downstream. Steady state configuration of the near wake is reached for a dimensionless time T approximately equal to 6. A comparison of the steady state lift coefficient predictions between the present TRNVLM code and the computational code due to Katz [30] is shown in Figure 7.6. The agreement between two codes are remarkable.

The above comparisons show that the Vortex Lattice computer code developed by the author predicts the same results of the standard code prepared and listed in the reference [30] by Katz.

7.2 Applications with the Research Geometry

Present computer code, TRNVLM is capable of predicting the unsteady wing loading during maneuvering flight along a three-dimensional path. The TRNVLM code, in its current state, simulates diving, climbing, pitching, heaving and rolling motions or combination of these motions where predictions by experiments and other numerical techniques are difficult and/or limited.

Both the steady and unsteady characteristics of the chosen research geometry (see Figure 4.1) were investigated. However, before studying with the complex geometry, the aerodynamic characteristics of the chosen wing was investigated. Figure 7.7 shows the variation of steady lift coefficient with the angle of incidence. The variation is found to be linear up to 20 degrees. With the addition of underwing external stores and pylons the lift coefficient values are modified while the slope of the new curve is almost equal to the previous case.

Figure 7.8 shows the instantaneous vortex wake structure behind the wing at an angle of incidence, 5^{0}. The roll-up of the vortex sheet is clearly depicted in Figure 7.8b. The time dependent lift build up on the wing is shown in Figure 7.8c. The transient lift variation dominates upto the nondimensional time, T=6. The steady state lift value reaches to 0.37. The wing tip separation is also included during this series of computer experiments.

As it was cited in various references, the configuration panelling will require careful modeling. In order to assess the requirements for the number of panels to adequately represent the wing configuration,

fine and sparse panel configurations were used to estimate the lift coefficient for the current wing configuration. The convergence of the program is illustrated in Fig. 7.9. Quite a lot of panels are required to have a reasonably precise answer. Figure 7.9 shows the variation of the steady lift coefficient with the number of subsurfaces used in representing the trapezoidal wing geometry. The angle of attack value appears as a parameter. The range of experimentation for the number of panels extends from 4 to 150 subsurfaces. Although the values do not differ for the lower angle of incidence values, at higher angles of incidence, as the panel number increases, the values reach an almost asymptotic value. It was observed that after N_w=40, the lift coefficient values are nearly stationary. From this observation, a minimum number of panel number quantity, N_w=42, (3 X 14), are chosen as an input data to TRNVLM for wing surface paneling. This choice is a also adequate for a reasonable computer run time.

The fuselage, external store and pylon geometries are represented by 6 X 6, 8 x 9, and 4 X 4 panels respectively. Hence, a total of 166 subsurfaces were used for the configuration modeling.

7.2.1 Effect of the External Store Installation Position and Size on the Wing Lift Characteristics

Before a detailed analysis with the research configuration described above, we performed short but critical computer experiments with the present code on an arbitrarily chosen wing and store configurations. Figure 7.10 illustrates the steady lift coefficient

variation with incidence for the configuration with and without underwing store installation. The computed lift curves show the same behavior with varying values of angle of incidence. At lower angles of attack, less than 15 degrees, the lift curve for the wing/ store/ fuselage lies above the wing/fuselage combination. Further, at 0 degree of incidence there is an induced positive lift on the wing due to store presence. At a higher incidence, the presence of the store decreases the wing's lift. Both lift curve slopes are equal at high angles of attack.

Figure 7.11a shows the time history of the wing lift coefficient with and without an external store. The store aspect ratio is greater than the previous case which was studied above. The steady state lift value of the wing/ store/ fuselage combination exceeds the wing/ fuselage alone. Contrary to the observations presented with Fig. 7.10, for this particular size and orientation of the store under the wing, the lift value is augmented at high angle of incidence. The corresponding wake configuration is obtained gradually by releasing vortex rings from the edges (See Fig. 7.11b). The roll up of the wake at the sides are clearly observed for the two cases under investigation. The flow field aft of the store continuously causes modifications on the strength of the vortex rings releases from the trailing edge. Consequently, the wake developing under the presence of the external store causes higher roll-up structure due to the modified near trailing edge flow field. The rotational fluid region occupied by the wing/ store/ fuselage trailing edge wake exceeds that of the wing/ fuselage combination.

7.2.3 Computer Experiments with the Research Geometry

The computer experimental results with the research configuration will be presented in this section.

Unsteady Wake Development: Effect of angle of incidence

The wake of an aircraft has a major effect on the aircraft's aerodynamic characteristics, such as tail plane loads on wing/tail plane configurations and wing pressures. For this reason, it is essential that a computational code can model wakes accurately.

Figure 7.12 shows an overall plan view of the instantaneous structures of the trailing edge wakes for different angle of attacks. The separated trailing edge wake does not carry any tip separation effects. The shed vortex rings deform continuously under the influence of fuselage/ pylon/ store combination. The continuous spill of the flow from the lower surface of the wing combines with the upper surface flow and then forms the classical wing tip vortices. The clockwise rotating wing tip vortex (viewed from the rear) induces downwash velocity on the developing wake. Along wing/ fuselage junction the wake is attached to the fuselage surface. The similar vortex roll-up but in the counterclockwise direction takes place as the wake develops in the streamwise direction. The downstream wake development is highly influenced by the presence of the underwing store. At $\alpha = 20^{\circ}$ there exist additional secondary roll-up in the clockwise direction at about three root chord distances from the trailing edge of the store. Such kind of wake characters can also appear for negative angle of incidence. In negative angle of attacks, the secondary vortex,

rotating counter clockwise (viewed from the rear) tends to spiral into a large vortex core. Similar types of vortex formation can also be observed behind wing/ trailing edge flap combination [22].

Figures 7.13 through 7.21 show the main features of the trailing edge wake development as a function of angle of incidence at a nondimensional time, $T = U_\infty t / CR = 8.3$. The pictures are presented at various view angles. Figure 7.13 shows the case for 0° of incidence. Figure 7.13a is the wire diagram representation of the wake and the research geometry. The instantaneous wake structure is represented with the instantaneous deformed shapes of the shed vortex rings. The transient wake development near the wing/fuselage juncture shows both a twist and also a light roll-up in the counterclockwise direction. Figure 7.13b shows the same configuration with hidden surfaces and lines. The side view of the complete wake development is shown in Fig. 7.13c. The roll up of the trailing edge wake is viewed from the rear parallel to the wing's surface (see Fig 7.13d-e). The wake is deflected down by forming a bowl shape. The wake exhibits a strong antisymmetry thus causing antisymmetric loading on the wing.

Figures 7.14a-e present the wake structure for a positive angle of attack (climb mode), $\alpha = 10°$. Figure 7.14b shows the streamwise vortex filaments separating from the trailing edge. A passive tracers emanating from the wing tip shows the basic character of tip vortex roll-up. The distortion of the near wake due to the presence of the external store is shown from different view angles in Figs. 7.14d and e. The wavy spanwise distribution of the wake sheet modifies the pressure loading on the wing surface. The wake deflects downwards near the store trailing edge thus creating unsteady velocity perturbations on the store surface.

At a positive angle of attack value α=20 degrees, the lateral size of the wake, hence the extend of the rotational region, increases (see Figures 7.15a-c). The secondary roll-up of the wake sheet with the influence of store complicates the final wake shape. This new vortex mechanism controls the final wake shape and also modifies the classical wake formation. The upward deflected wake shape with the presence of secondary spiral between the wing tip and wing/fuselage juncture is the important character of the transient wing motion during the forward-climb mode.

The direction of the wake deflection is downward for the negative values of angle of incidence (dive mode). Figure 7.16 shows the instantaneous wake structure from different view points. The wake sheet deflects slightly upward near the trailing edge of the wing and then deflects downwards (see Fig. 7.16c). The secondary spiral rolls-up in the clockwise direction in contrast to our observations for the case of positive incidence. The roll-up process is augmented at higher dive angles. Figures 7.17a-d show the case at α=-20°. The initial upward deflection of the wake sheet after shedding from the wing trailing edge is more evident in this case.

Unsteady Wing and External Store Loading

The transient development of the force coefficients for the research geometry that was suddenly put into forward climbing and diving motion is reported in this section. In the first part of the presentation, the wing lift coefficient variation due to wing forward motion will be discussed. This discussion will be followed by presentation of the 3-D transient force development on the external store during unsteady maneuver.

Wing Loading

The transient lift coefficient variation with time for the wing is presented in Figure 7.18 for α= 0.0. During the early phases of geometry acceleration, the unsteady component $\partial\phi/\partial t$ is very large, hence it dominates the overall lift value. Immediately, after the wing has reached its steady-state speed, the lift drops due to the influence of the starting vortex and also due to the change in downwash velocities. Contrary to the classical observations, the lift fluctuates under the influence of external store and then shows smooth behavior. The initial lift loss continues almost two chord distance of motion. A recover will then turn into a flat asymptotic steady lift coefficient value.

Figure 7.19 depicts the transient lift development for the climb mode where the wing/fuselage/pylon/store geometries are suddenly set into climb motion. The length of the transient lift variation is small compared to Fig. 7.18. A relatively short length of transient lift development shows slight fluctuations in the lift value. This turns into a steady state value after one root chord distance for the climb mode at α= 10 degrees. That is clear that the presence of the store slightly modifies the effect of initial acceleration by causing additional perturbations. Figure 7.20 shows the transient variation for α =20 degrees. After a short distance of transient lift development, the final steady state value of the lift builds up on the wing's surface.

The transient nature of the lift coefficient for the negative incidence (dive mode) are shown in Figures 7.21 and 7.22. At α = -10 degrees, after a large jump

in the lift, the lift coefficient begins to fluctuate up to T=2 and then attains its final value. As the dive angle increases, the transient lift portion decreases and the wing lift coefficient reaches its final value. (see Figure 7.22).

The final steady state lift coefficient values are plotted on Figure 7.23. The variation is almost linear for the range -10 to 10 degrees. There is a positive lift value at 0 degree of incidence due to the presence of external store. The variation of the steady state lift coefficient is not symmetric with respect to the angle of attack values. While the lift coefficient values are observed to be higher for the positive values of the angle of incidence (climb mode), the values drops nearly 30% for the negative angle of incidence (dive) values. We also plot the steady state lift coefficient values for the wing system without an underwing external store system on this Figure. It is very interesting to note that at positive angle of incidence (climb mode) the lift value decreases. On the other hand at negative angle of attack values (dive mode) the lift is augmented. The downward shift of the lift curve predicts zero lift at zero degree of incidence.

External Store Loading

Understanding of the transient force development on the external store is extremely important since the characteristic values set the initial conditions for store separation. For this reason the instantaneous pressure distribution over the store surface is integrated over the subsurfaces and the normal force values are determined. By resolving the normal force components in three directions, the transient force component history is obtained.

Figure 7.24 shows the variation of the steady state external store force coefficient values as a function of angle of attack. The x-component of the store force values are found to be all positive. The streamwise x-force component decreases as the climb angle increases. On the other hand, this value increases for the negative incidence. Hence during the dive mode, the store is subjected to higher streamwise loads. This final observation is also valid for the other two force components. Both the y- and z- directional force values are negative and reach maximum values at negative angle of attack values. The outward force component, F_{cy}, spanwise force, is believed to be due to the largely outward air flow beneath the wing lower surface. Surprisingly, the force component F_{cz}, is all negative for the parameter range under investigation. Thus, store is subjected to downward forces which is partly due the downwash velocity of the trailing wake and the nonlinear interaction between the store and pylon/wing configurations.

The series of 5 Figures (Figures 7.25-17.29) present the unsteady force coefficient development on the external store during steady forward flight. The transient force build-up on the store is different than the wing's transient lift development. Since, we assume that there is no wake shedding from the store geometry, the perturbations coming from both the neighboring bodies and the developing wake modify the transient force development. For all the cases investigated, the transient force development zone extends upto nearly two root chord lengths. The spanwise force fluctuates during the early transition period then reaches a steady state value.

Transient Velocities at a Reference Point

A reference point (Xp/CR=1.3, Yp/CR=-0.434, Zp/CR=-0.11 is chosen near the trailing edge of the external store so as to study the character of the velocity perturbations induced by the complex configurations and the trailing edge wake. This computer experimentation aims at understanding the magnitude and also the direction of the induced velocities near the store. This information is important when the store separation process is modelled under the effects of the unsteady wake roll-up.

Figure 7.30 shows the time variation of the streamwise velocity at the reference point. For 0 degrees angle of incidence, the nondimensional velocity attains a value near .85 . For positive angle of incidence (climb mode) this value drops to a value of .82. On the other hand, for the negative incidence values the velocities increase and reaches to a value of .9 for α =-10 and .93 for α =-20 degrees. Hence, during diving, the streamwise induced velocity increases. This causes a decrease on the pressure coefficient values on the store surface. Such an observation is also validated by Figure 7.24, where we showed that the streamwise force component increases with the negative angle of incidence values.

The nature of the spanwise velocity variation at the reference point is shown in Figure 7.31. The sign of the velocities are worth to discuss. While the positive velocities (towards fuselage) are observed for positive angle of incidence, the direction of the velocity vector is outward for negative incidence. For symmetric flow conditions (zero incident yaw velocity) a spanwise velocity components may reach upto 40% of the free streamwise velocity at high positive angle of incidence.

Finally, the transient development of vertical velocity component at the reference point is shown in Fig. 7.32. The induced velocity due to external flow, wake roll up and body singularities yield negative (downward) velocity magnitudes at the reference point. It is interesting to note that induced velocities for positive angle of incidence are even higher than the values which correspond to the negative values. Hence, strong downward velocities are mainly due to the unsteady wake roll-up near the trailing edge.

Roll and Pitch Motions During Steady Flight

In the present study, a nonlinear and unsteady vortex lattice code applied for calculating the unsteady force and wake characteristics for complex wing /fuselage/ pylon /store maneuvers. Figure 7.33 shows wake oscillation patterns behind the system undergoing a roll motion under zero angle of incidence. The roll amplitude is 10 degrees and the whole configuration sinusoidally rolls with respect to x- symmetry axis. The oscillation reduced frequency is $k=2\pi f.CR/2U_{\infty}=0.95$ The sinusoidal roll motion of the system is reflected in the wake structure. The roll-up of the tip vortex sheet disappears and wake vorticity field forms crests and troughs. The wavy nature of the wake continues with growing nature.

The time dependent lift coefficient variation is depicted in Figure 7.34. The transient lift coefficient oscillates with the same frequency of the roll motion. Roll motion at zero angle of incidence results in higher positive lift values. Furthermore, at the peak positive amplitudes of the roll, the lift coefficient attains maximum values since the apparent angle of attack also increases.

The induced force components on the external store during roll motion is depicted in Figure 7.35. The force components fluctuate with the given roll frequency. However, the presence of secondary harmonics show that during the roll motion the nonlinear loads becomes significant. This nonlinear behavior may be due to the Biot Savart induction from developing wake structure behind the configuration.

Figures 7.36a-c show the computed wake shape for the simultaneous dive and roll motion. The configuration was set suddenly into forward dive motion while it executes roll with respect to wing midspan. Due to combined dive/roll motion, the near wake structure is modified drastically. This modification is reflected in the transient lift coefficient development (see Figure 7.37). The oscillatory nature of the lift coefficient with a single dominant frequency (as it was observed earlier) is modified slightly with the nonlinear effects. The frequency of the nonlinear effects are almost twice the main frequency. The time mean average value of the lift coefficient is nearly equal to the value plotted in Figure 7.25. for α=-20 degrees.

Figure 7.38 shows the transient force coefficient variation for the external store system. The higher harmonics present in all three components show that the nonlinear effects are dominant and play an important role on the store loading. Due to transient motion, the streamwise force component also fluctuate in phase with the input motion.

One of the simplest but yet an important maneuver is the oscillatory pitching motion of the system during diving. The system is put into pitching mode with respect to wing apex while diving. Figures 7.39a-c

shows instantaneous complex wake structures at different view planes. The pitching motion results in sinusoidal change in angle of attack. The vortex sheet separated at the trailing edge forms continuous sheet of vorticity with unsteady complex character.

The transient lift coefficient varies sinusoidally with the same frequency of pitching (see Figure 7.40). There is no secondary harmonics as opposed to the observation in roll motion simulation. The transient store force coefficient variations are shown in Figure 7.41.

The character of the induced velocity fluctuations at the reference point is shown in Figures 7.42-7.44. For the roll maneuver with and without dive, there exist secondary harmonic components in the variation of the streamwise velocity component (See Figure 7.38). The pitch/dive mode results in pure sinusoidal variation with an approximately 180 degrees phase lag. The transient variation of V/U_{∞} and W/U_{∞} are shown in figures 7.39 and 7.40.

Above results and discussions reveals that the unsteady nature of the force components on the wing and external store systems are due to both the nonlinear interactions between maneuvering configuration and the unsteady wake roll-up behind the system. However, more computer experiments are needed to clarify this complex nature.

shows instantaneous complex wake structures at different view planes. The pitching motion results in sinusoidal change in angle of attack. The vortex sheet separated at the trailing edge forms continuous sheet of vorticity with unsteady complex character.

The transient lift coefficient varies sinusoidally with the same frequency of pitching (see Figure 7.40). There is no secondary harmonics as opposed to the observation in roll motion simulation. The transient store force coefficient variations are shown in Figure 7.41.

The character of the induced velocity fluctuations at the reference point is shown in Figures 7.42-7.44. For the roll maneuver with and without dive, there exist secondary harmonic components in the variation of the streamwise velocity component (See Figure 7.38). The pitch/dive mode results in pure sinusoidal variation with an approximately 180 degrees phase lag. The transient variation of V/U_{∞} and W/U_{∞} are shown in figures 7.39 and 7.40.

Above results and discussions reveals that the unsteady nature of the force components on the wing and external store systems are due to both the nonlinear interactions between maneuvering configuration and the unsteady wake roll-up behind the system. However, more computer experiments are needed to clarify this complex nature.

CHAPTER VIII

EXTERNAL STORE SEPARATION UNDER UNSTEADY WAKE SHEDDING

In the second phase of the project, author aims at simulating store separation under various aircraft maneuvers. The flow grid network method developed by Meto [56] will be used for this purpose. The philosophy of the method is shown in Figure 8.1.

The store separation analysis consisted of calculating the aerodynamic forces and moments on the store in several locations in the vicinity of the maneuvering wing [56]. The store aerodynamic characteristics are evaluated using the Nonlinear Vortex Lattice Method combined with a flow grid method.

In the modified version of TRESSP [56], author solves for the new attitude of the store at a specified interval of time in the store trajectory and then uses this new wing/fuselage/pylon/store physical relationship to calculate a new flow field. Using the new flow field, the aerodynamics is updated and the process is repeated for a complete store trajectory.

The characteristics of the external store dynamics after release from the wing was investigated by employing an unsteady flow grid method. The external store moves through the nonuniform flow field consisting of the freestream plus the disturbance flow field created by the wing/pylon/fuselage/store including unsteady wake effects. The instantaneous state of the underwing flow field that depends on the time history of the aircraft motion taken to the instant is simulated so as to evaluate the store carriage and release performance.

As it was outlined briefly in Chapter I, the separation effects are critical for store initial trajectory. Since such an initial condition set the stage for the rest of the trajectory we need to know the initial aerodynamic loading on the store as soon as it separates from the pylon. At and just after the separation the aircraft induced velocity perturbations are very critical. During air-to-air or air-to-ground weapon delivery, the continuous maneuver of the aircraft may effect the initial conditions. Moreover there may be cases which will deviate from standard conditions although the pilots are instructed to fly strictly defined delivery conditions.

Since the computer experiments are still being done, no results will be presented for this phase of the project. The complete results will be presented on the report covering the second year activity of the project.

CHAPTER IX

FUTURE DIRECTIONS

In the present report, we described an extension for the familiar Vortex-Lattice Method that can treat unsteady lifting flows. Some of the capabilities of the computational approaches were demonstrated on a variety of simple cases. Moreover, trailing edge vortex wake dynamics were studied for pitching, heaving and rolling motions, where predictions by experiments and other computational techniques is very limited. Currently, the computer code is being modified with the inclusion of leading edge separation.

The computer code was tested against known steady and unsteady solutions. Flat rectangular wings of various aspect ratio were used to compare the theoretical lift coefficient slope with the computer code's predictions.

The store separation module based on TRESSP computer code [57] is prepared and is currently being tested. This will be the major future activity.

The present report brings a single case study. Hence, a single store station is tested with a generic store geometry. Preliminary exercises have shown that the position of the store has a drastic influence on the wing loading. For this reason more parametric runs are needed for complete understanding.

The plan of the future activity is reported separately under the proposal for continuation.

REFERENCES

[1] Arnold, R.J. and Epstein, C.S., " Store Separa tion Fligt Testing", AGARD Flight Test Technique Series, Vol.5, AGARD-AG-300, April 1986.

[2] Triplett, W.E., "Wind tunnel correlation Study of Aerodynamic Modeling for F/A-18 Wing-Store Tip-Missile Flutter ", Journal of Aircraft, Vol.21, No.5, 1984.

[3] -----, "Integration of Externally Carried Weapon Systems with Military Helicopters", AGARD ADVISORY REPORT No.247, April, 1990

[4] Huttsell, L.J. and Noll, T.E., "Wing Store Active Flutter Suppression-Correlation of Analyses and Wind-Tunnel Data", vol. 16, No.7, 1979.

[5] Arnold, R. J. and Knight, J.B., "Weapon Delivery Analysis and Ballistic Flight Testing ", AGARDograph 300, Flight Test Techniques Series-Volume 10., 1992

[6] Baxendale, A.J., " Application of a Multiblock CFD System to Obtaining Flowfield Predictions About Wing Body Pylon Store Configurations", Proceedings of ICAS-90,1990.

[7] Luckring, M.J., " Recent Progress in Computational Vortex Flow Aerodynamics ", AGARD Conference Proceedings 494, 1991.

[8] Nurman, E.m. and Rizzi, A., " Application of Euler Equations to Sharp-Edged Delta wings with Leading Edge Vortices", AGARD CP412, Paper no. 15, 1986.

[9] Hoeijmakers, H.W.M., Jacops, J.M.J.W., Berg., J.I., " Numerical Simulation of Vortical Flow Over a Delta Wing at subsonic and Transonic Speeds", ICAS Paper 90-3.3.3, 1990

[10] Legendre, R. "Ecoulment au voisinage de la pointe avant d'une aile a forte fleche aux incidence moyennes", La Recherche Aeronautique, Vol. 30, 1952.

[11] Brown, C. and Michael, W. Jr.,"On slender wings with leading edge separation", NACA TN 3430, 1955.

[12] Mangler, K.W. and Smith, J.H.B., " A Theory of the flow past a slender delta wing with leading edge separation", Proc. Roy. Soc. Vol. A 251, 1959.

[13] Gersten, K., "A nonlinear lifting surface theory specially for low aspect ratio wings", AIAA Journal, Vol. 1, 1963.

[14] Cohen, M.J. and Nimri, D., "Aerodynamics of slender rolling wings at incidence in separated flow", AIAA Journal, Vol. 14, 1976.

[15] Tavares, S.T., "Aerodynamics of Maneuvering Slender Wings with Leading Edge Separation", Ph.D. Thesis, M.I.T., Sept. 1990.

[16] Jones, R.T., "Properties of Low Aspect Ratio Pointed Wings Below and Above the speed of Sound", NACA Report 835, 1946.

[17] Munk, M., "The aerodynamic forces on Airship Hulls", NACA Report 184, 1921

[18] Polhamus, E.G., "Predictions of vortex lift characteristics by leading edge suction analogy", J. of Aircraft, vol. 8, 1971

[19] Lamar, J.E., "Extension of Leading Edge Suction Analogy to Wings with Separated Flow Around the Side Edges at Subsonic Speeds", NASA TR R-428, 1974.

[20] Bartlet, G.E. and Vidal, R.J., " Experimental Investigation of Influence of Edge Shape on the Aerodynamic Characteristics of Low Aspect Ratio Wings at Low Speeds ", J.Aero. Sci., Vol. 22, 1955.

[21] Shepshelovich, M., " vortex Lift Prediction for Cambered Wings ", Proc. 18th Israel Annual Conference on Aviation and Astronautics, 1976.

[22] Hoeijmakers, H.W.M., " Panel Methods for Aerodynamic Analysis and Design ", AGARD FDP Special Course on Engineering Methods in Aerodynamic Analysis and Design of Aircraft, Ankara, Turkey, May 1991.

[23] Cenko, A., Tinoco, E.N., Dyer, R.D. and DeJongh, J., " PAN AIR Applications to Weapons Carriage and Separation", Journal of Aircraft, Vol. 18, No. 2, 1981.

[24] Maskew, B., "Prediction of Subsonic Aerodynamic Characteristics- A Case for Low-Order Panel Methods ", AIAA Paper No. 81-0252, 1981.

[25] Tinoco, E.N., Johnson, F.T., and Freeman, L.M., "The Application of a Higher Order Panel Method to Realistic Supersonic Configurations" , AIAA Paper 79-0274, 1979.

[26] Morino, L. (Editor), Computational Methods in Potential Aerodynamics, Springer Verlag, 1985.

[27] Carmichael, R.L. and Erickson, L.L., " PAN AIR A Higher Order Panel Method for Predicting Subsonic or Supersonic Linear Potential Flows About Arbitrary Configurations", AIAA Paper 81-1255, 1981.

[28] Kaykayoglu, C.R., Ozturk ,I., Meto, S. and Bayar,C ," Development of Computational Aerody namic Codes for Simulating Military Air craft/Store Carriage and Release ", Paper Submitted to the Bulletin of Istanbul Technical University, 1991

[29] Hoeijmakers, H.W.M. and Bennekers, B., " A Computational Method for the Calculation of the Flow About Wings with Leading Edge Vortices", AGARD CP-247, Paper 25, 1979.

[30] Katz, J., Low Speed Aerodynamics, McGraw-Hill, Inc., 1991.

[31] Konstadinopoulos, P., Thrasher, D.F., Mook, D.T., Nayfeh, A.H. and Watson, L., "A Vortex - Lattice Method for General, Unsteady Aerodynamics", Journal of Aircraft, 22, No.1, pp. 43-49, 1985.

[32] Katz, J., "Lateral Aerodynamics of Delta Wings With Leading Edge Separation", AIAA Journal, 22, No. 3, pp. 323-385, 1984.

[34] Katz, J. and Kern, D., "Effect of Vertical-Ejector Jet on the Aerodynamics of Delta Wings", Journal of Aircraft, 27, No. 5, pp. 408-412, 1990.

[42] Portnay, R., Rom, J., Zorea, C., "Investigation Into Formation of Wing Tip Vortices", TAE Report 199, 1974.

[43] Almosnino, D., Rom., J. and Zorea, C., " Calculation of the Nonlinear Aerodynamic Coefficients of wings of Various Shapes and Their Wakes, Including Canard Configurations", Proceedings of 11th ICAS Conference, vol 1, September 1978, pp. 333-344.

[44] Straganac, W.T. and Mook, D.T. " Numerical Model of Unsteady Subsonic Aeroelastic Behavior", AIAA Journal, Vol. 28, No. 5, 1990.

[45] Kandil, A.O., Mook, D.t., and Nayfeh, A.H., " Nonlinear Prediction of the Aerodynamic Loads on Lifting surfaces", Journal of Aircraft, Vol. 13, 1976.

[46] Nuhait, A.O. and Mook, D.T., " Numerical Simulation of wings in Steady and Unsteady Ground Effects ", Journal of aircraft, Vol. 26, No. 12, 1989.

[47] Bayar, C., " Vortex Lattice Method simulation of Thick Wing Unsteady Aerodynamic", Ph. D. Study (Continues)

[48] Rusak, Z., Wassertrom, E. and Seginer, A.," Numerical Calculation of nonlinear Aerodynamics of Wing-Body configurations ", AIAA Journal, Vol. 21, 1983.

[49] Uchiyama, N., Mikkilineni, R.P., and Wu, J.M., " The Analysis of Wing-Body Combinations at Moderate Angle of Attack", AIAA Paper No.78-62, 1978.

[50] Atta, E.H. and Nayfeh, A.H. " Nonlinear Aerodynamics of Wing-Body Combinations ", AIAA Paper 78-1206, 1978.

[51] Kandil, O.A., Mook,D.T. and Nayfeh, A.H.," A Numerical Technique for Computing Subsonic Flow Past Three Dimensional Canard-wing Configurations with Edge Separations", AIAA Paper 77-1, 1977

[52] Rusak. Z, Wasserstrom, E. and Seginer, A, " Numerical Calculation of Nonlinear Aerodynamics of Wing-Body Configurations", AIAA Journal, Vol. 21, No. 7, 1983.

[53] Rusak. Z, Seginer, A. and Wasserstrom, E., " Convergence characteristics of a Vortex Lattice Method for Nonlinear Configuration Aerodynamics", Journal of Aircraft, Vol. 22, No.9, 1985.

[54] Almosnino, D. and Rom, J., "Calculation of Symmetric Vortex Separation Affecting Subsonic Bodies at high Incidence ", AIAA Journal, Vol. 21, 1983.

[55] Ozturk, I., " A 3-D Panel Method in Linearized Subsonic Flow ", Master Thesis, Graduate School, Istanbul Technical University, July 1989.

[56] Meto, S., " Computer Simulation of an External Store Separation from a Military Aircraft with Panel Method " , Master Thesis, Graduate School, Istanbul Technical University, February 1991.

[57] Bayar, K.C., " Steady and Unsteady Aerodynamics of Wings ", Master Thesis, Graduate School, Istanbul Technical University, July 1991.

[58] Robinson, A. and Laurman, J. A., Wing Teory, Cambridge University Press, Cambridge, England, Chapter 1, 1956.

[59] Kaykayoglu, C.R. and Bozkurt, S., " Vortex Lattice Method simulation of Unsteady Separated Flows Around Maneuvering Wings ", Proceedings of Tenth Anniversary Symposium of the Department of Aeronautical Engineering, Middle East Technical University, 22-26 June, 1992.

[60] Graham, J.M.R., " A lifting Line Theory for the Rectangular Wing in Non-Stationary Flow ", The Aeronautical Quarterly, Vol. XXII, 1971.

[61] Anderson, J.D., Fundamentals of Aerodynamics, McGraw Hill Book Company, 1985

[62] Lamar, J.E., NASA TR R, p. 428, 1974

[63] Fang, J. and Luo, S., "Computation of the Subsonic Nonlinear Loads on Flat Plane Wings at High Angles of Attack ", Computational Mechanics, Balkema Press, pp. 1543-1547, 1991.

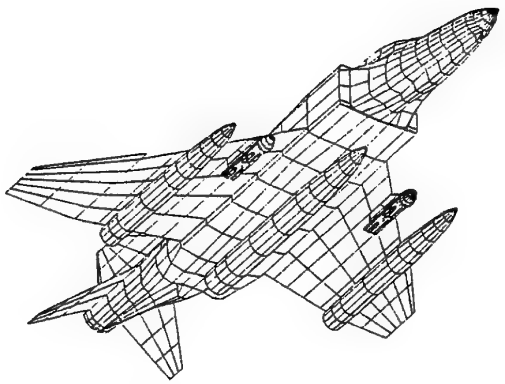

F-4 Aircraft Paneling including dispensers and fuel tanks: isometric view

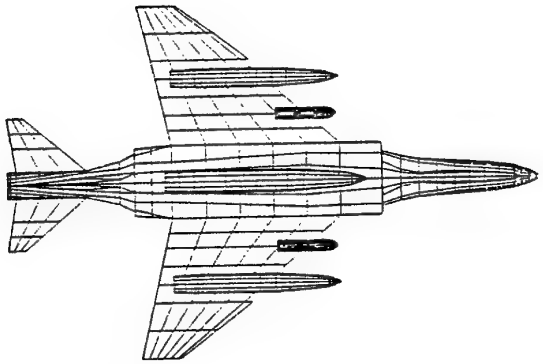

bottom view

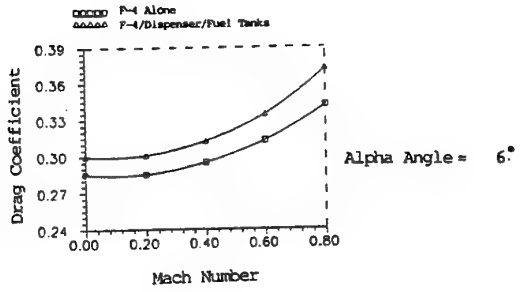

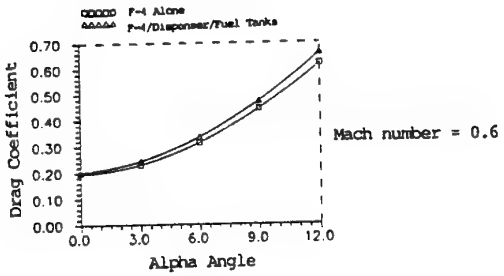

Figure 2.1 F-4 configuration with external stores and fuel tanks. Variation of form drag coefficient with Mach Number and Angle of Incidence.

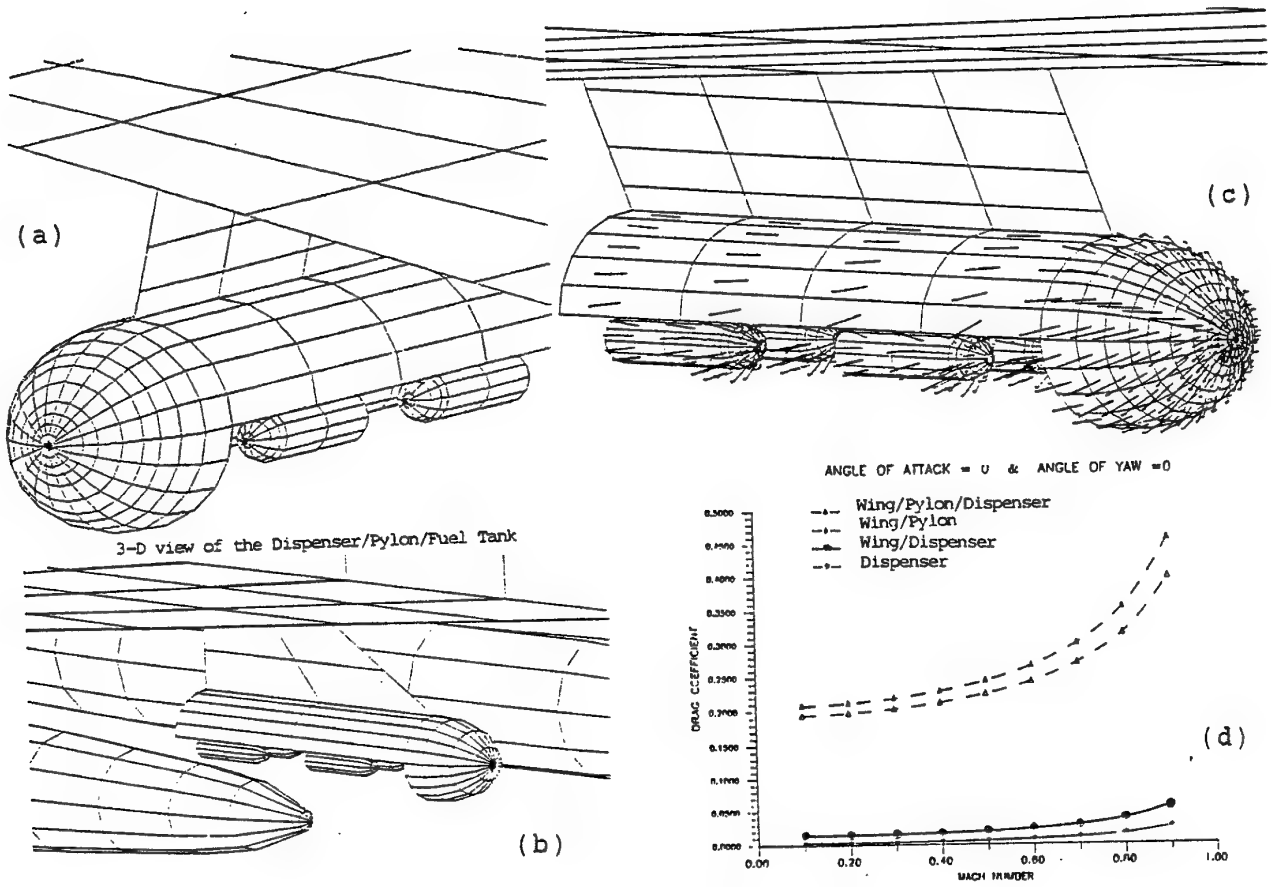

Figure 2.2 a,b) Geometry of wing/pylon/store combination and paneling density c) Surface velocity vectores on the dispenser d) Variation of drag coefficient as a function of free stream Mach Number.

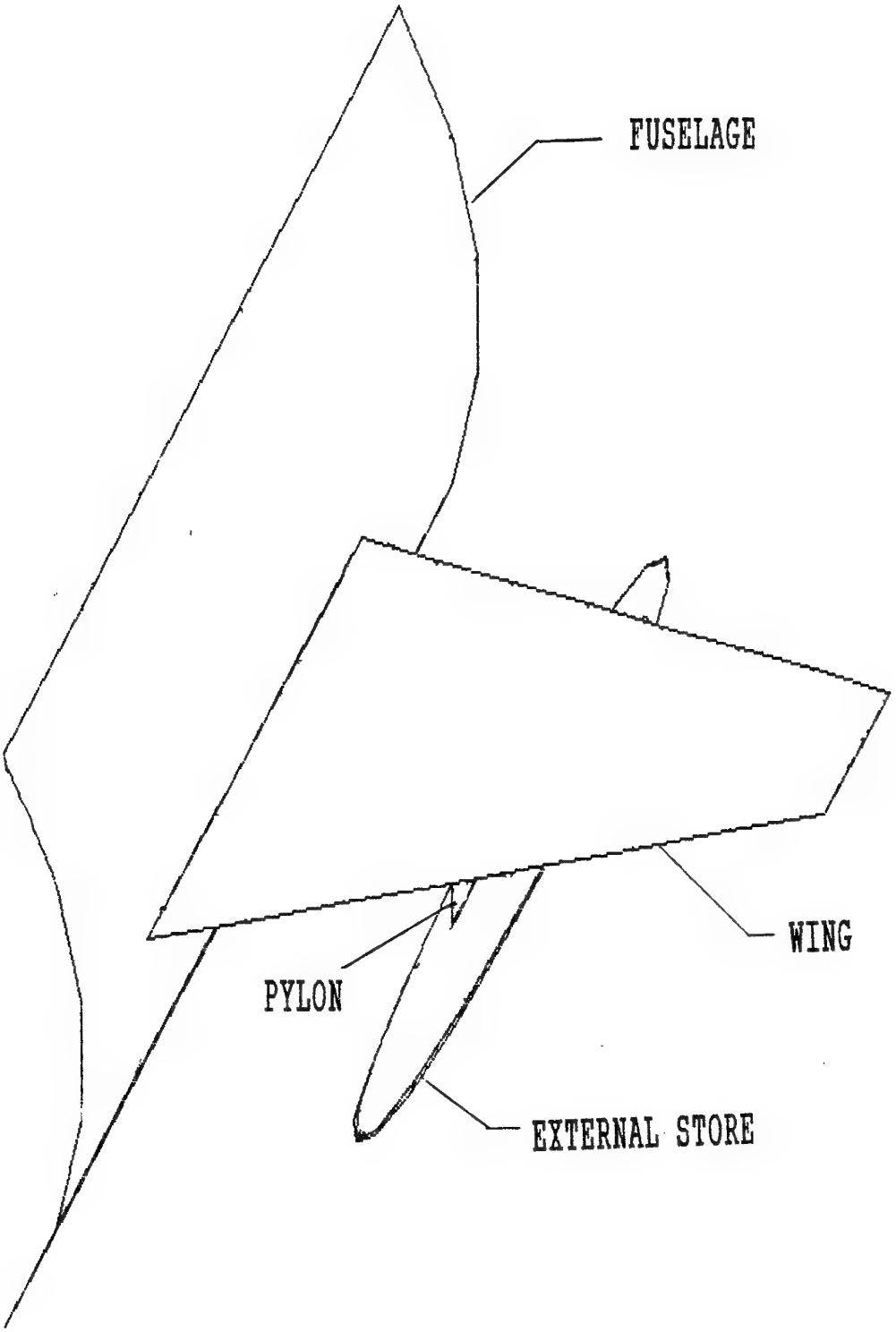

Figure 4.1 The geometry of the research configuration featuring wing/fuselage/pylon/store combination

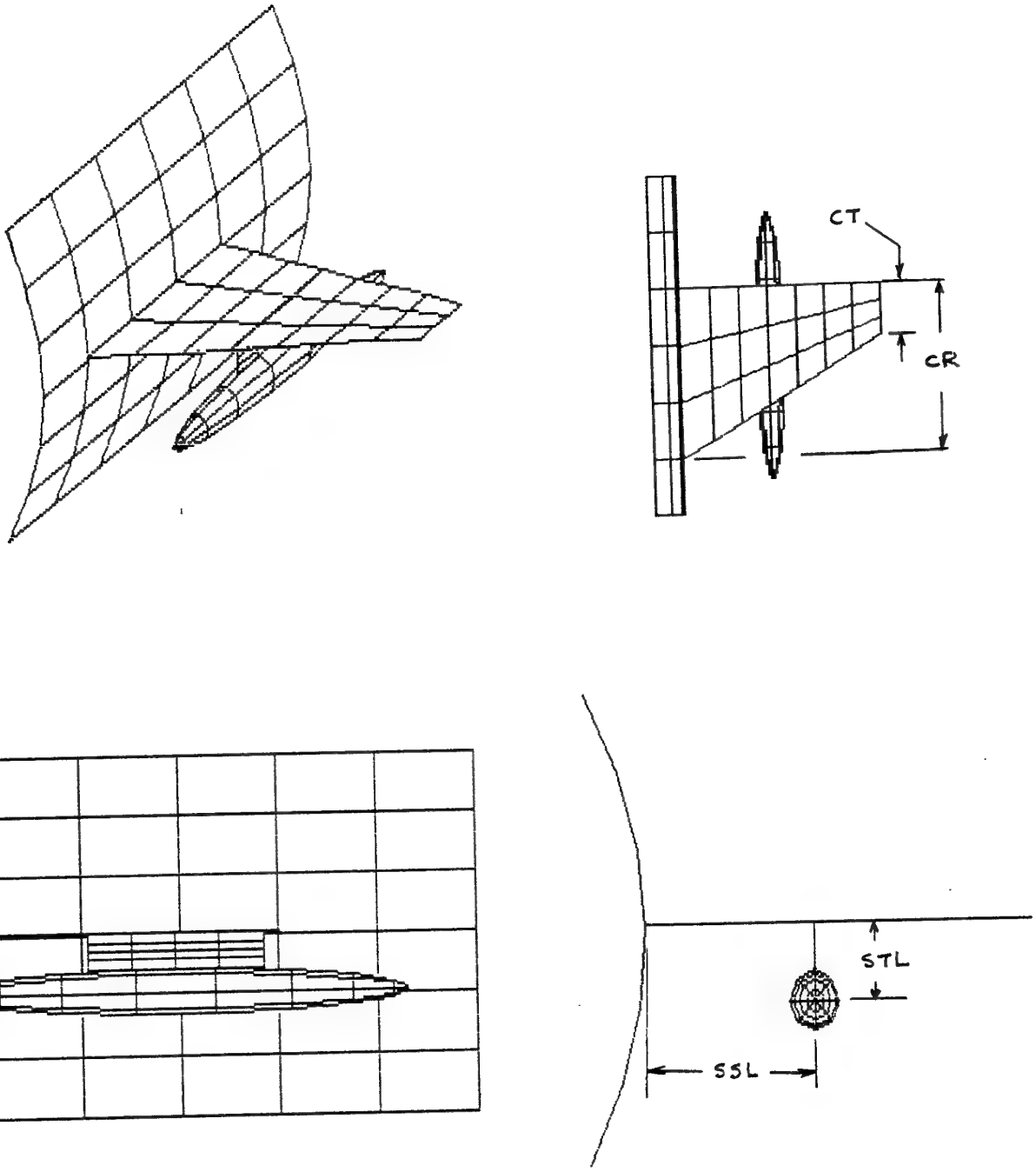

Figure 4.2 The properties of the research configuration at different view planes.

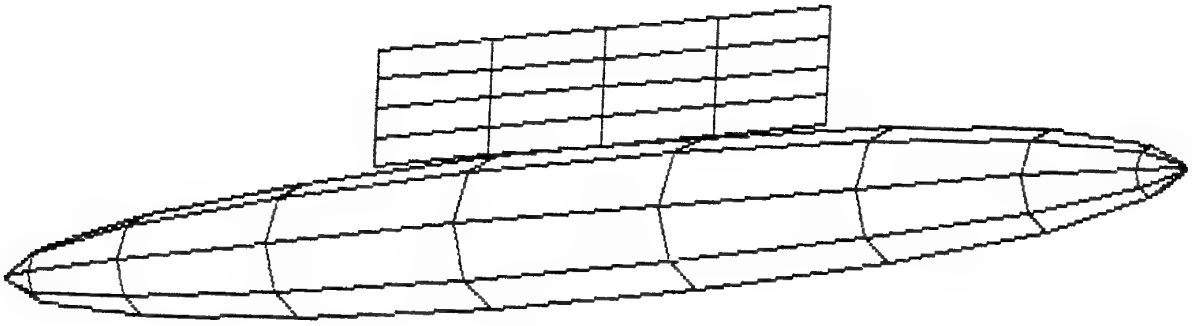

Figure 4.3 External store and pylon geometry.

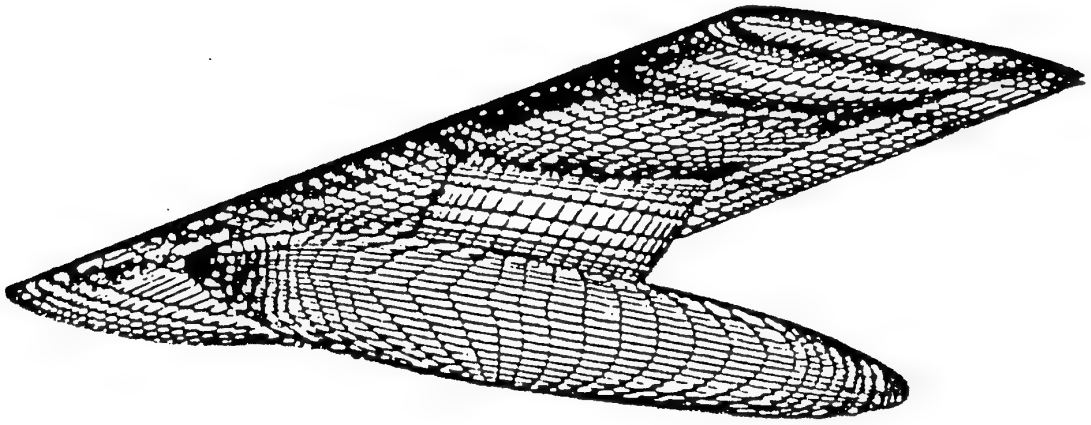

Figure 4.4 Research model used by Baxendale [6] at Aircraft Research Association in Bedford, U.K..

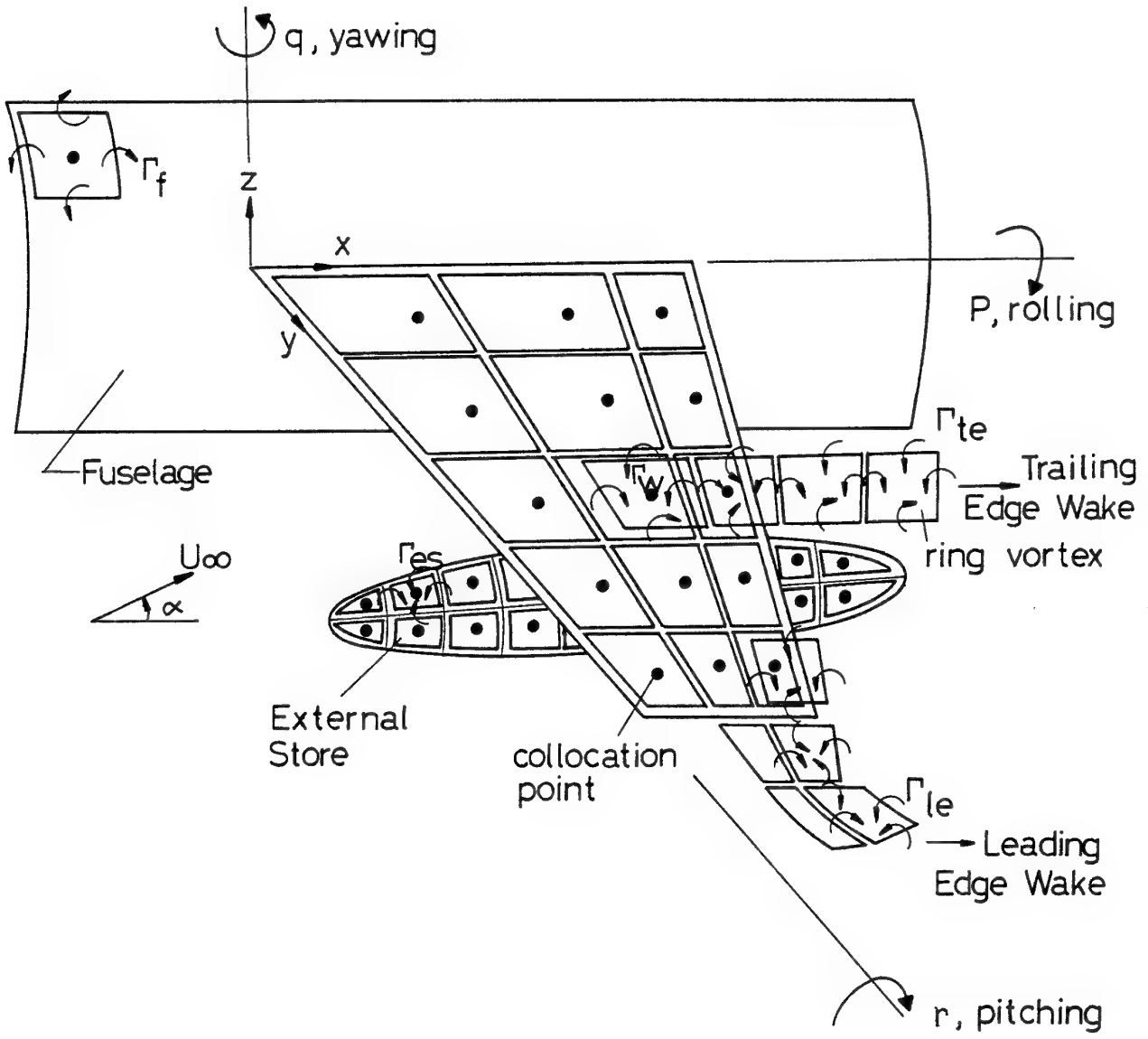

Figure 4.5 The vortex lattice discretization of the research configuration.

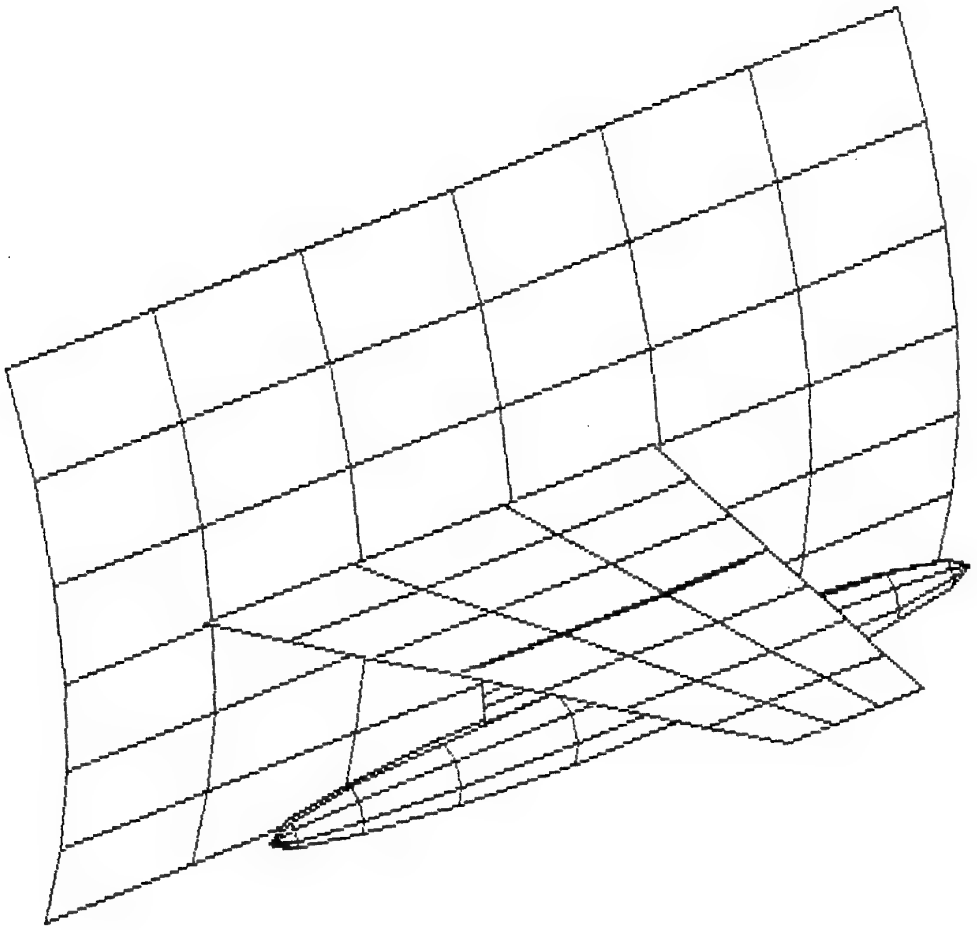

Figure 4.6 The vortex lattice representation of the research geometry.

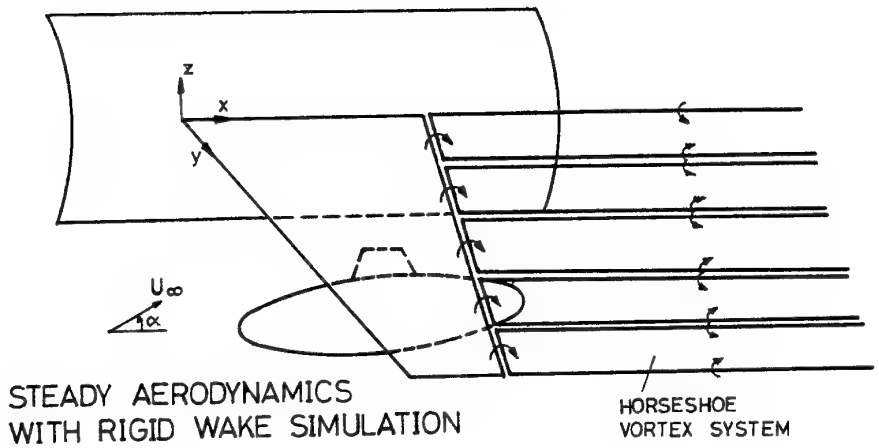

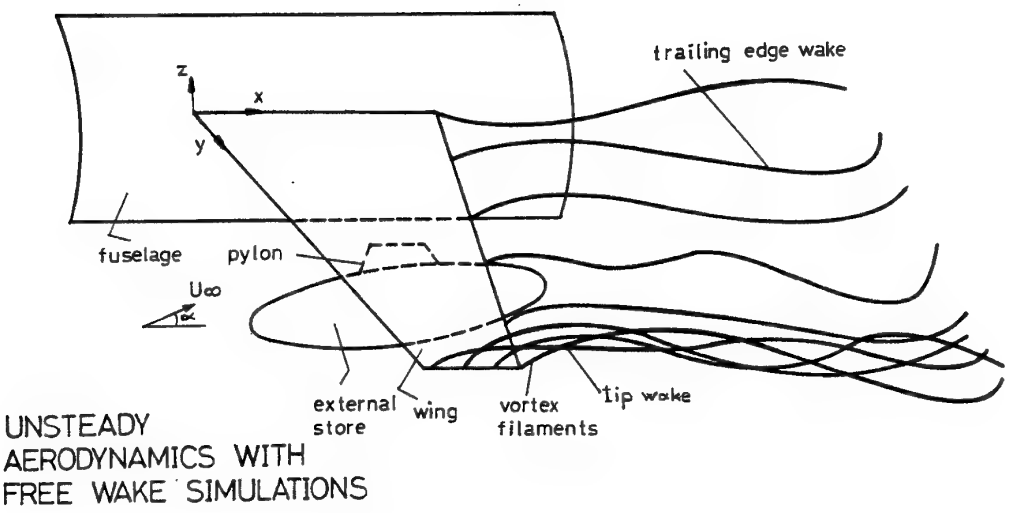

Figure 4.7 Essentials of the steady and unsteady wake models.

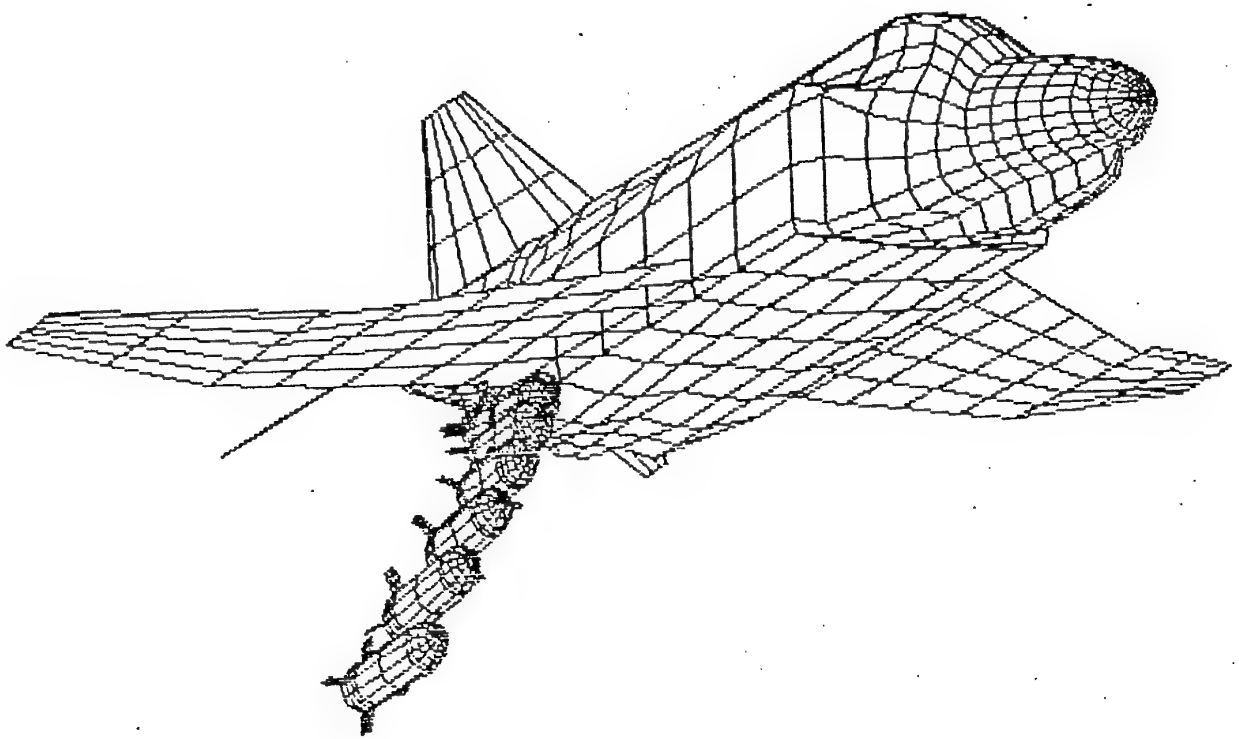

Figure 5.1 Simulation of a generic store seperation under steady flight conditions.

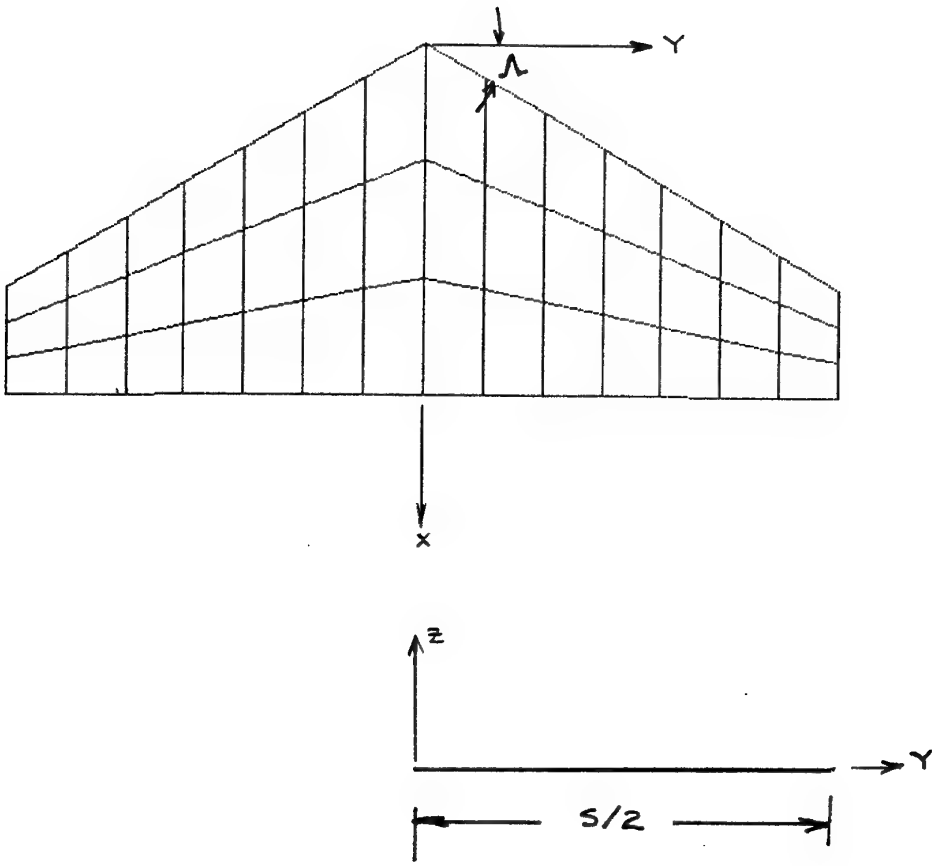

Figure 6.1 Reference Axes information and relevant directions.

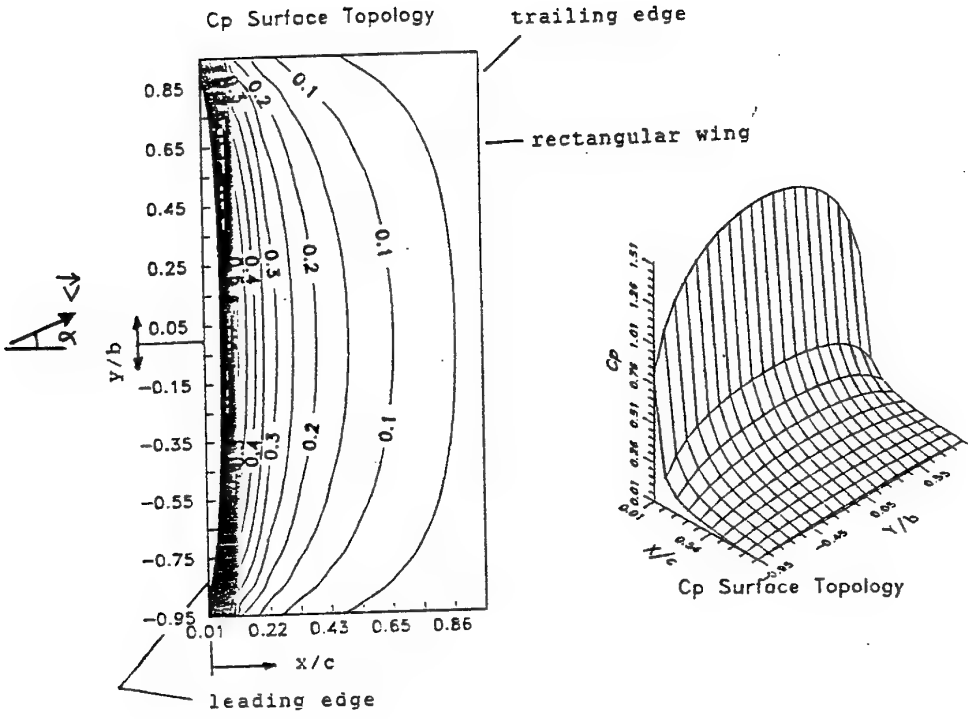

Figure 7.1 Chordwise and spanwise pressure coefficient distribution for thin rectangular wing.

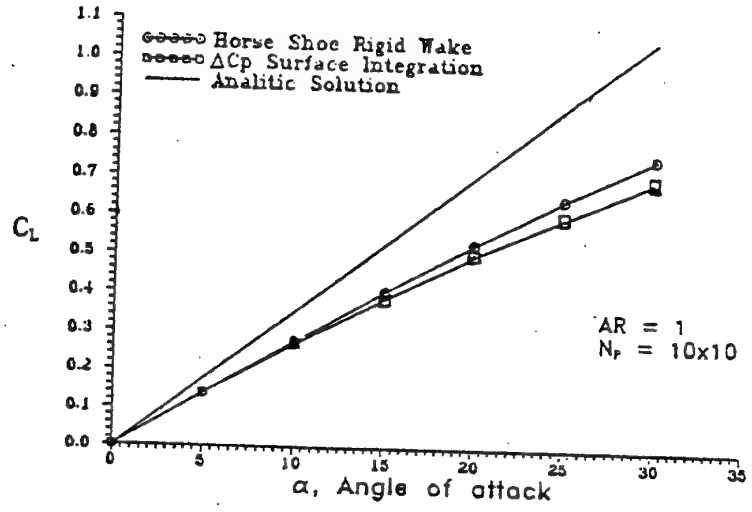

Figure 7.3 Comparison of different computation methods for the prediction of the steady state lift coefficient.

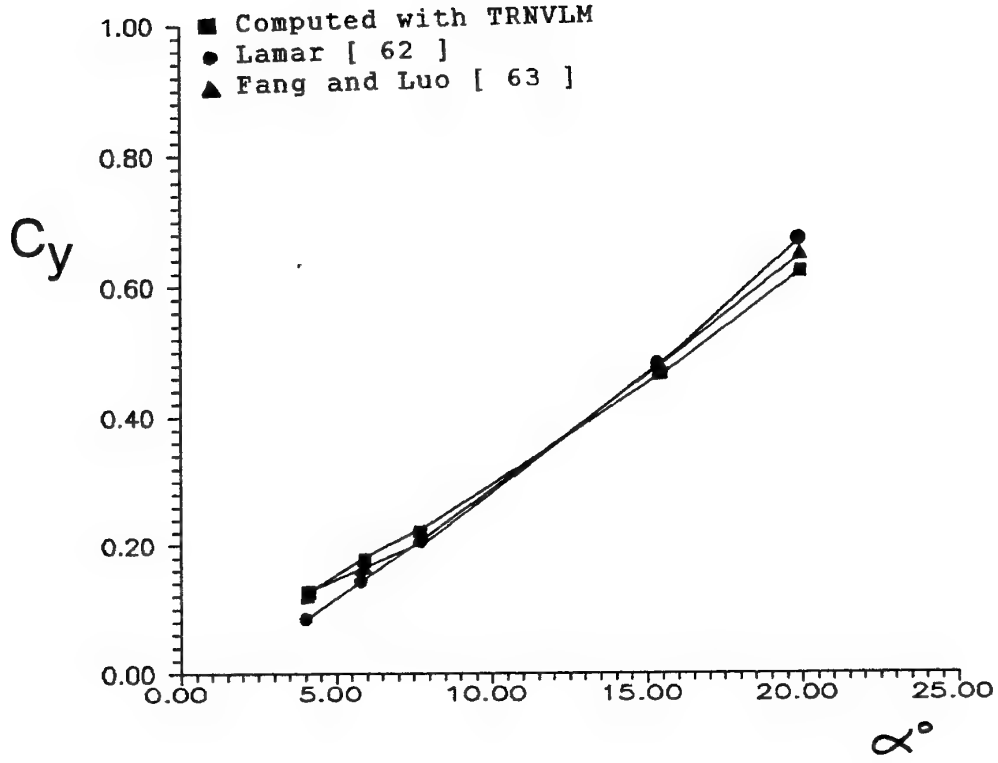

Figure 7.4 Comparison of the results of TRNVLM with the computational results of Fang[61] and the experimental results of Lamar [60]. (-■- Present Results, -▲-Fang's Computational Results, -●- Lamar's Experimental Results)

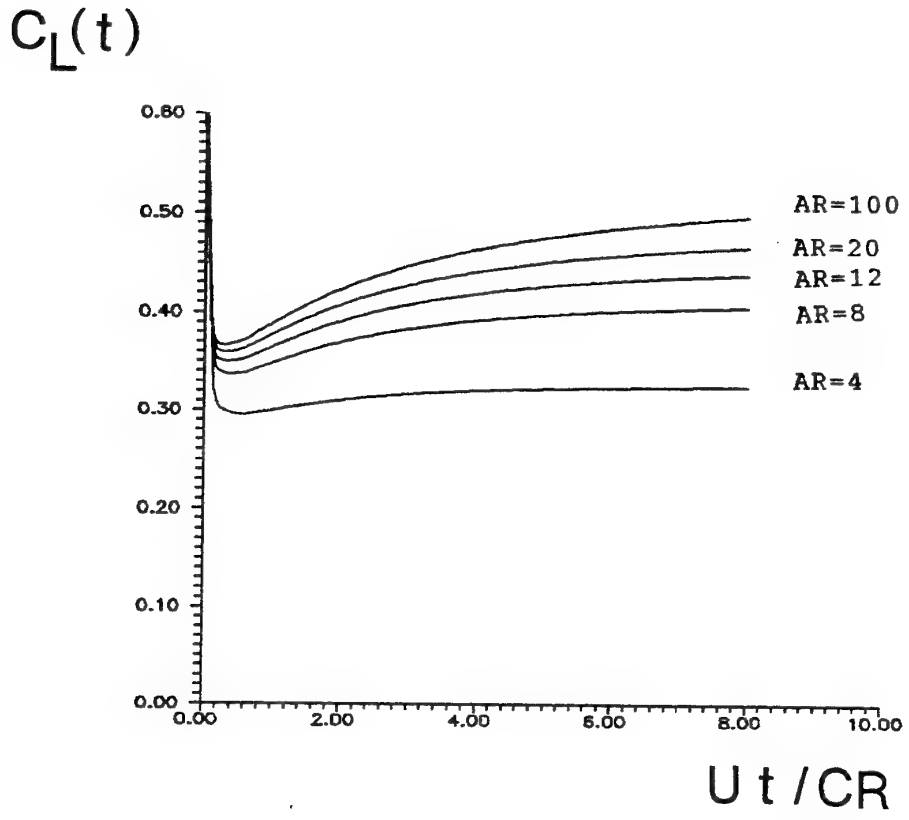

Figure 7.5 Transient lift coefficient variation with time for the thin rectangular wings of different Aspect Ratio that were suddenly set into a constant speed forward flight.

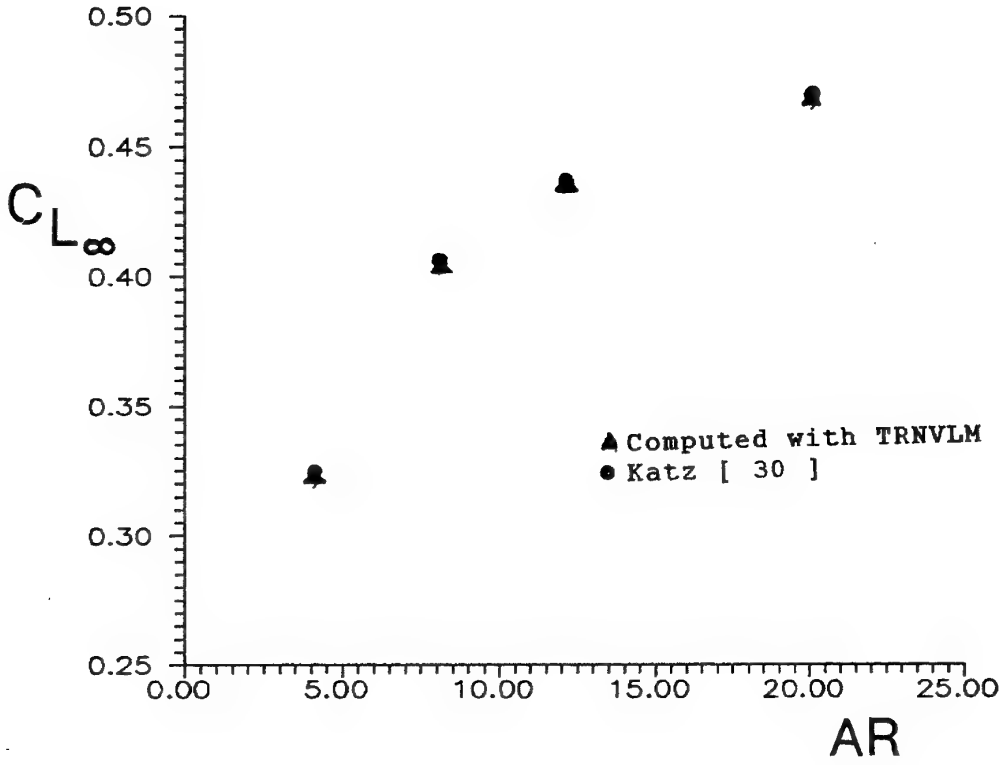

Figure 7.6 Comparison of the predictions of the Katz's [30] Vortex Lattice Computer code with the Predictions of TRNVLM.(—●— Katz's results, —▲— Present results).

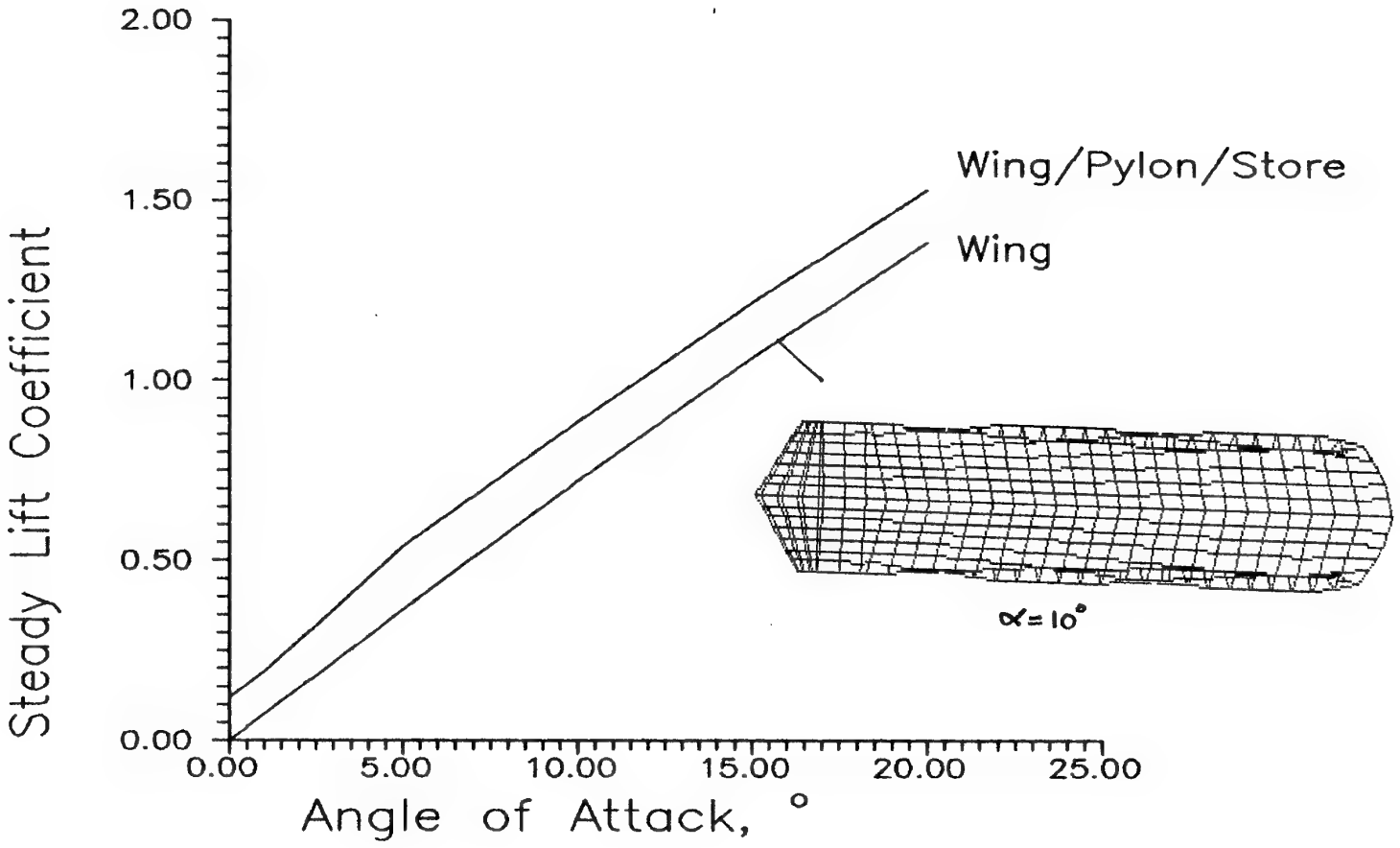

Figure 7.7 Lift coefficient variation as a function of angle of incidence: effect of pylon/store configurations on the lift coefficient.

Figure 7.8 a) Simulation of wake evolution by releasing vortex sheets from the wing's trailing edge. b) Properties of the vortex wake. c) Transient lift coefficient variation.

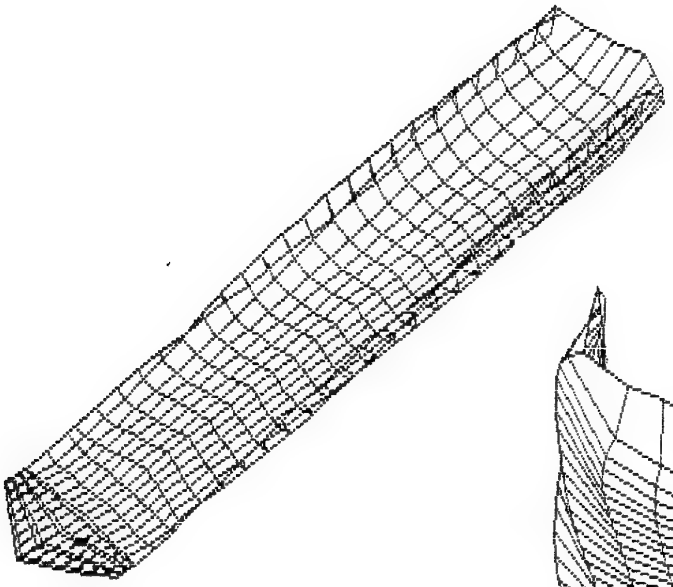

a.

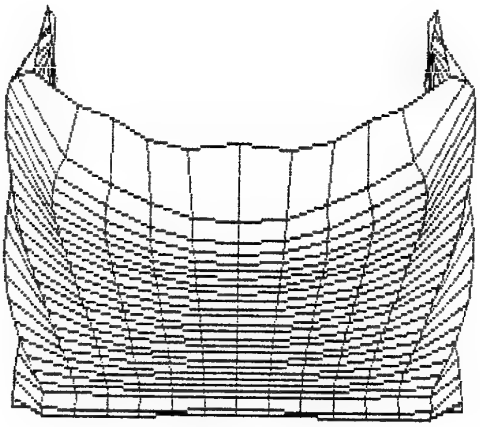

b.

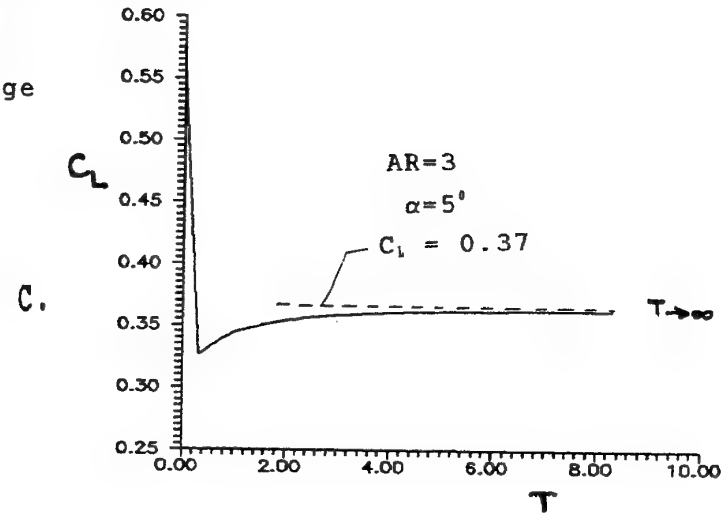

c.

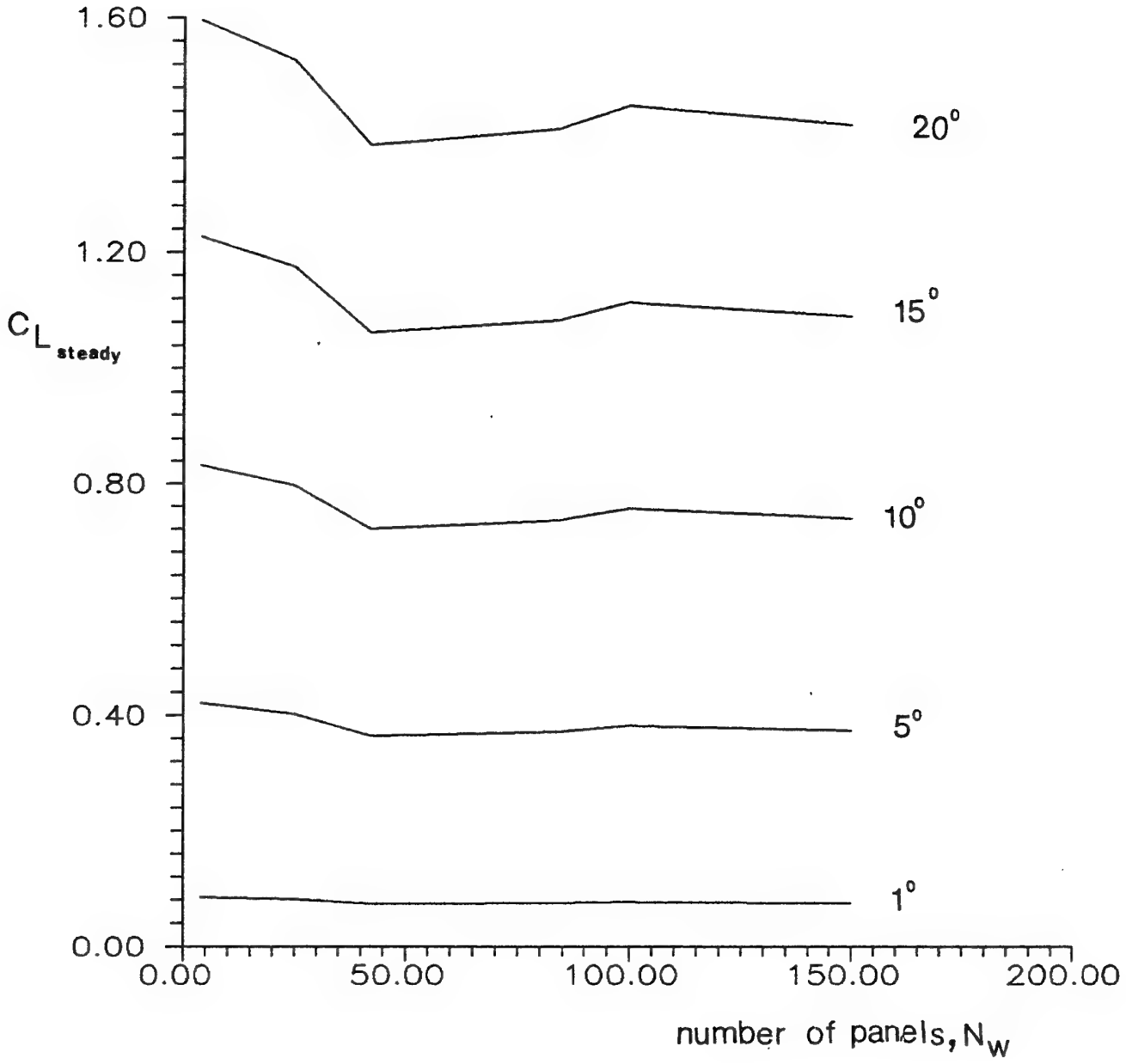

Figure 7.9 Effect of vortex ring density on the computed steady lift coefficient.

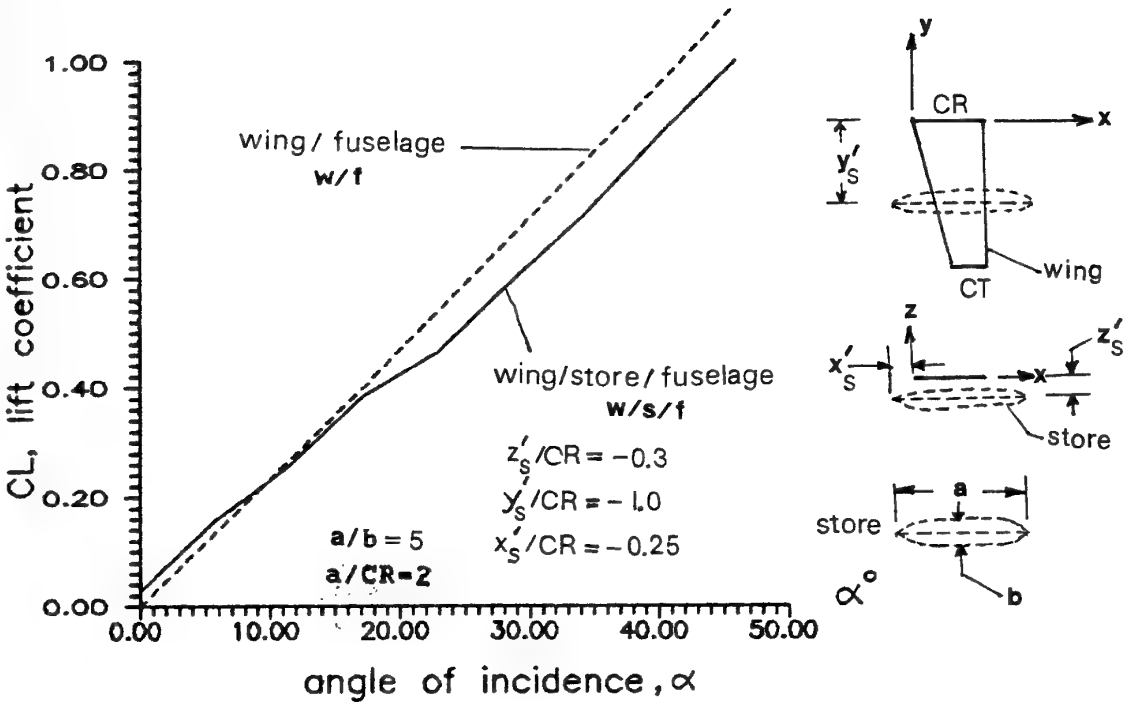

Figure 7.10 Computed lift curves for the wing/ fuselage configuration with and without external store.

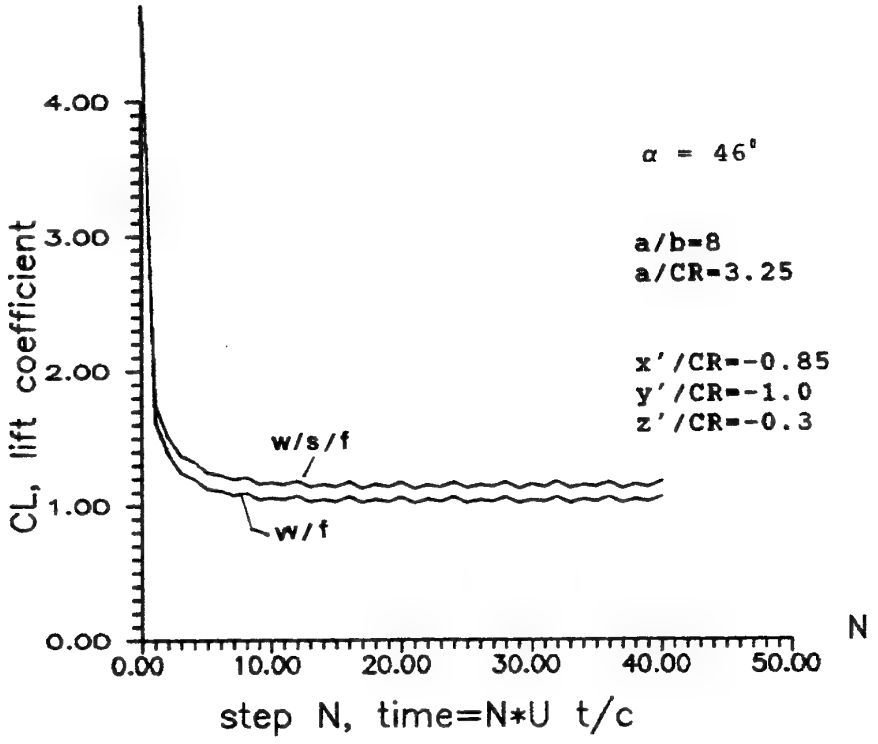

Figure 7.11a Comparison of the transient lift coefficient variation with time for the research geometries that were suddenly set into a constant speed forward flight.

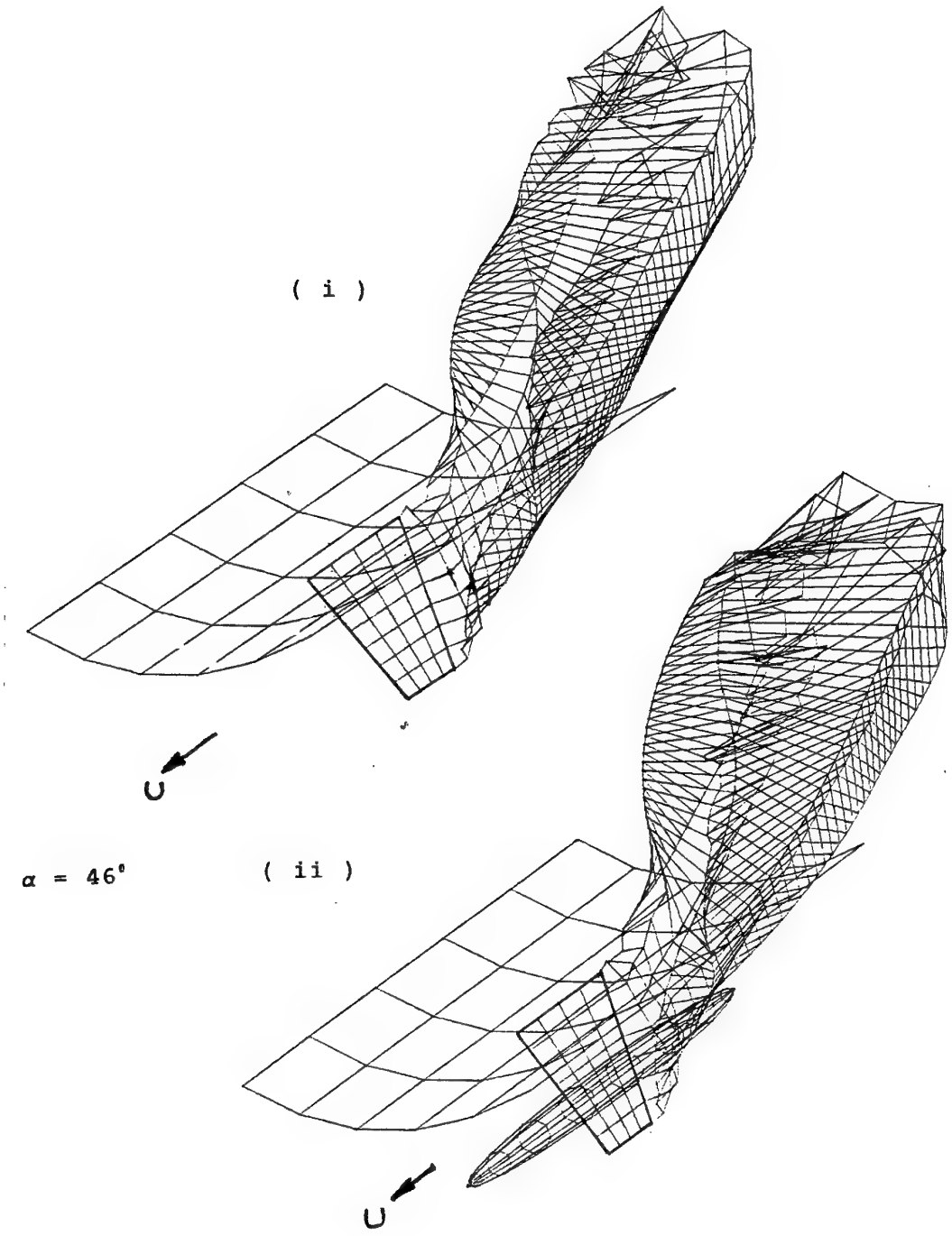

Figure 7.11b Simulation of the wake evolution by releasing vortex sheets from separation edges i) wing /fuselage combination ii) wing/ fuselage/ store combination

$\alpha=20^{\circ}$

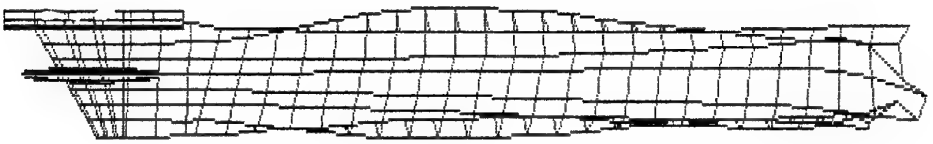

$\alpha=10^{\circ}$

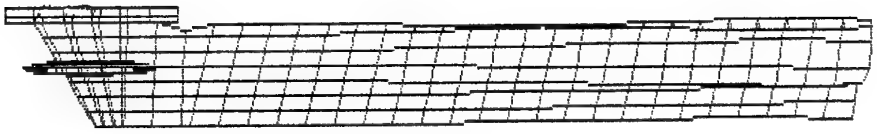

$\alpha=0^{\circ}$

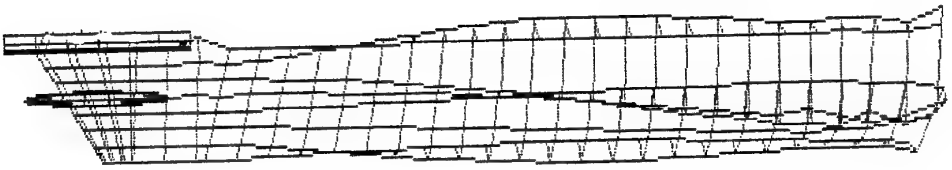

$\alpha=-10^{\circ}$

$\alpha=-20^{\circ}$

Figure 7.12 Computed shapes of separated trailing edge vortex wake structures behind the research configuration:effect of angle of incidence.

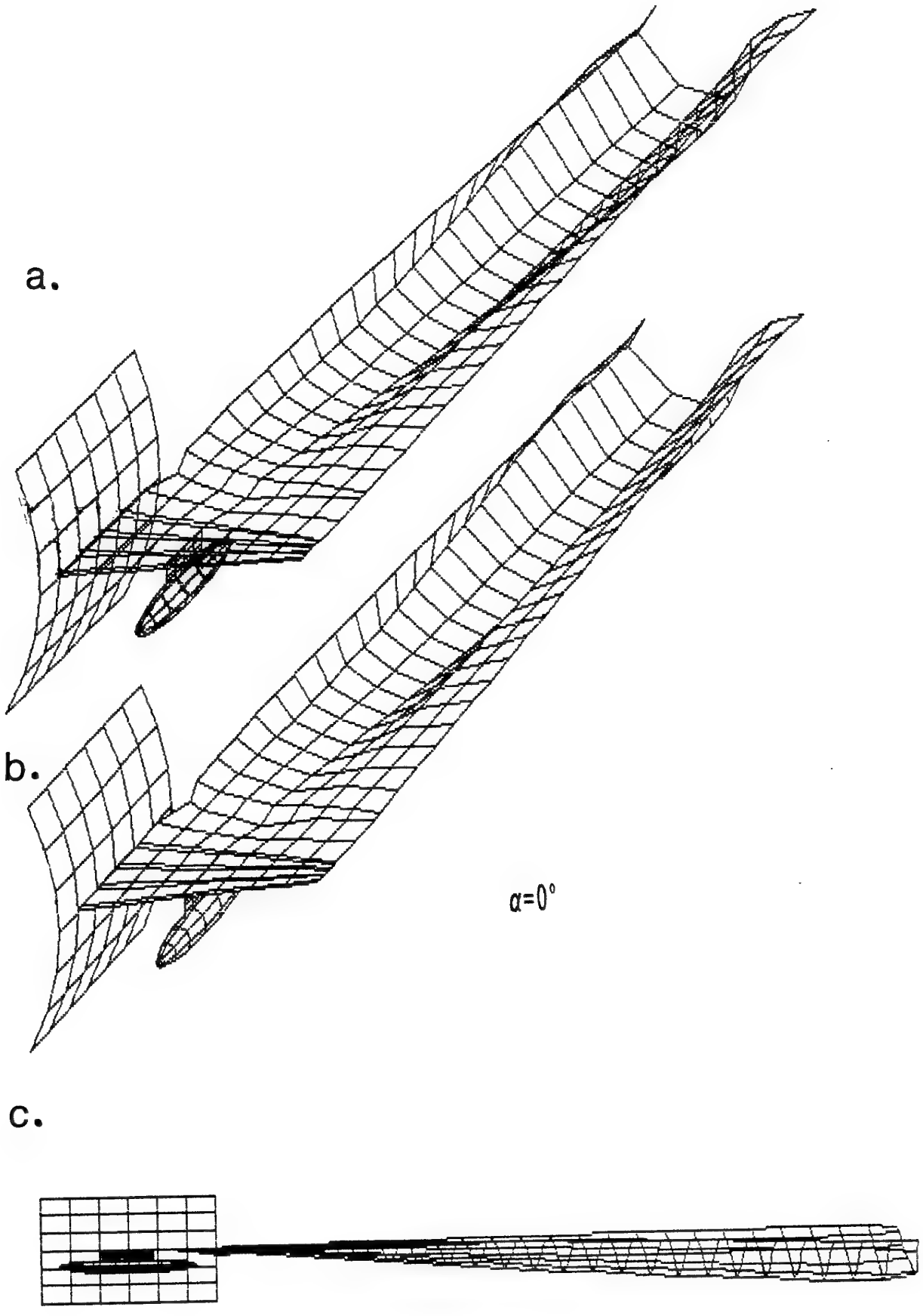

Figure 7.13

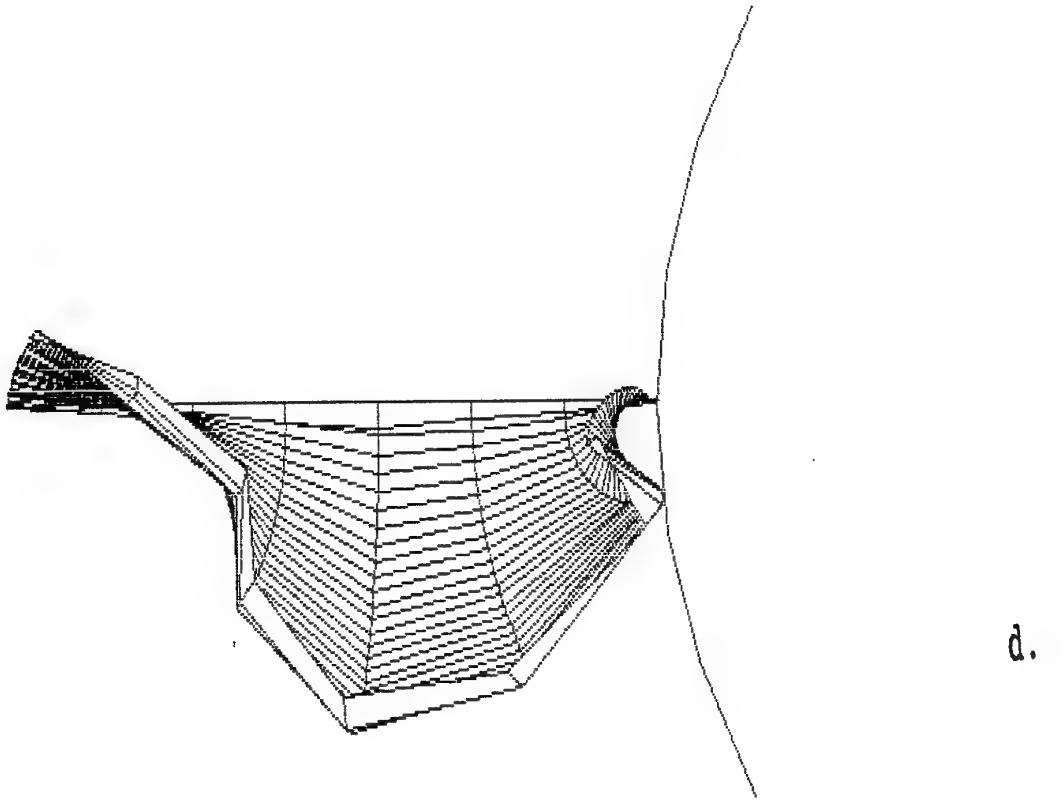

d.

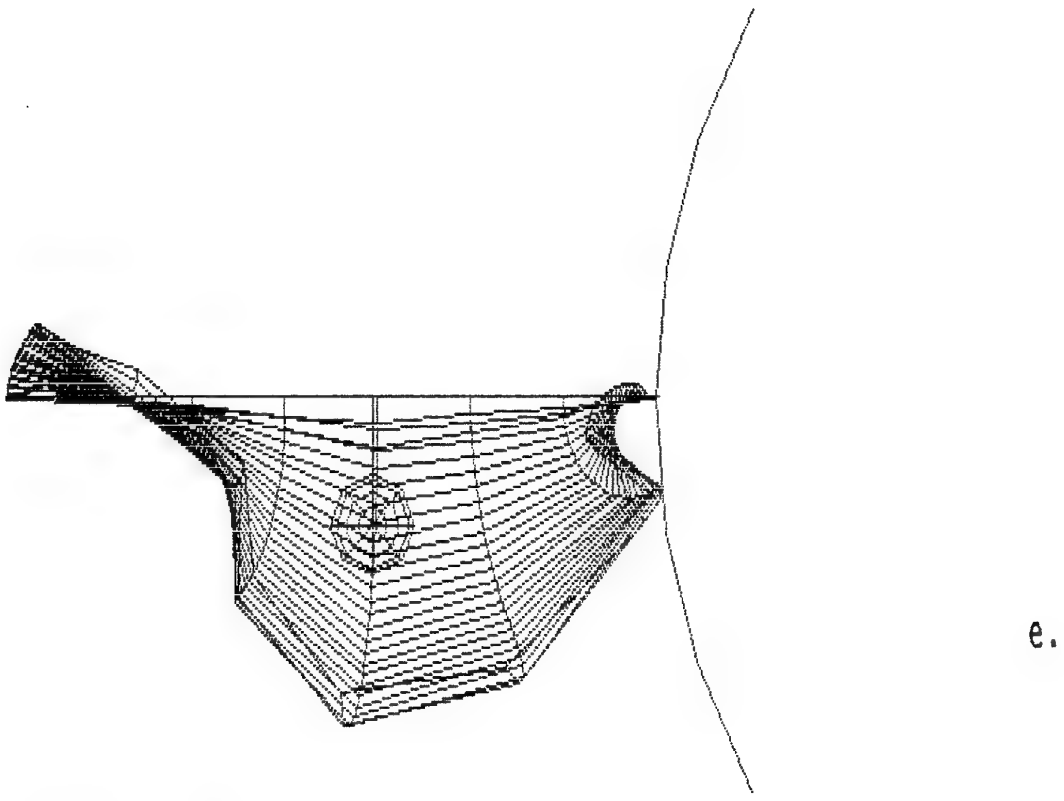

e.

Figure 7.13

Computed shape of a vortex wake structure behind the wing/ fuselage/ pylon/ store a) wire diagram representation b) representation with hidden surfaces and lines c) side view of the wake roll-up d) rear view of the wake with hidden surfaces e) rear view of the wake with wire diagram.

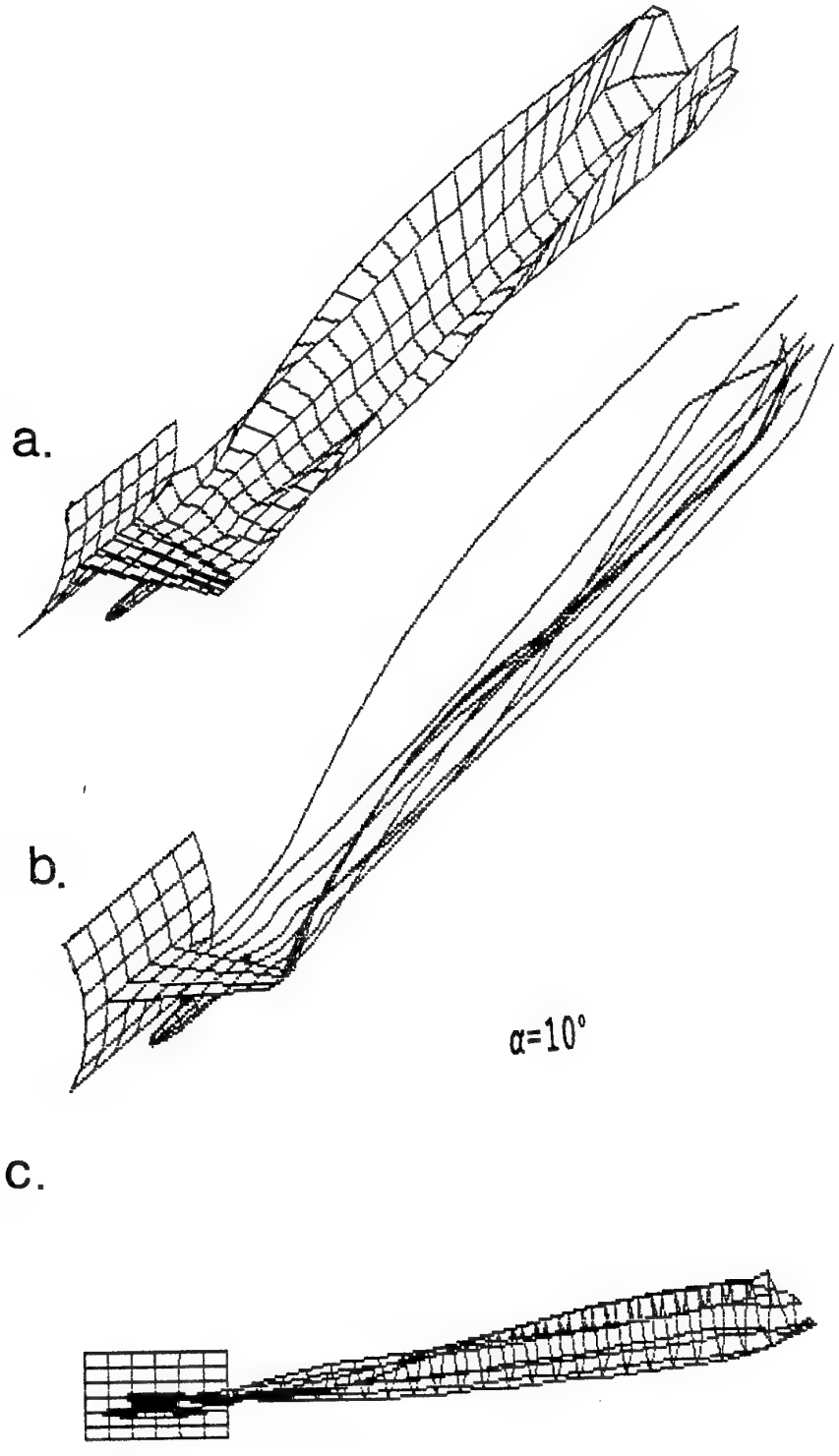

Figure 7.14

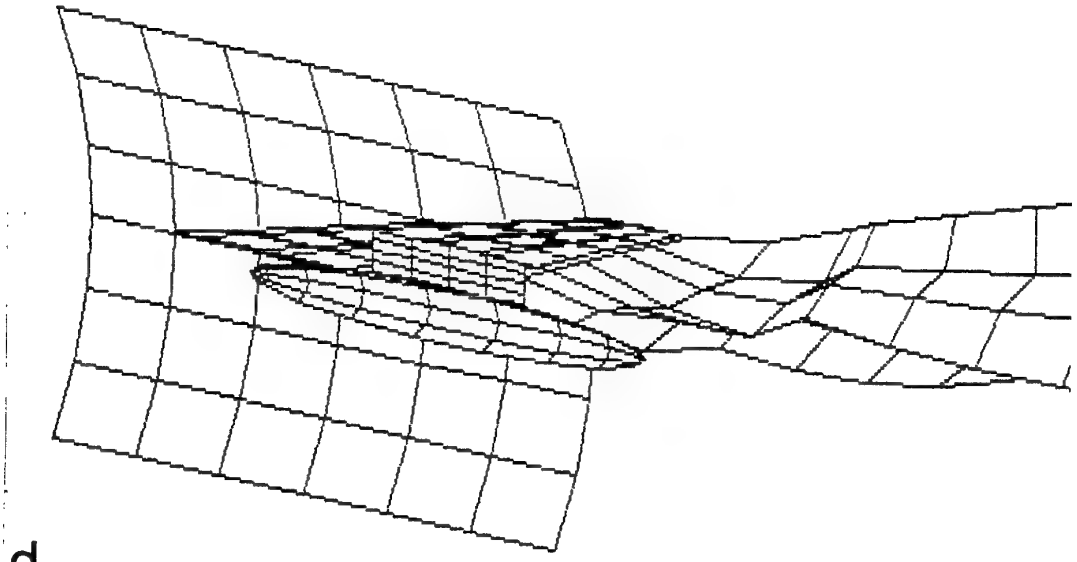

d.

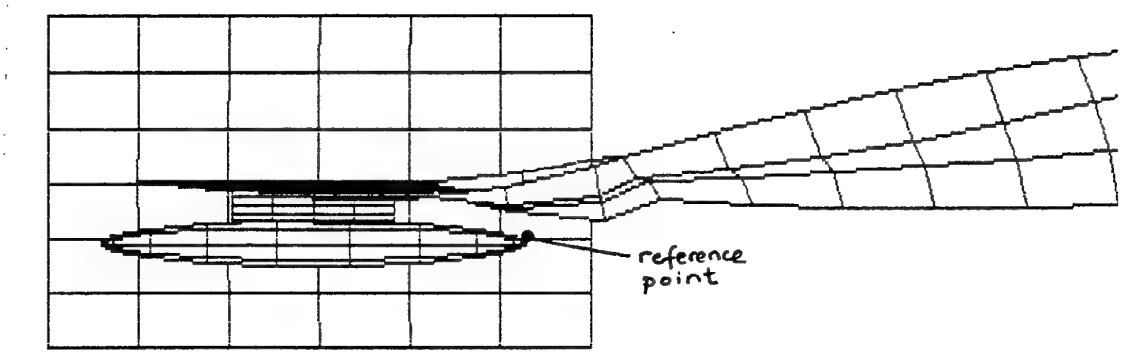

e.

Figure 7.14

Computed shape of a vortex wake structure behind the wing/ fuselage/ pylon/ store a) perspective hidden surface view of the vortex wake evolution b) representation of the wake with vortex filaments c) side view of the wake roll-up d) details of the near wake from different point of visualization e) side view of the near wake and deformation of the wake structure.

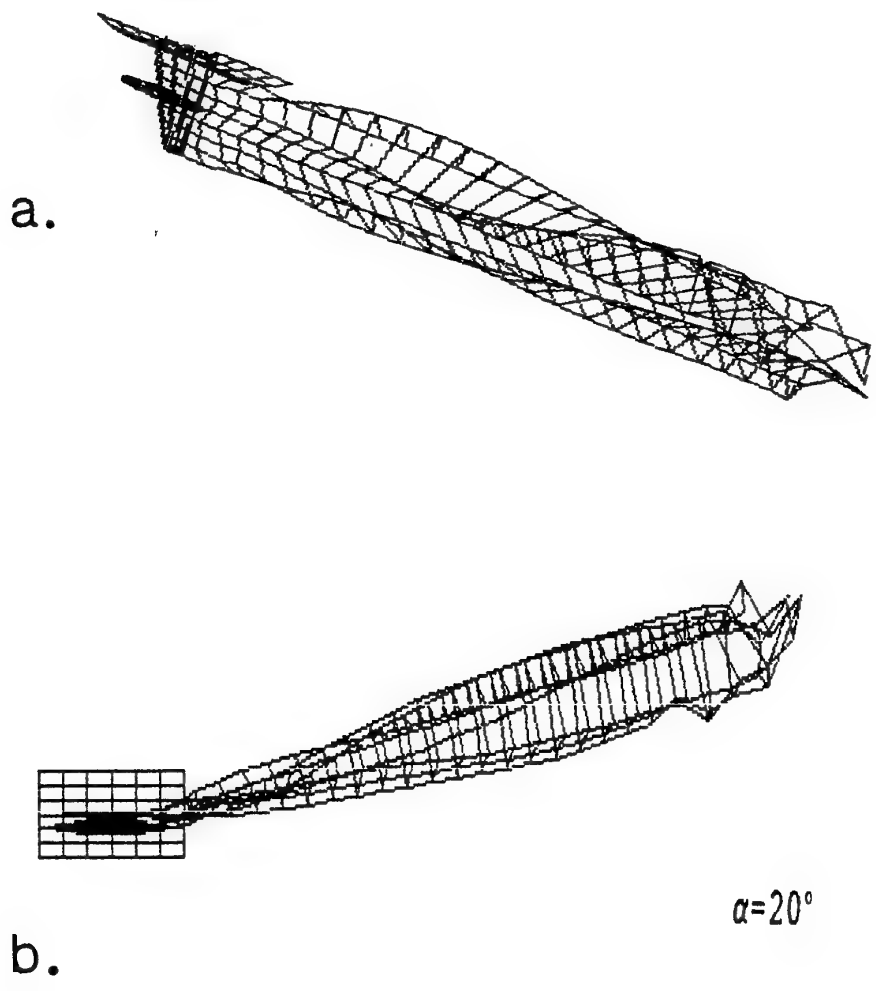

Figure 7.15

Computed shape of a vortex wake structure behind the wing/ fuselage/ pylon/ store a) perspective view of the vortex wake evolution formation of secondary roll-up with the influence of external store b) side view of the wake roll-up c) details of the near wake from different point of visualization:deformation of the wake structure.

C.

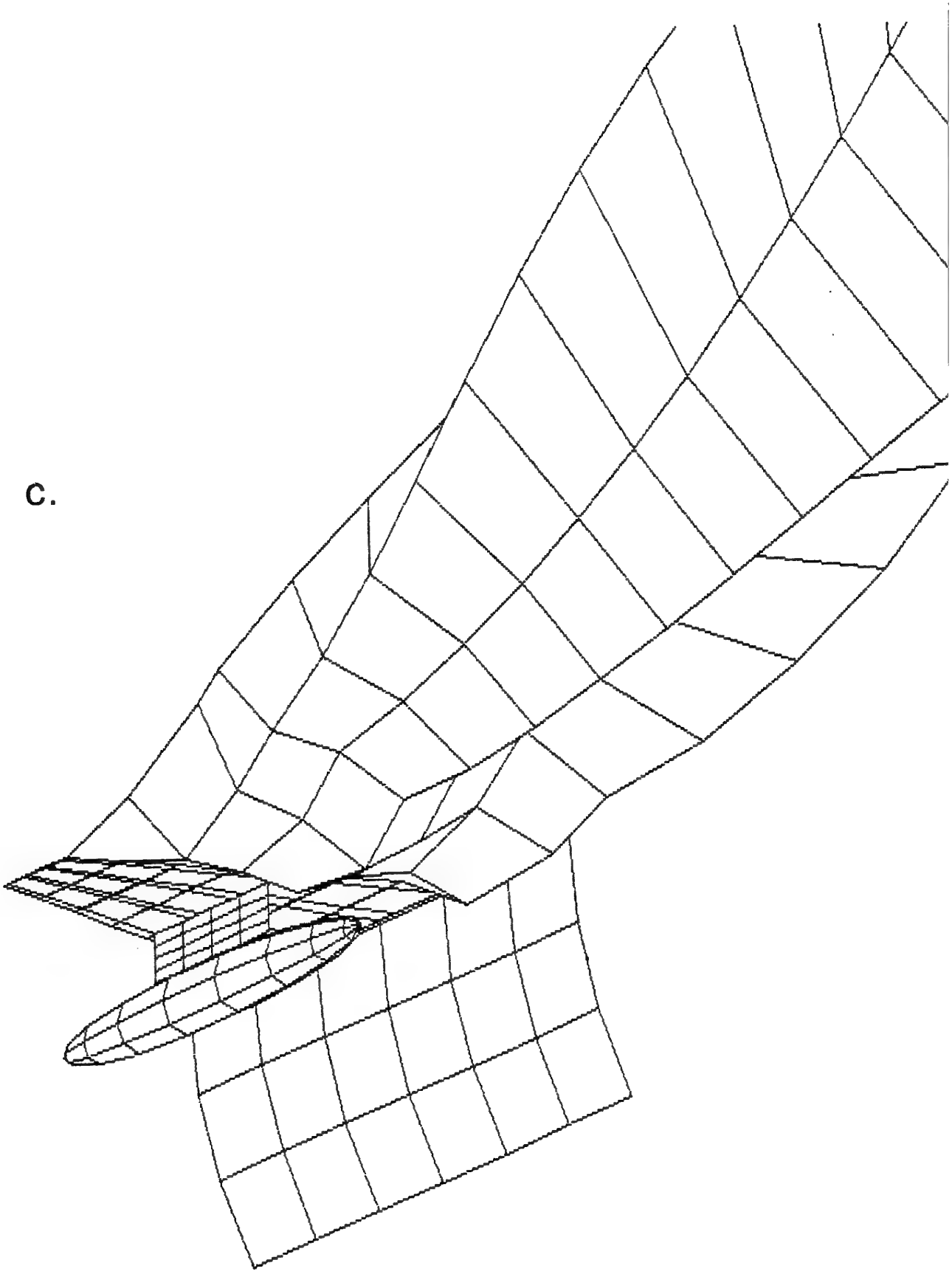

Figure 7.15

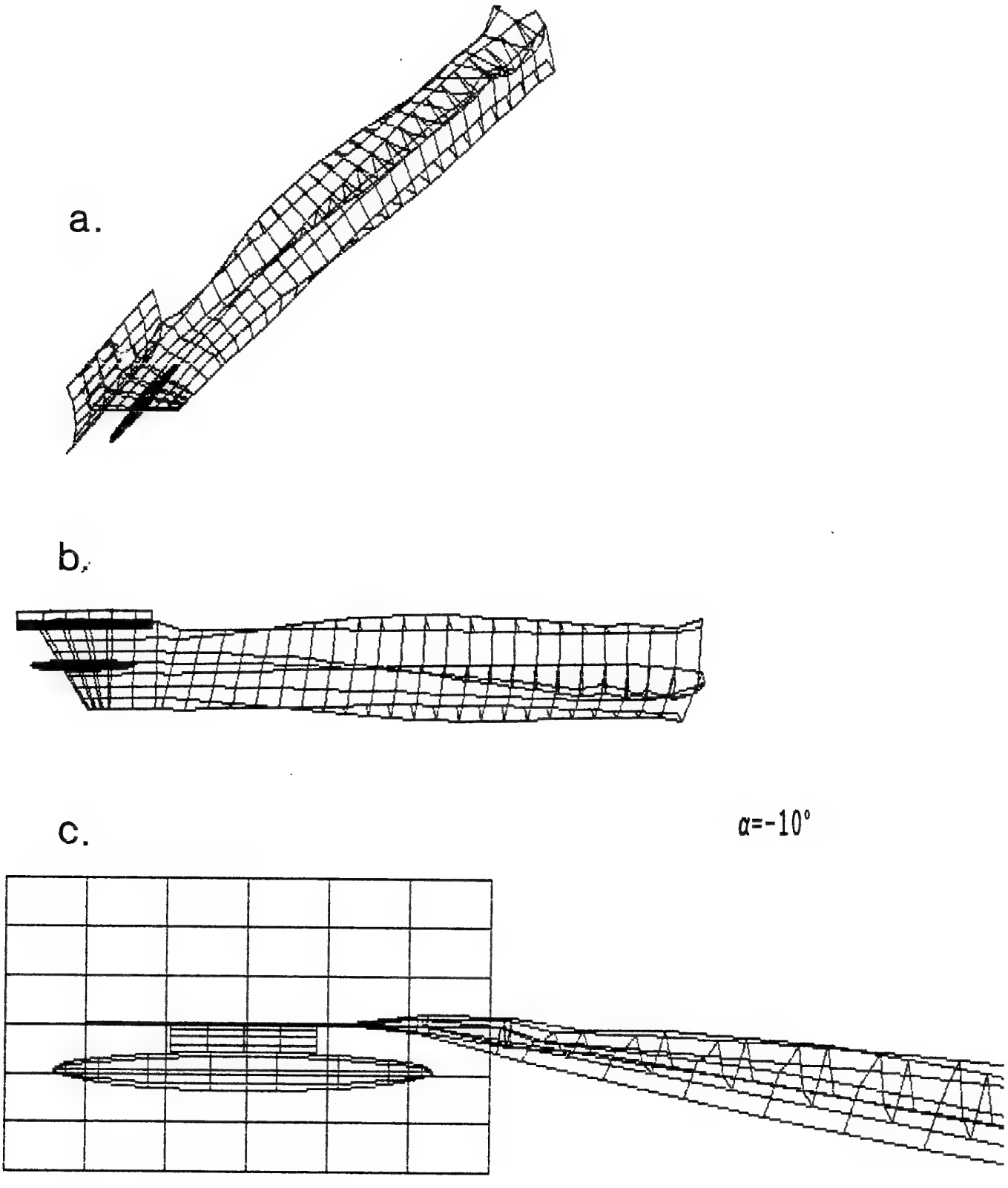

Figure 7.16

Computed shape of a vortex wake structure behind the wing/ fuselage/ pylon/ store a) perspective view of the vortex wake evolution formation of secondary roll-up with the influence of external store b) top view of the vortex wake c) side view of the wake roll-up.

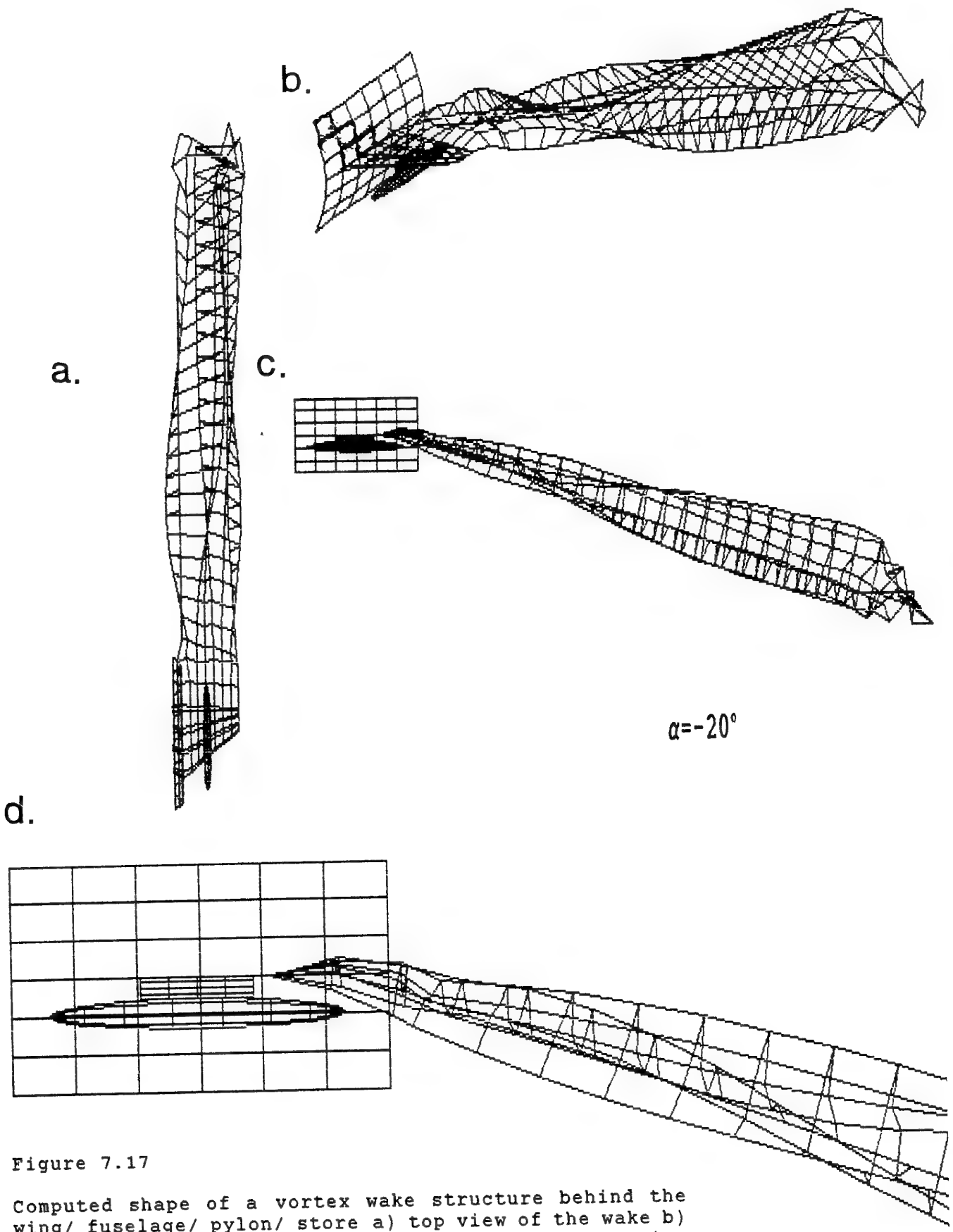

Figure 7.17

Computed shape of a vortex wake structure behind the wing/ fuselage/ pylon/ store a) top view of the wake b) perspective view of the vortex wake evolution formation of secondary roll-up with the influence of external store c) side view of the wake roll-up d) details of the near wake deformation.

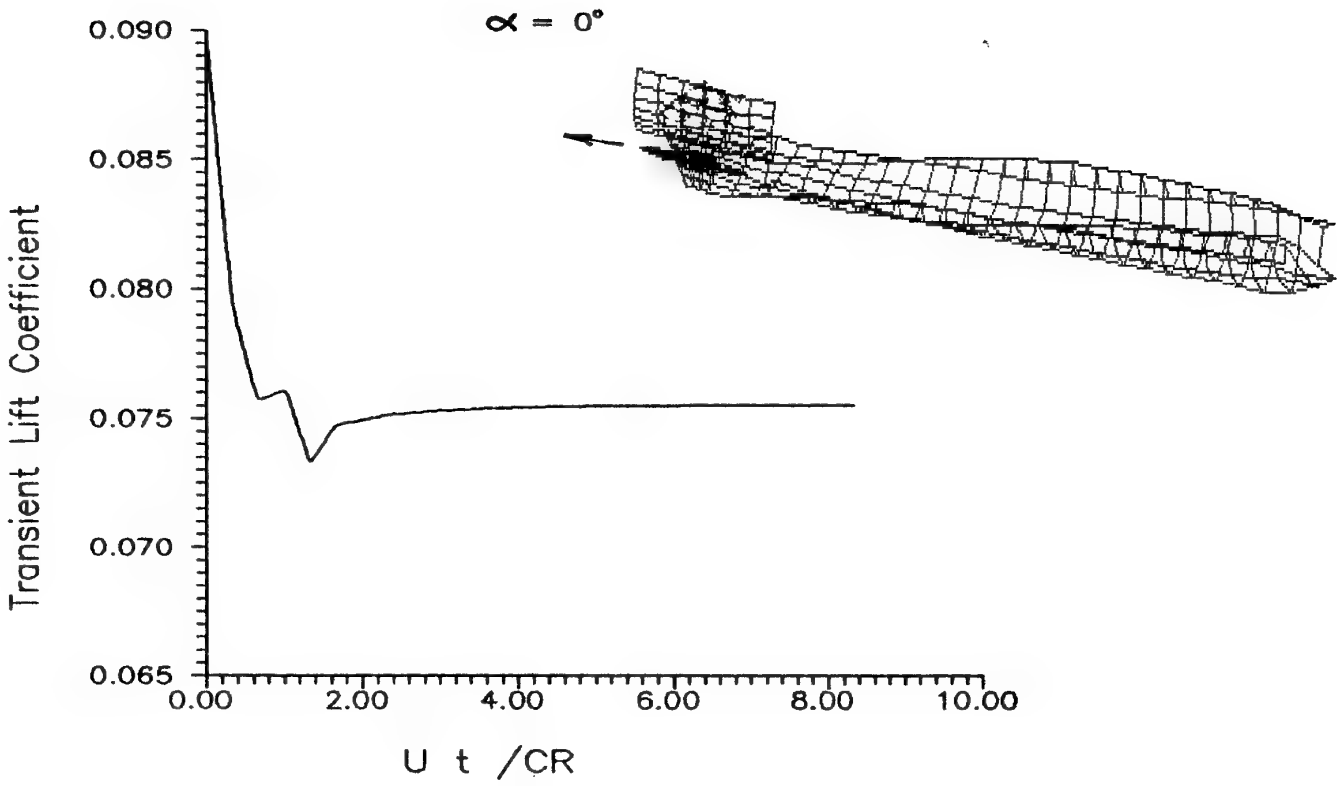

Figure 7.18 Transient lift of the wing that was suddenly set into forward motion (without tip separation).

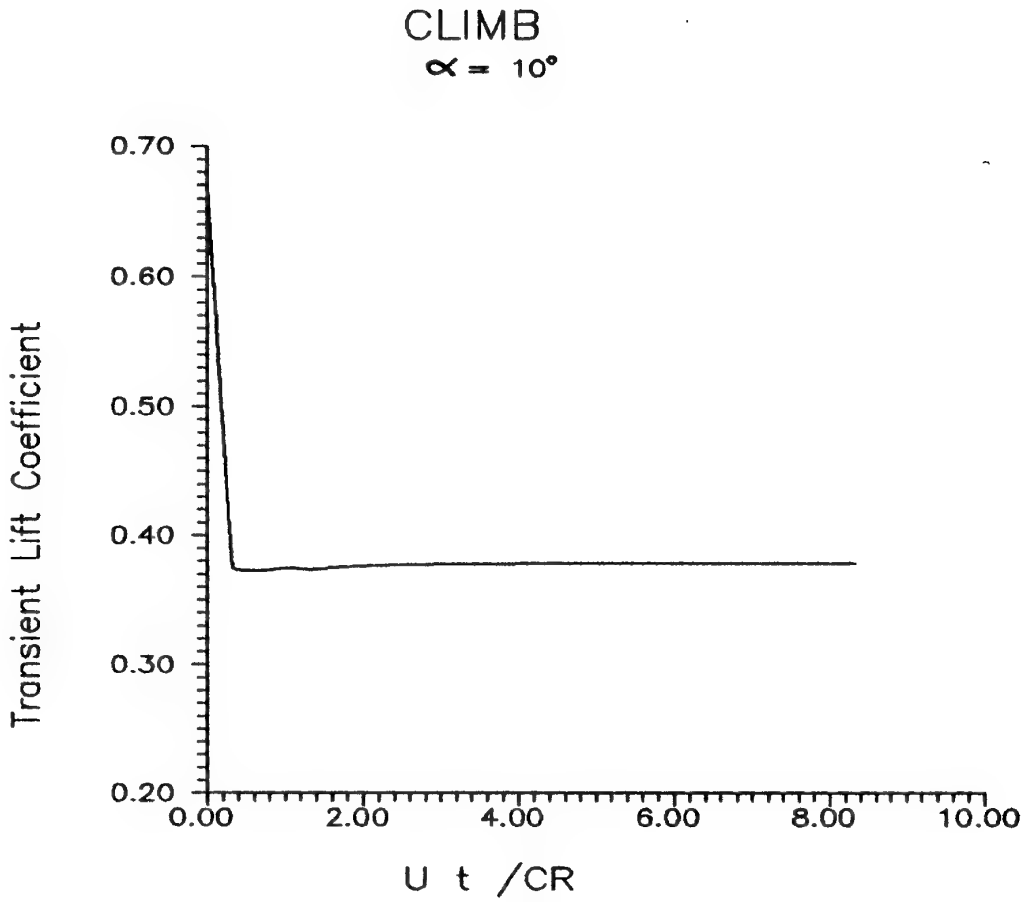

Figure 7.19 Transient lift of the wing that was suddenly set into forward climb motion (without tip separation).

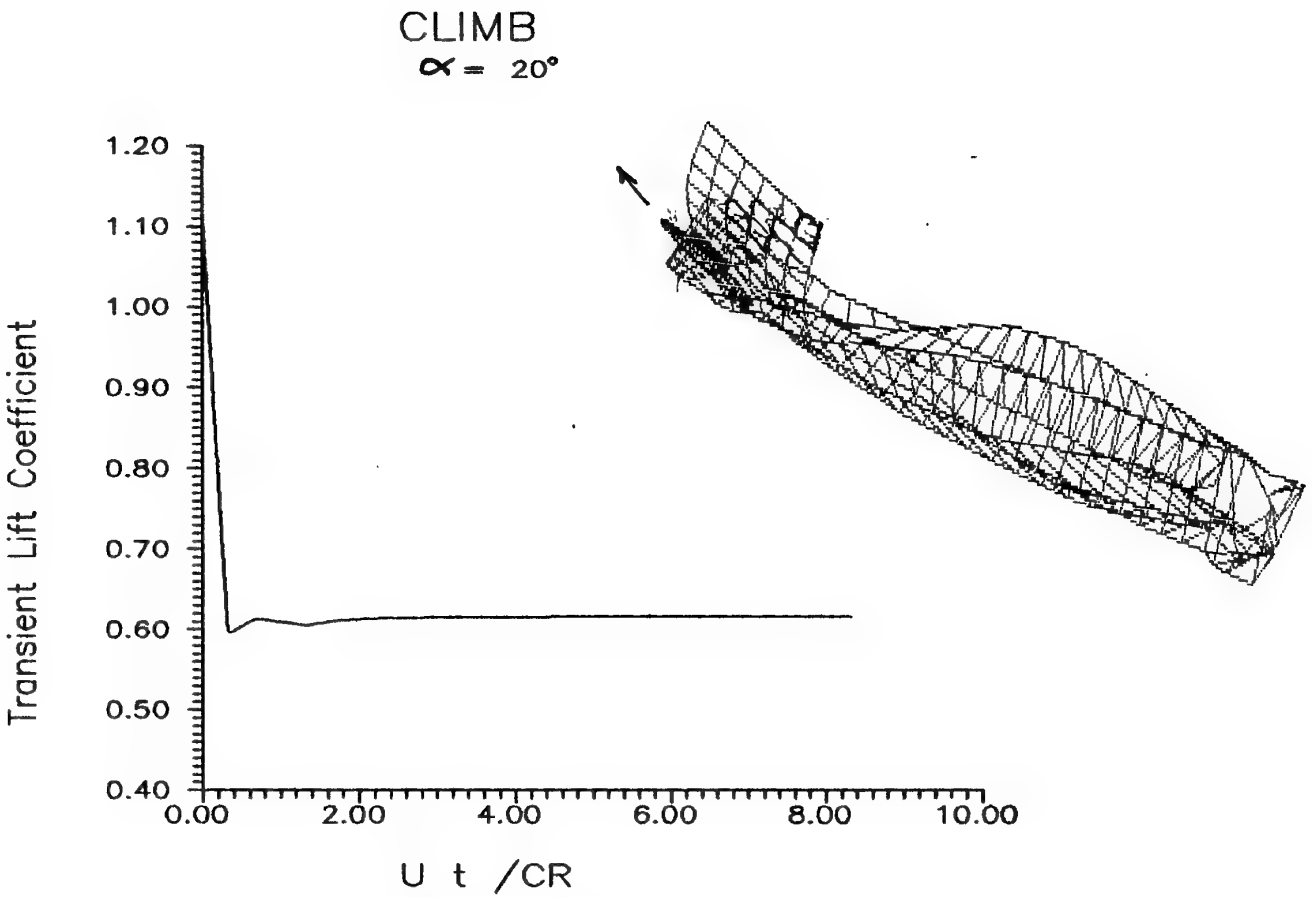

Figure 7.20 Transient lift of the wing that was suddenly set into forward climb motion (without tip separation).

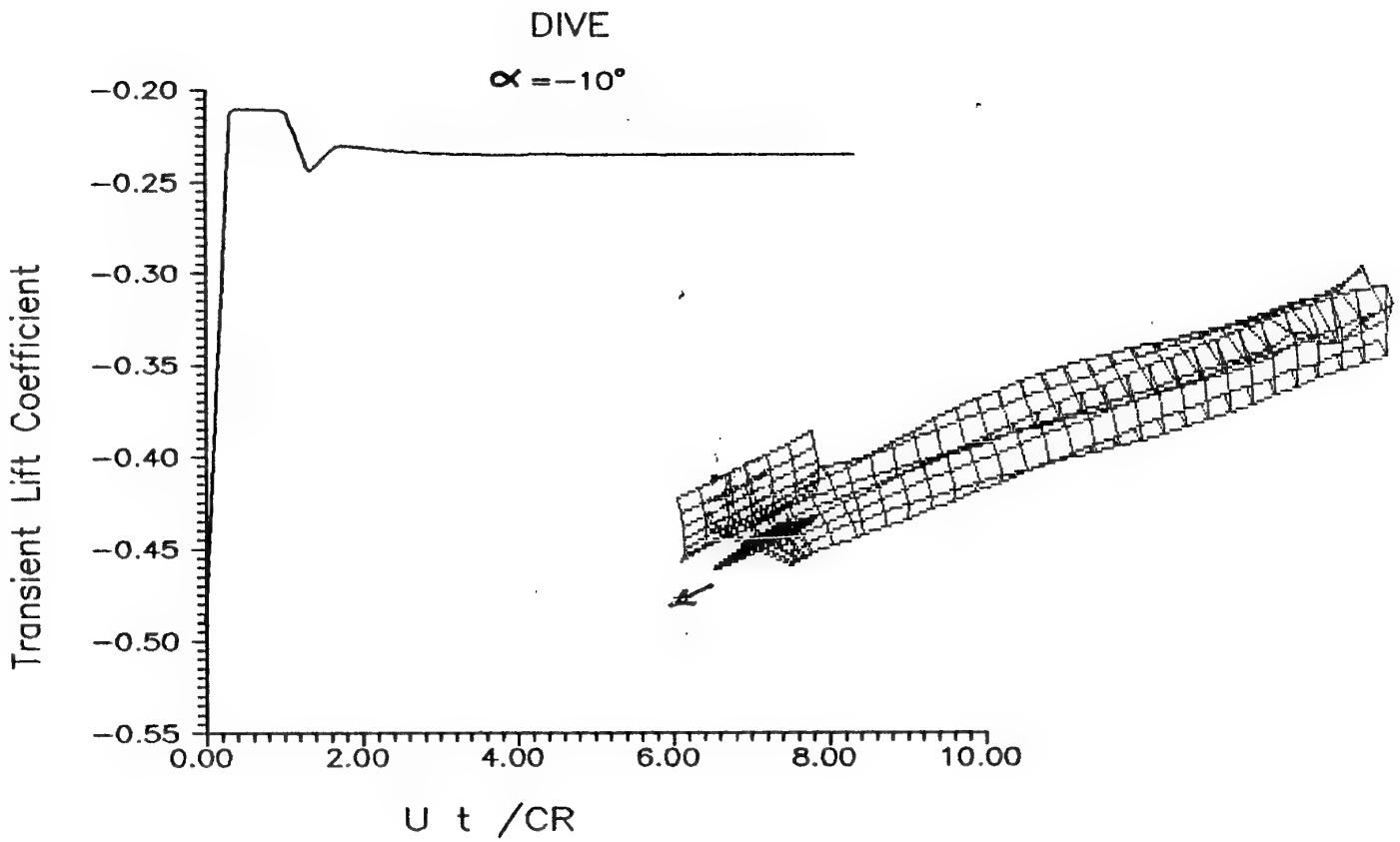

Figure 7.21 Transient lift of the wing that was suddenly set into forward dive motion (without tip separation).

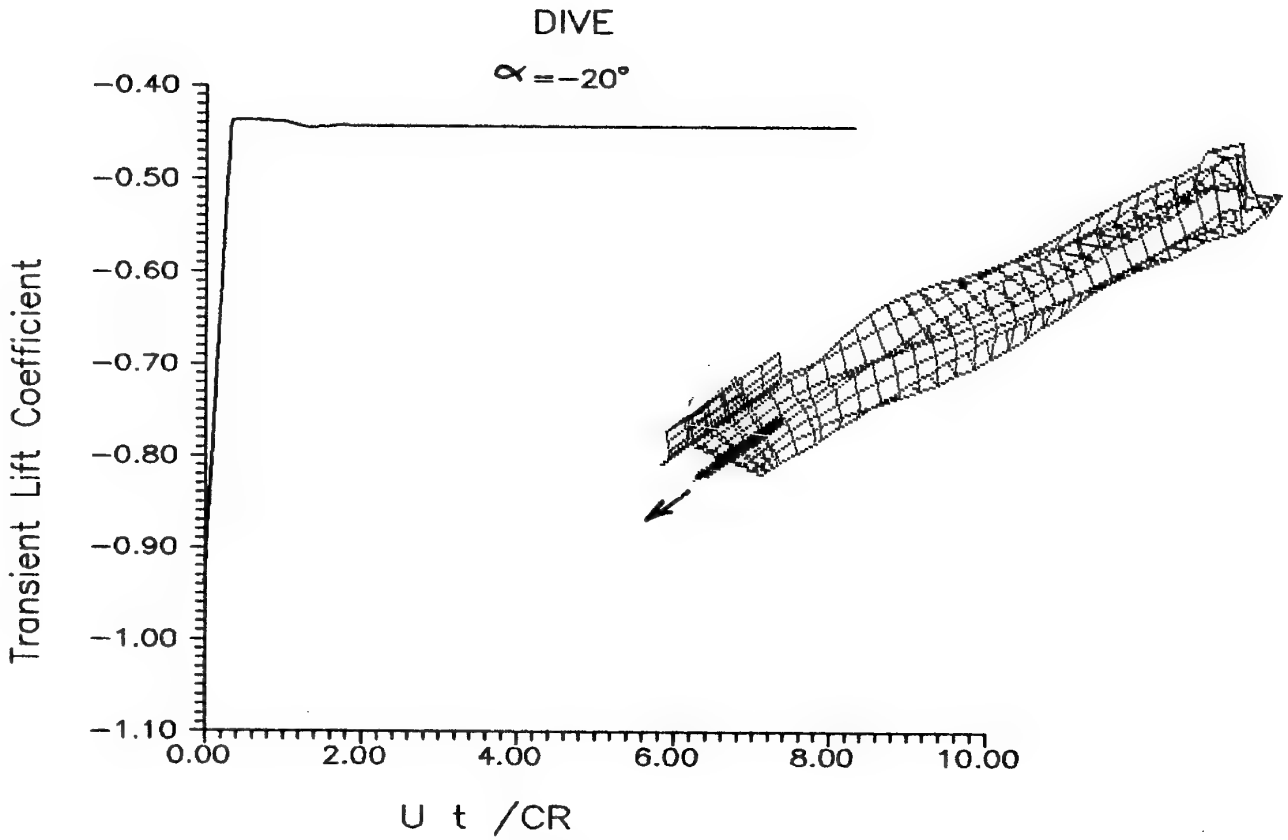

Figure 7.22 Transient lift of the wing that was suddenly set into forward dive motion (without tip separation).

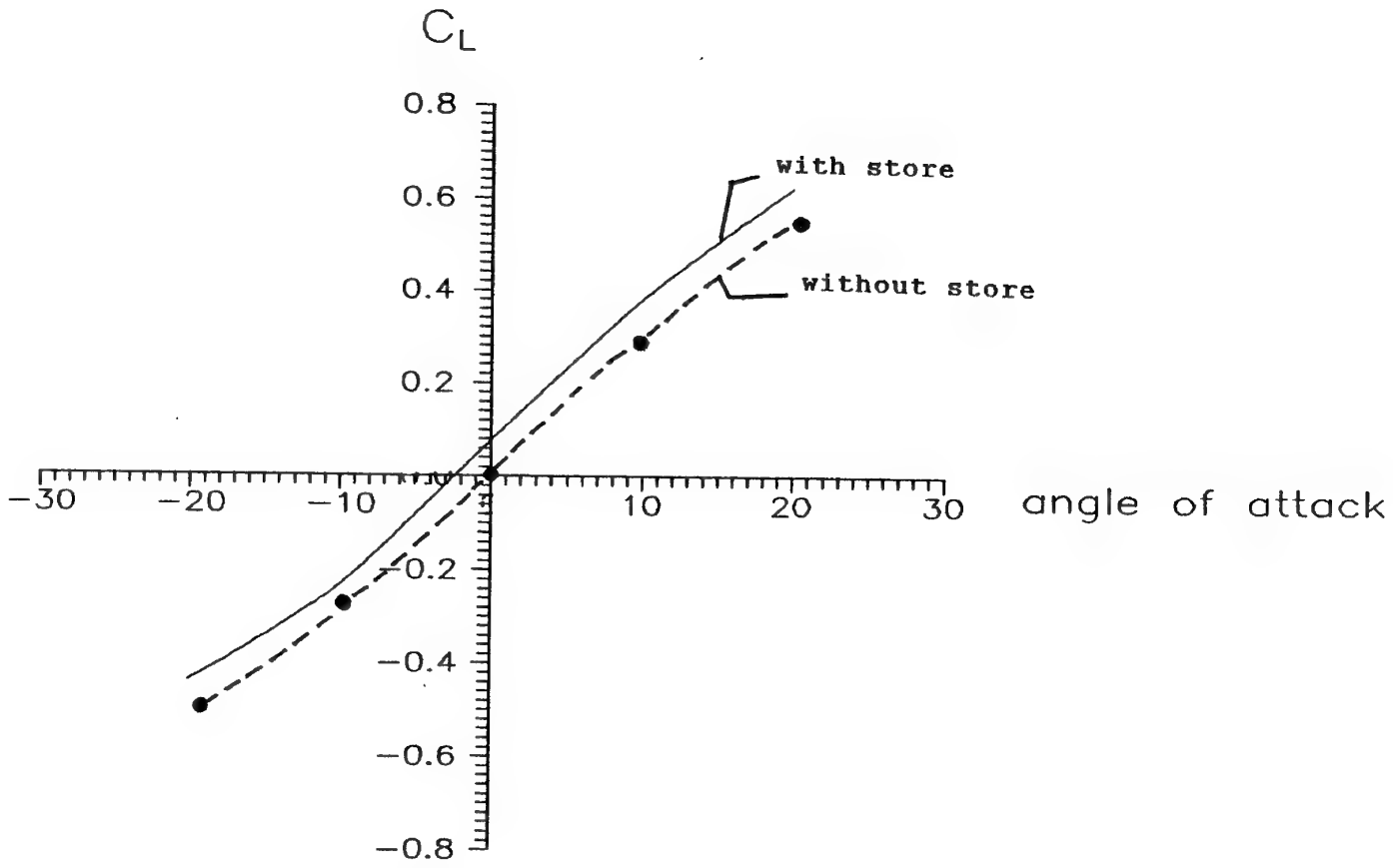

Figure 7.23 Variation of wing lift force with angle of attack.

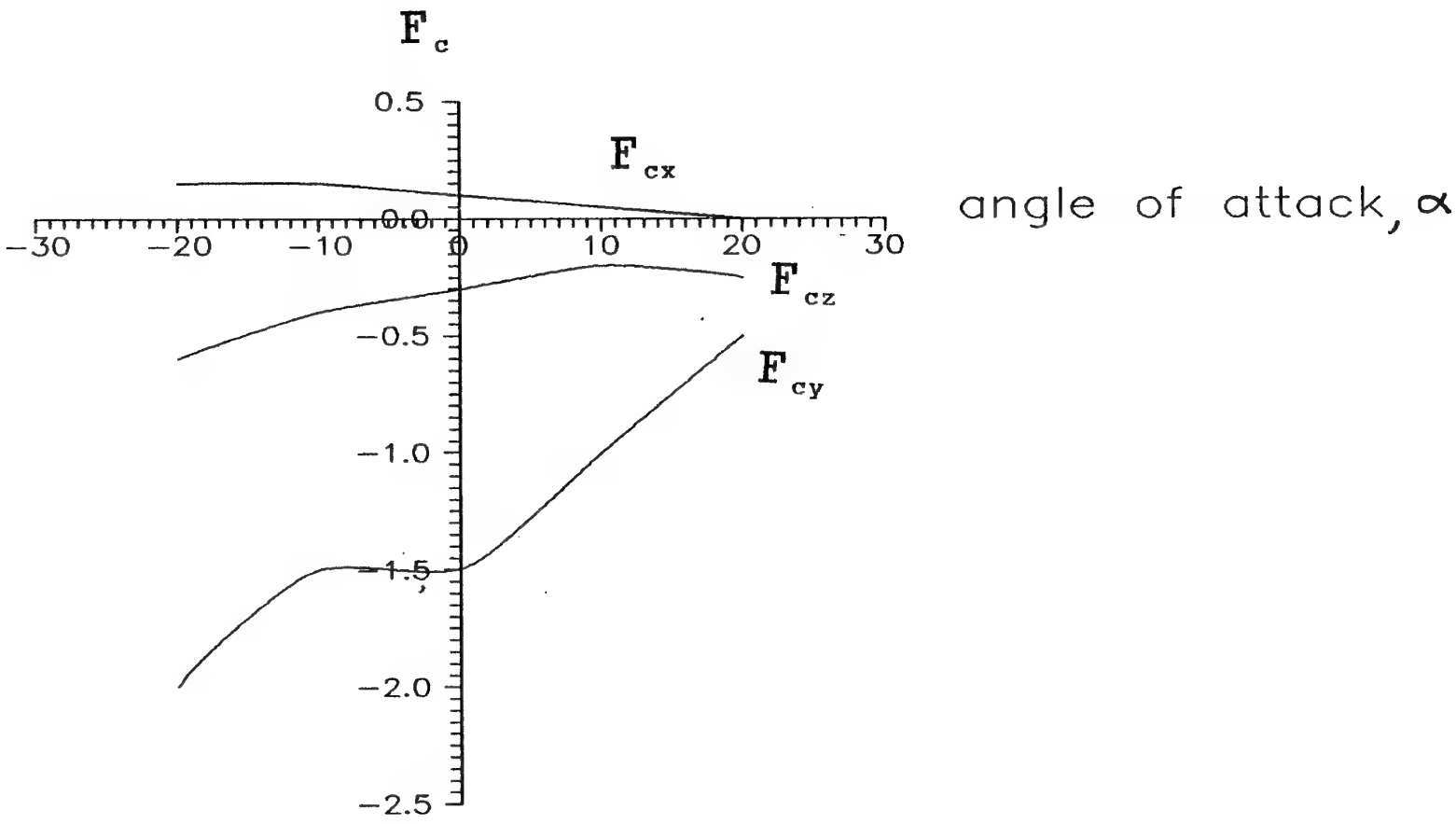

Figure 7.24 Variation of external store force components with angle of attack

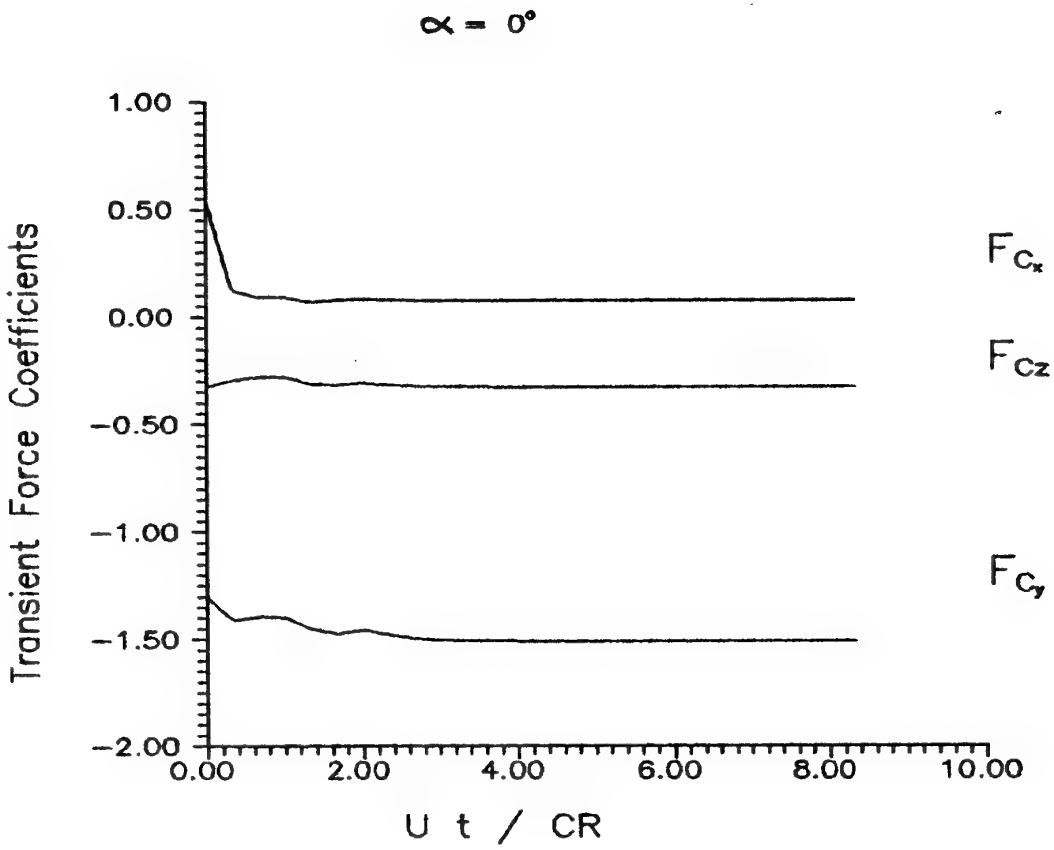

Figure 7.25 Transient force components of the underwing external store that was suddenly set into forward motion.

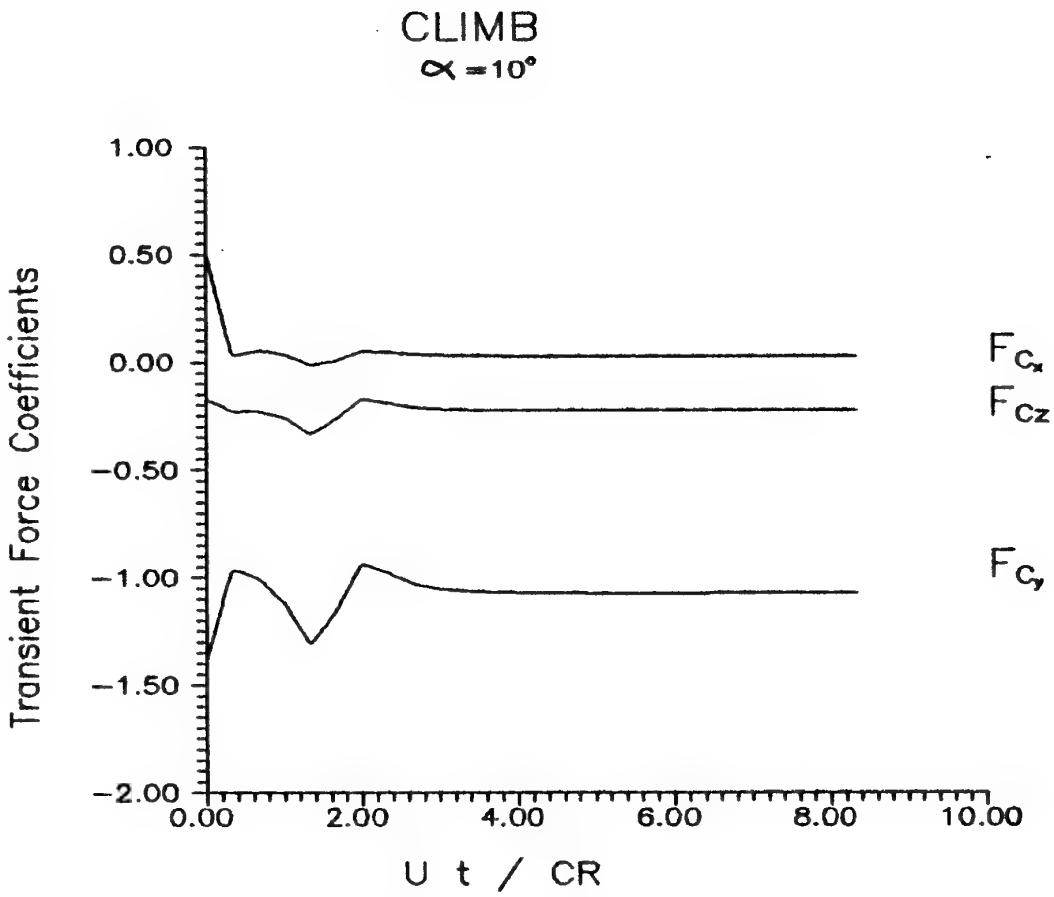

Figure 7.26 Transient force components of the underwing external store that was suddenly set into forward motion.

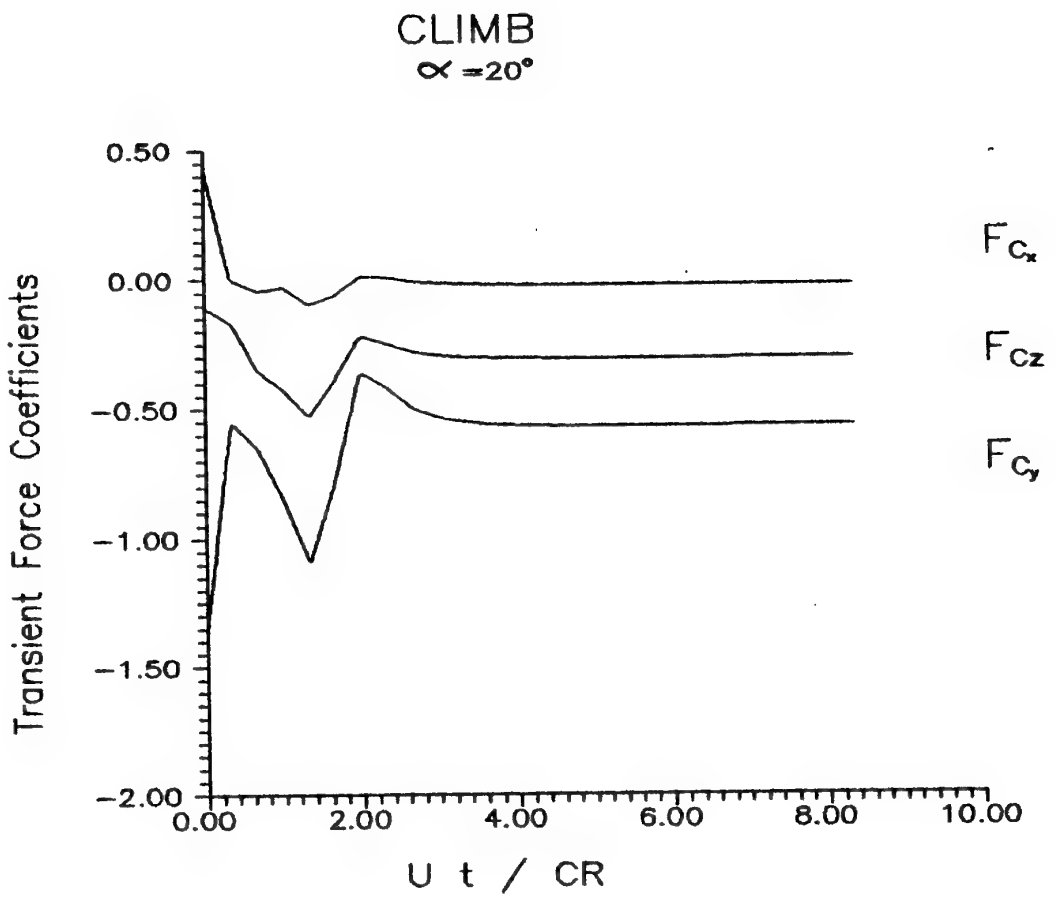

Figure 7.27 Transient force components of the underwing external store that was suddenly set into forward motion.

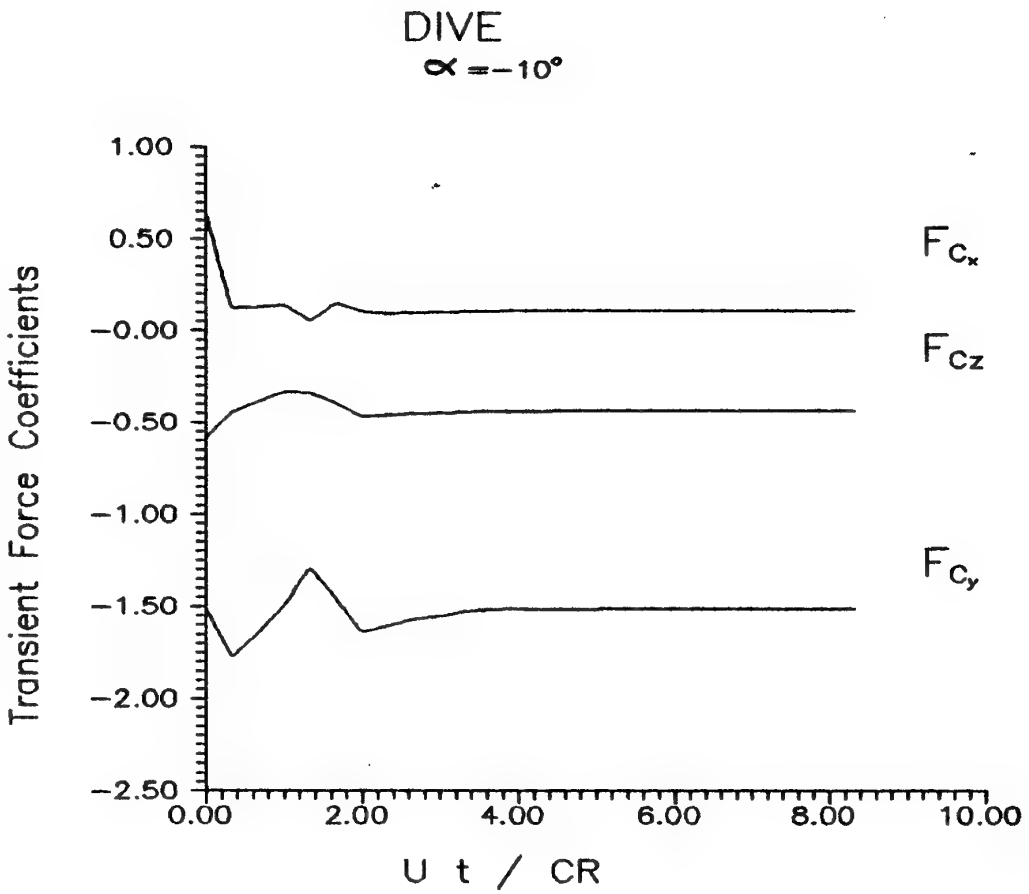

Figure 7.28 Transient force components of the underwing external store that was suddenly set into forward motion.

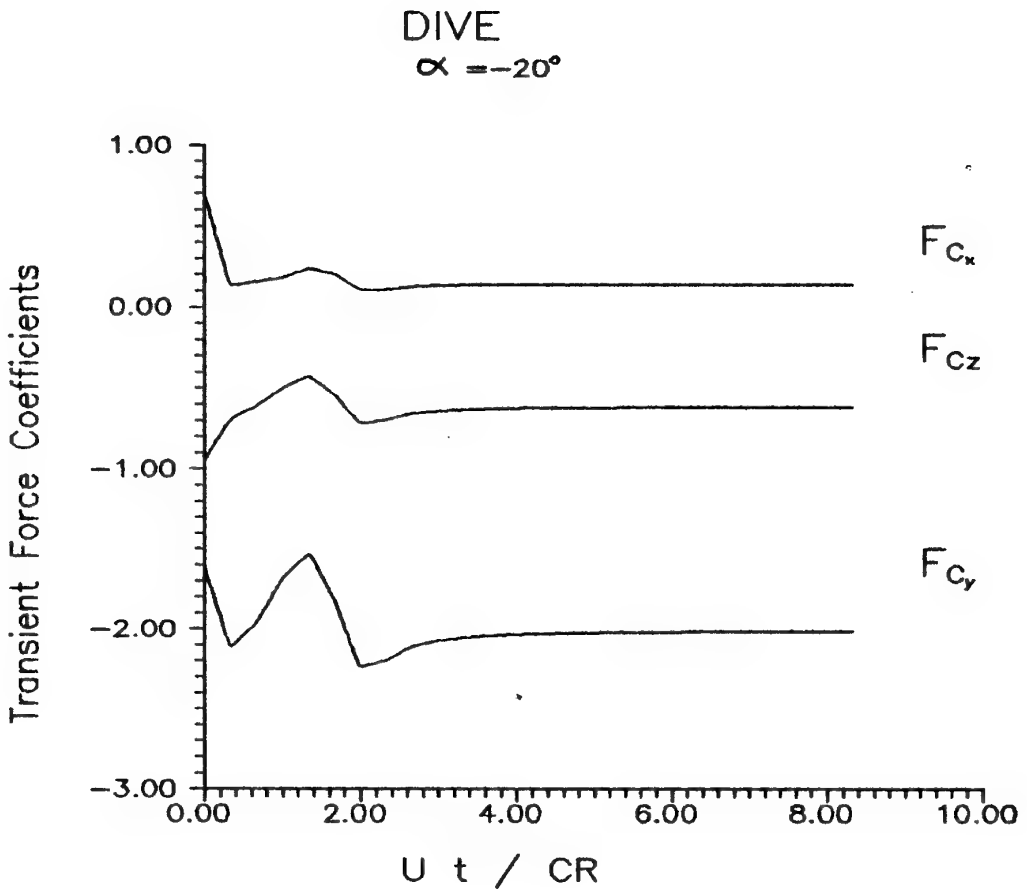

Figure 7.29 Transient force components of the underwing external store that was suddenly set into forward motion.

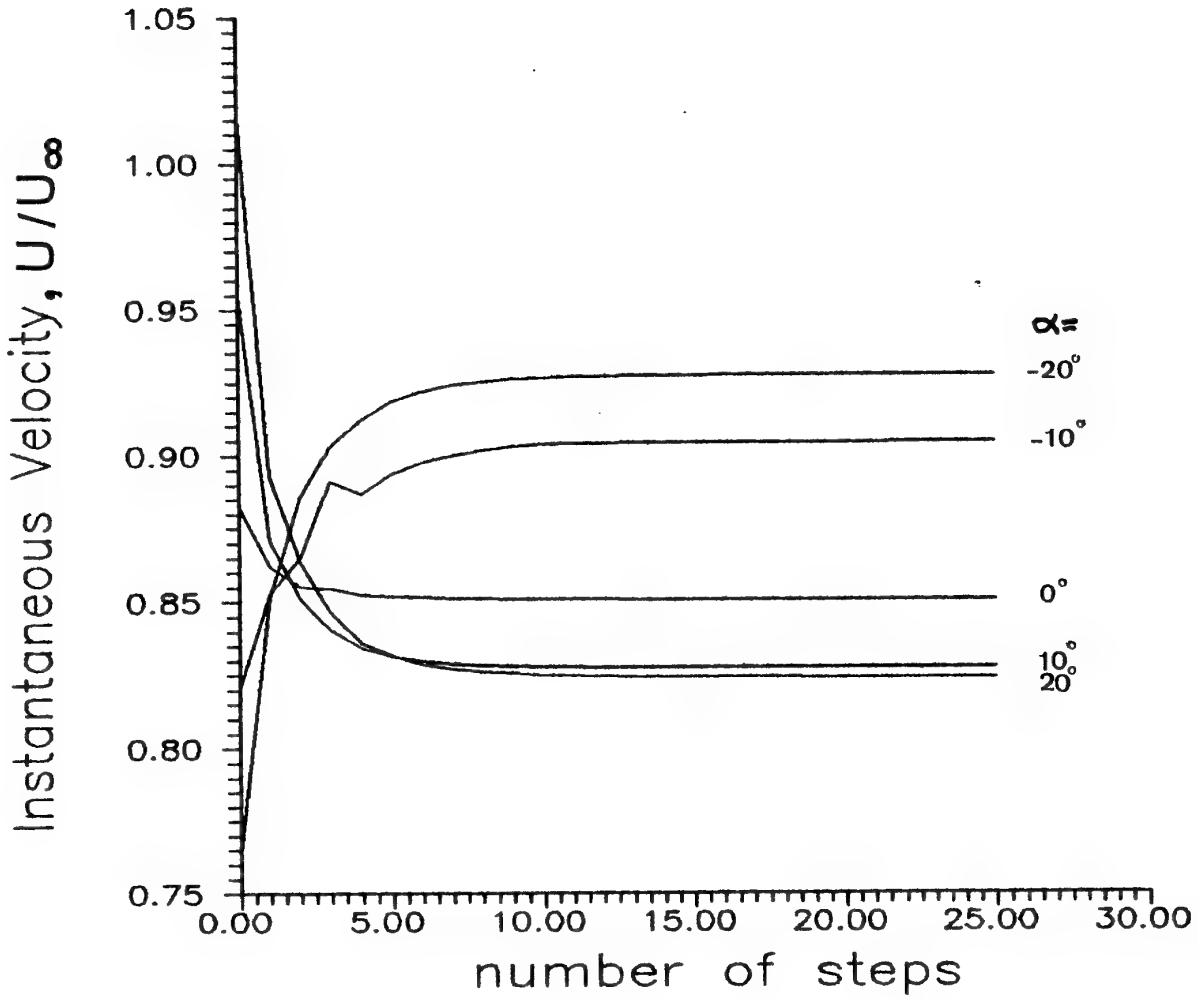

Figure 7.30 Time dependent streamwise velocity variation at the characteristic reference point near the external store trailing edge.

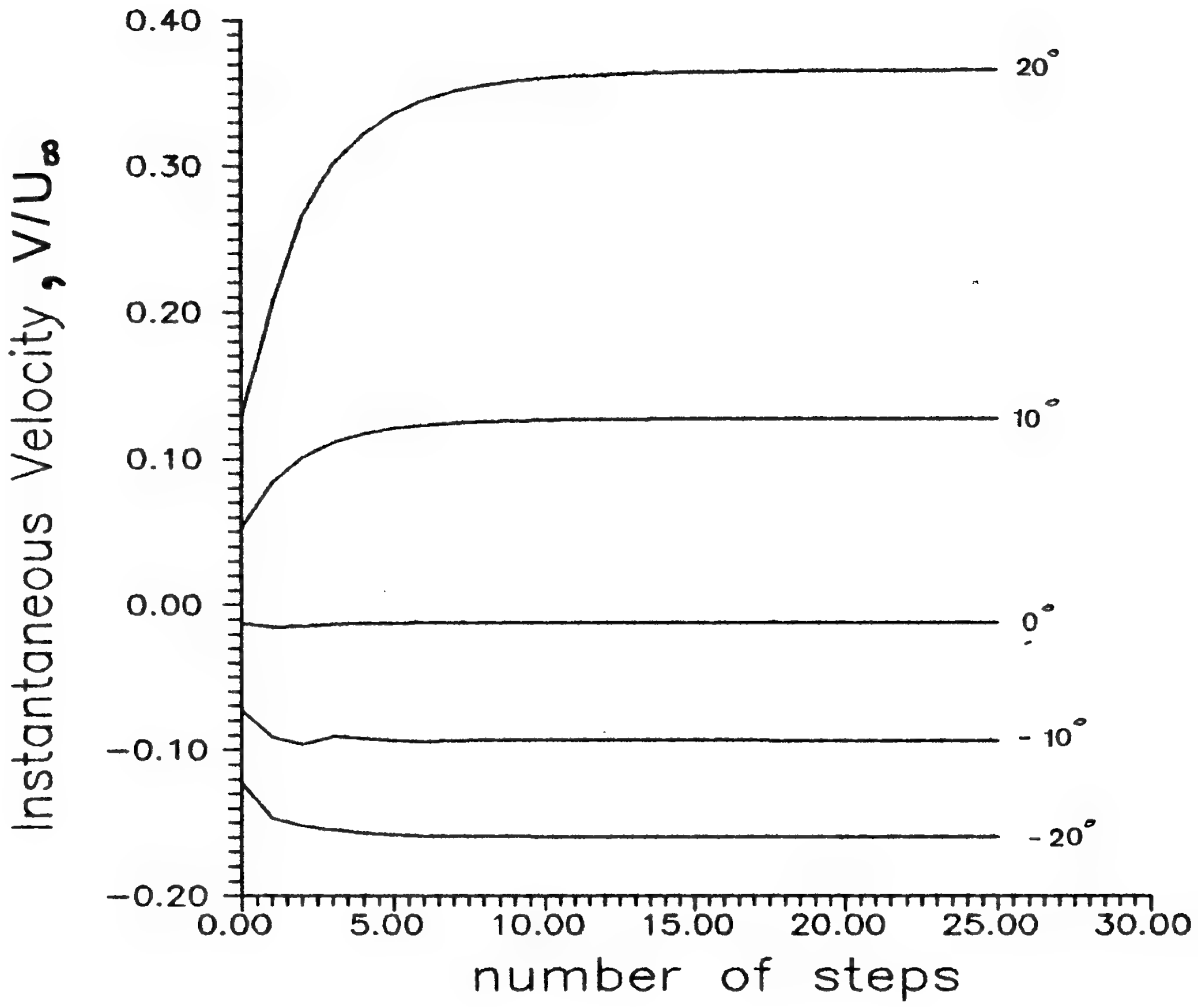

Figure 7.31 Time dependent spanwise velocity variation at the characteristic reference point near the external store trailing edge.

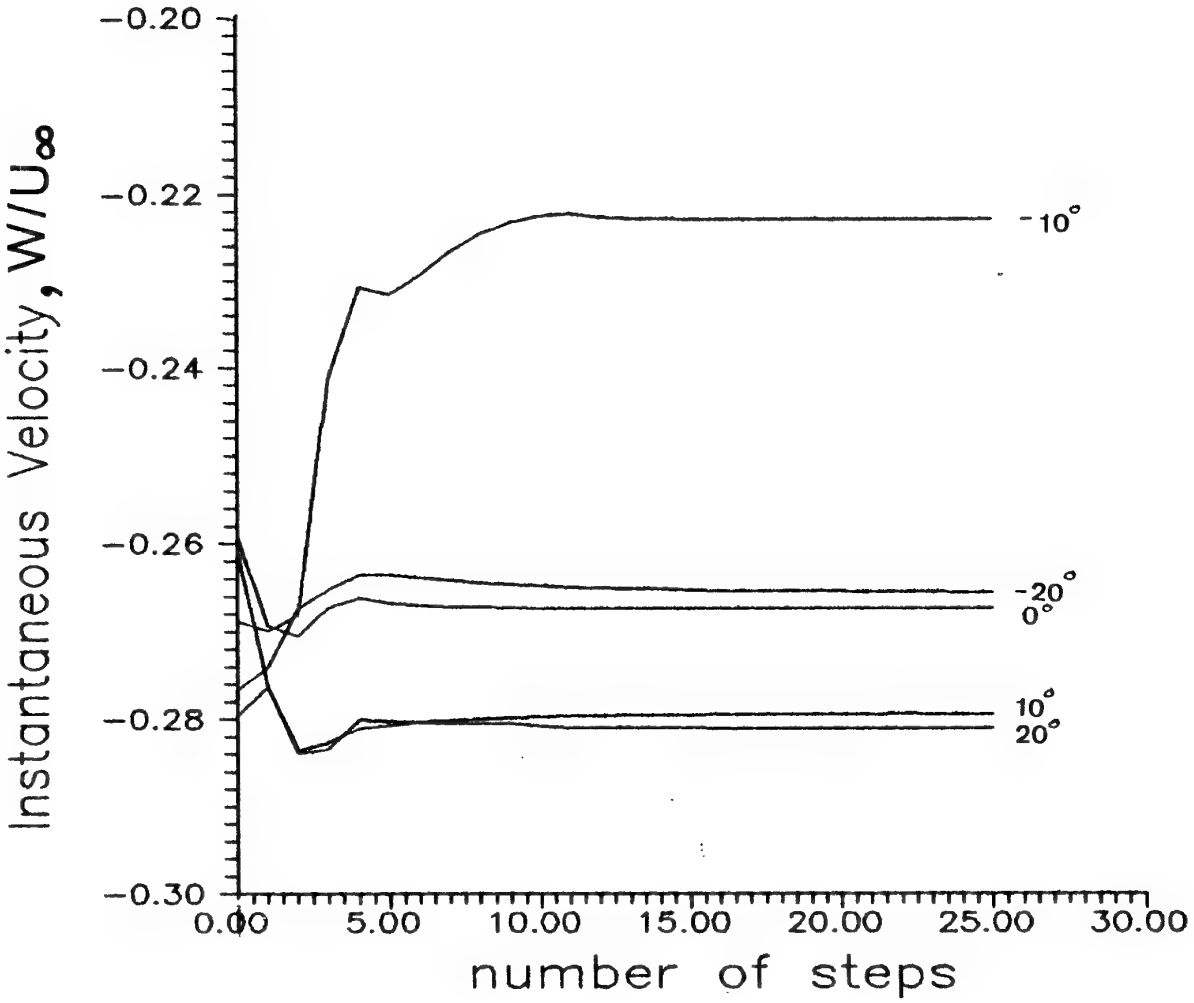

Figure 7.32 Time dependent vertical velocity variation at the characteristic reference point near the external store trailing edge.

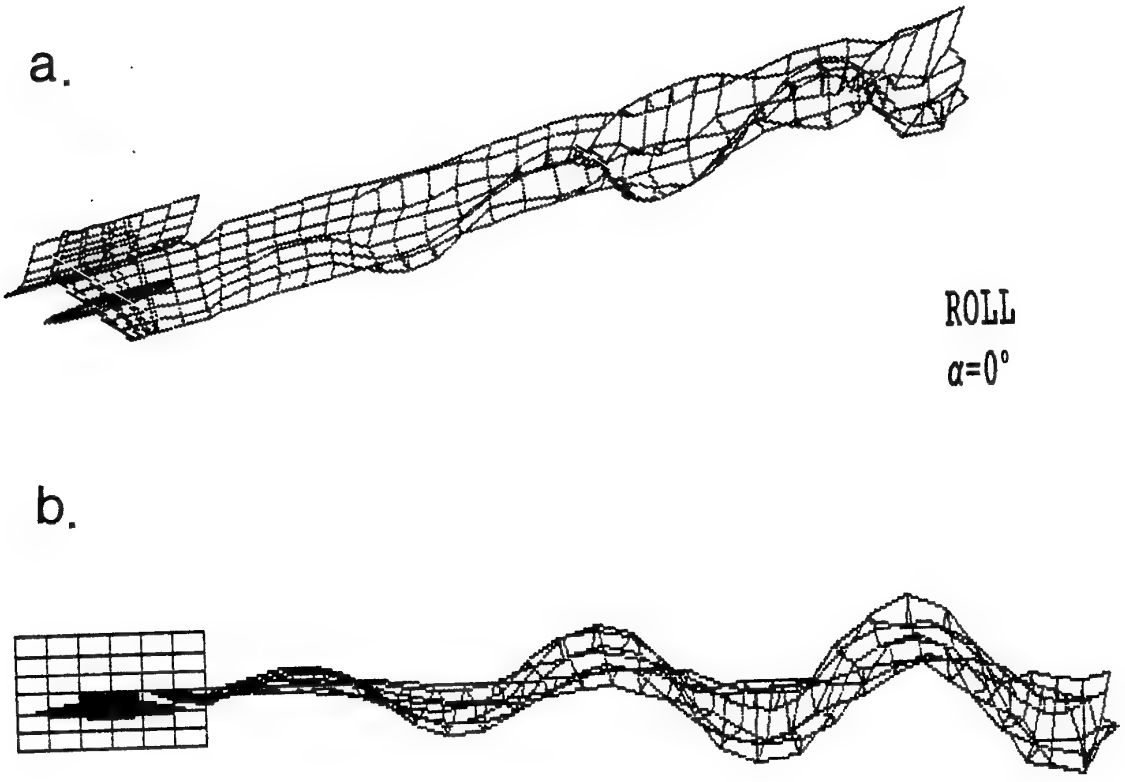

Figure 7.33 a)Perspective view of the computed vortex wake structure behind the configuration performing sinusoidal roll motion after 30 steps.b) side view of the oscillatory wake.

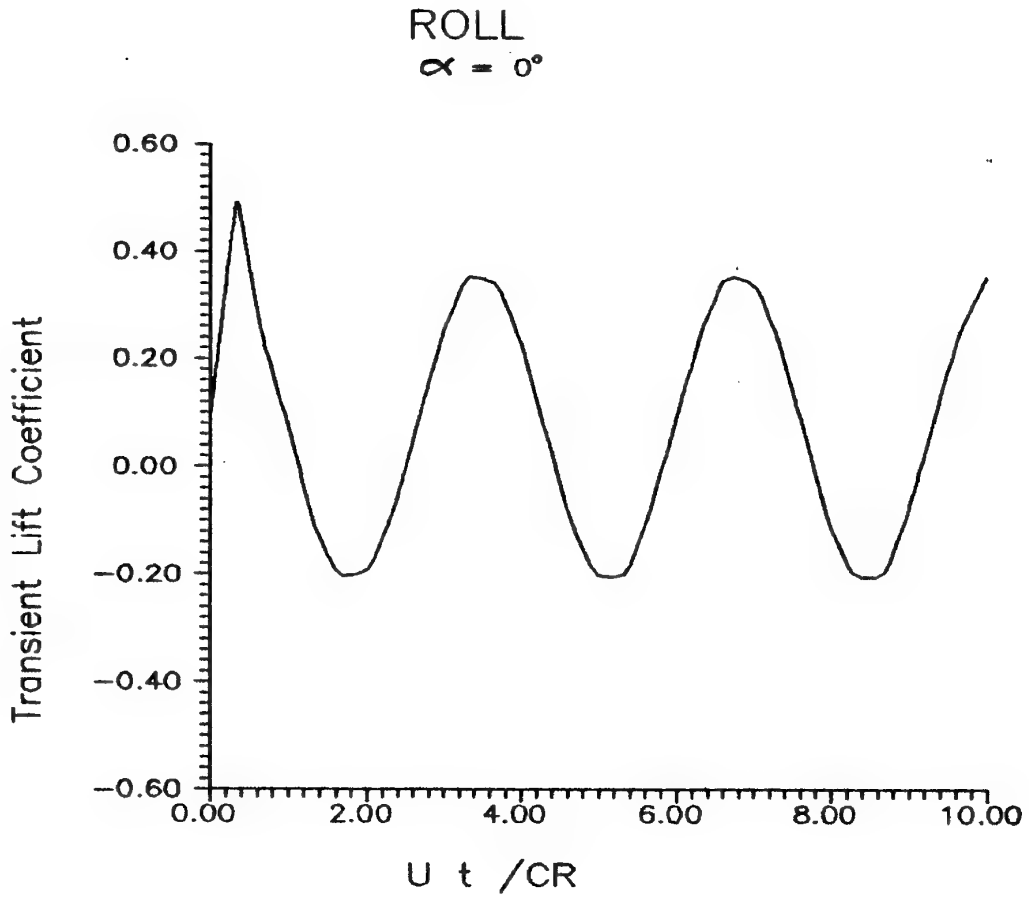

Figure 7.34 Time-dependent lift of a wing performing sinusoidal roll motion at 0° angle of attack.

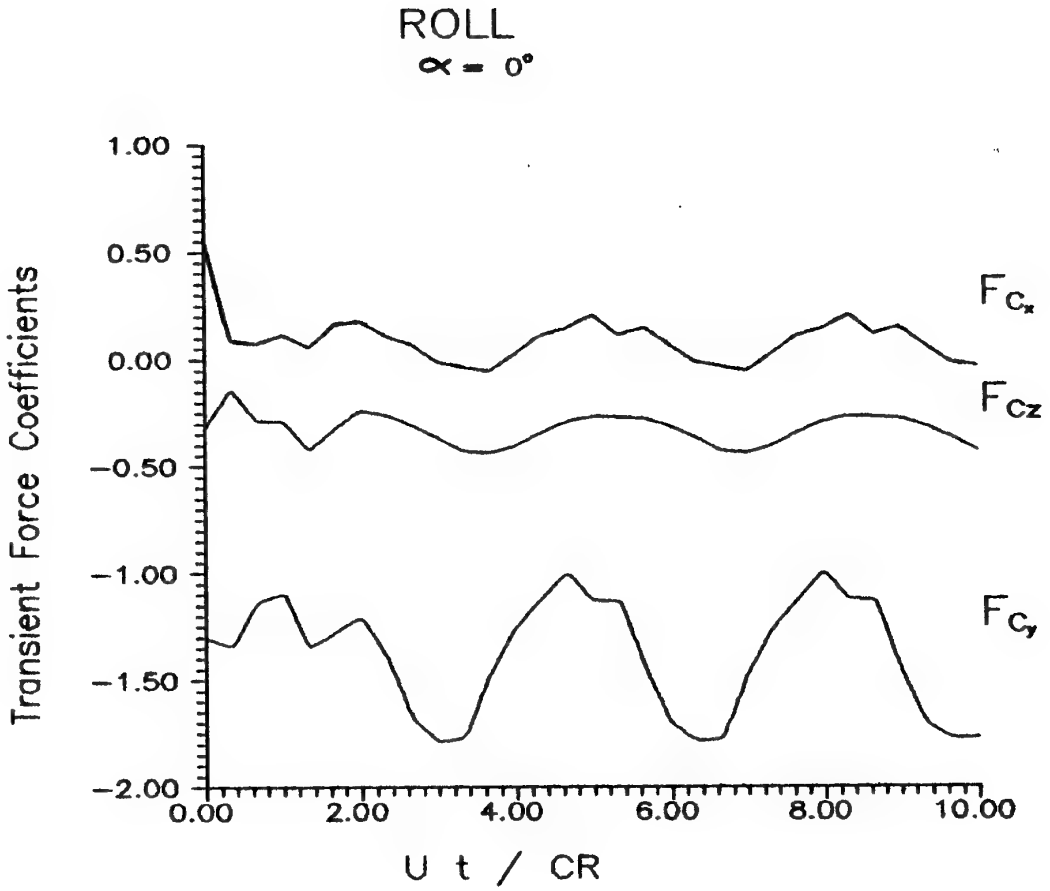

Figure 7.35 Time-dependent force components of an external store performing sinusoidal roll motion with the wing at 0° angle of attack.

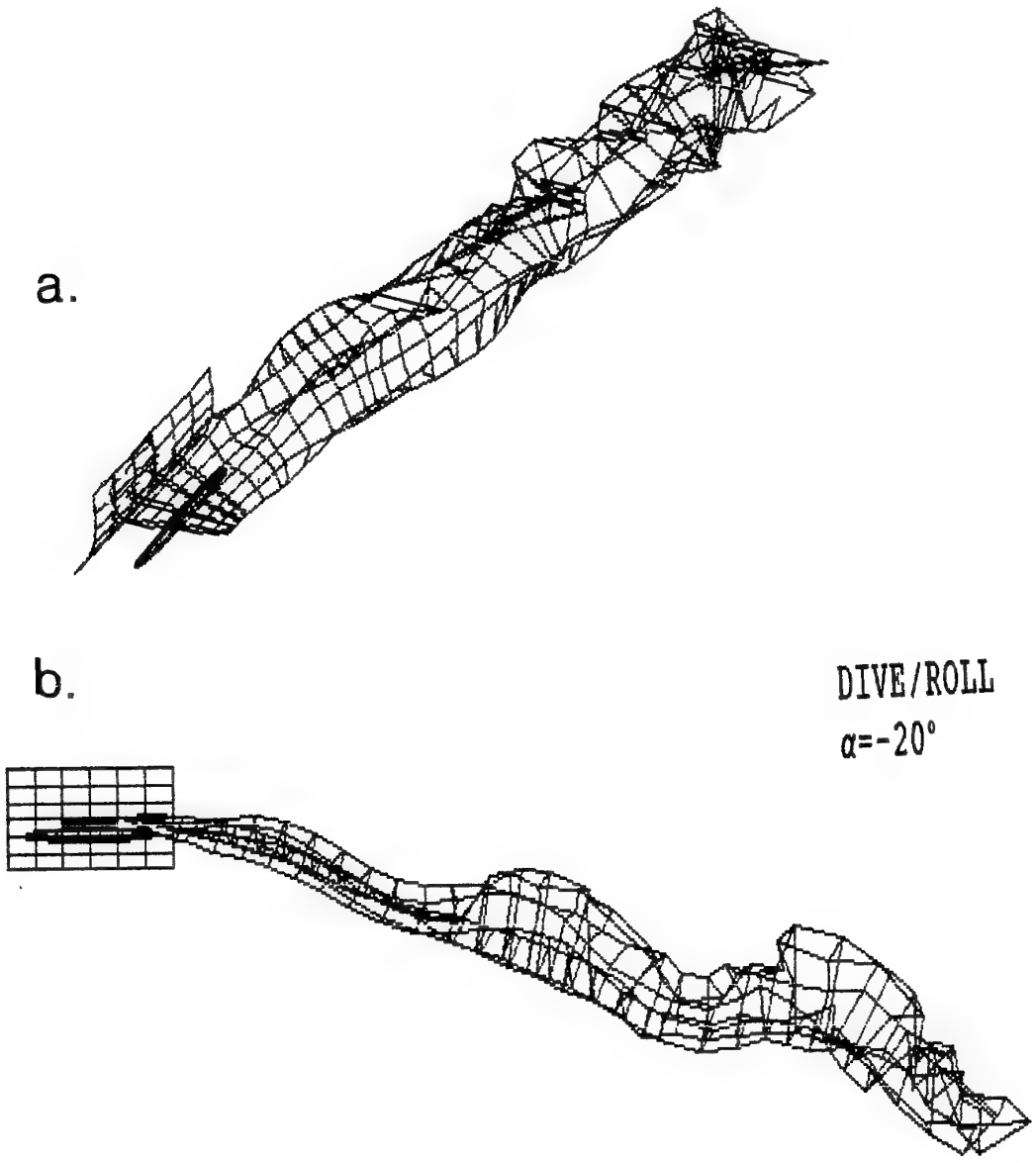

Figure 7.36 a)Perspective view of the computed vortex wake structure behind the configuration performing sinusoidal roll motion during diving after 30 steps.b) side view of the oscillatory wake. c) details of the near wake during dive/roll motion.

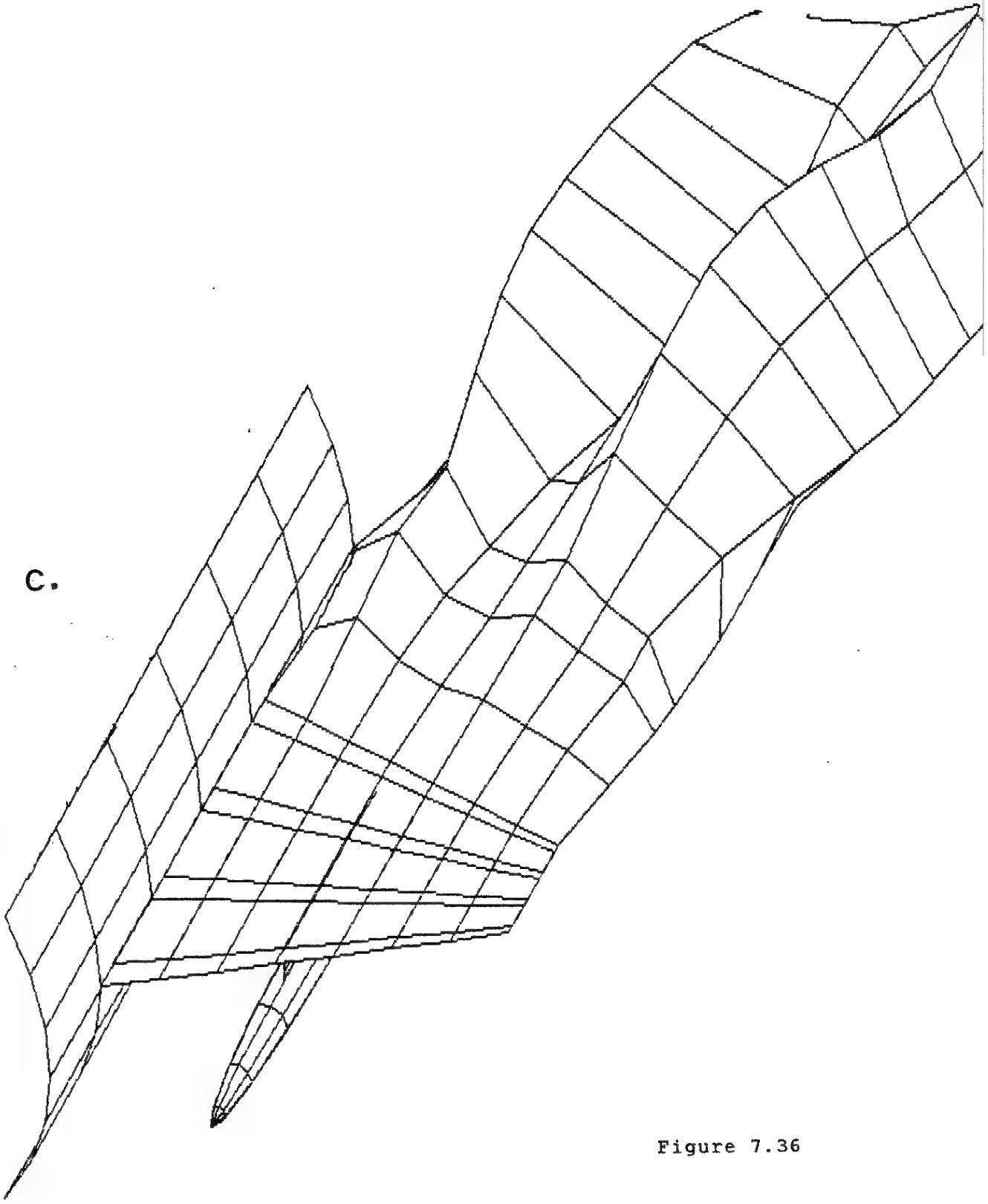

c.

Figure 7.36

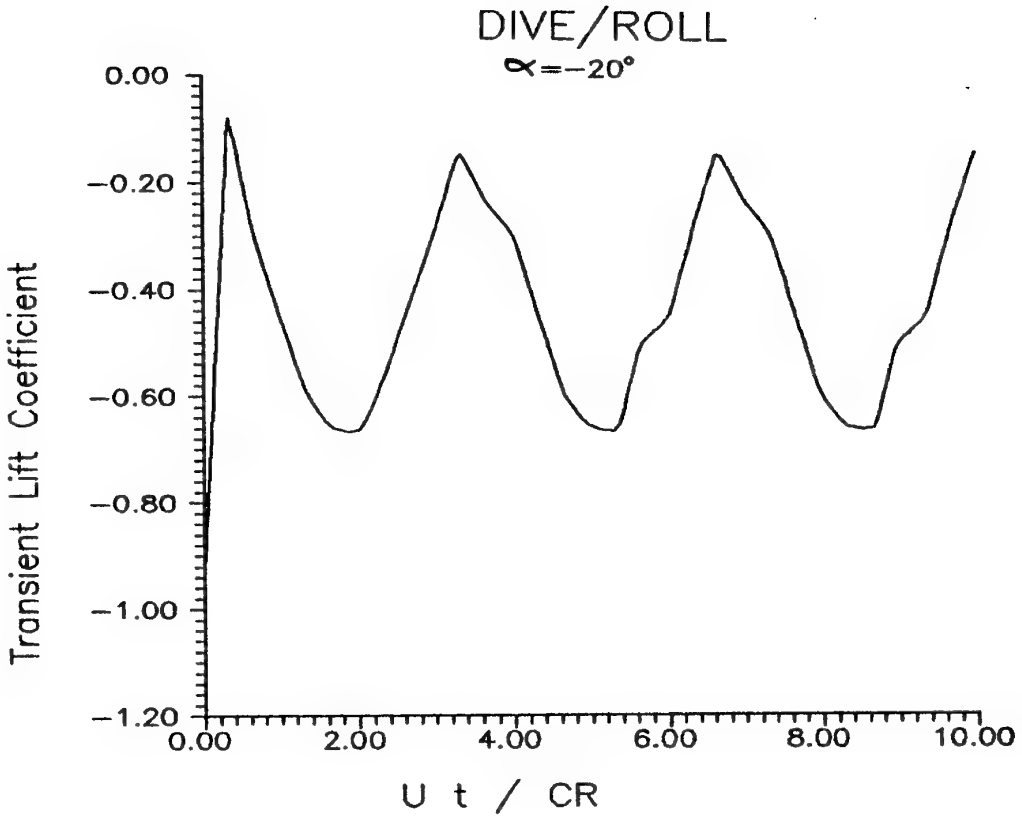

Figure 7.37 Time-dependent lift of a wing performing sinusoidal roll motion during diving at -20° angle of attack.

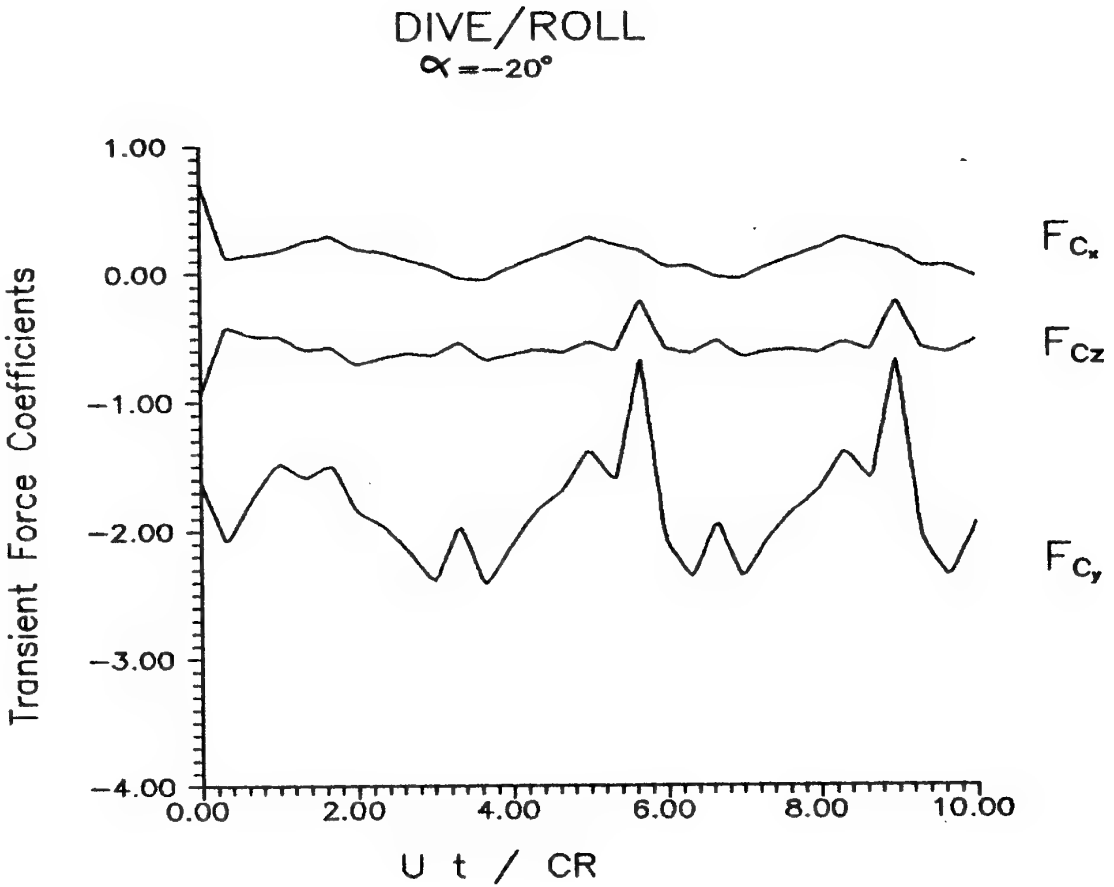

Figure 7.38 Time-dependent force components of an external store performing sinusoidal roll motion during diving with the wing at -20° angle of attack.

a.

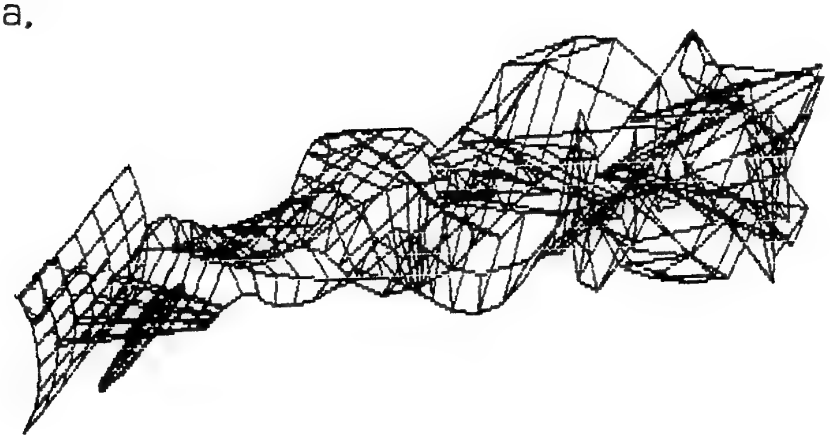

b.

DIVE/PITCH

α=-30°

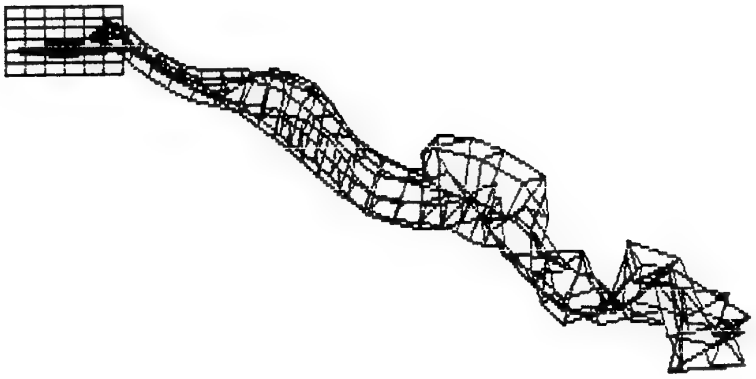

Figure 7.39 a)Perspective view of the computed vortex wake structure behind the configuration performing sinusoidal pitch motion during diving after 30 steps.b) side view of the oscillatory wake. c) details of the near wake during dive/roll motion.

C.

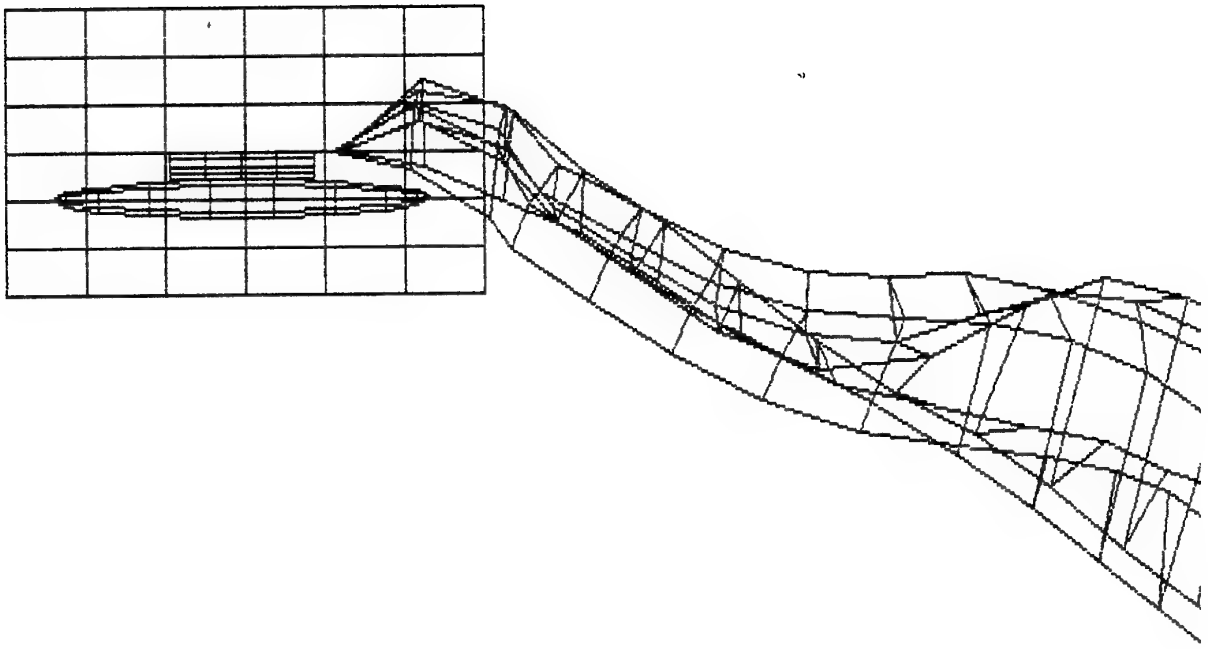

Figure 7.39

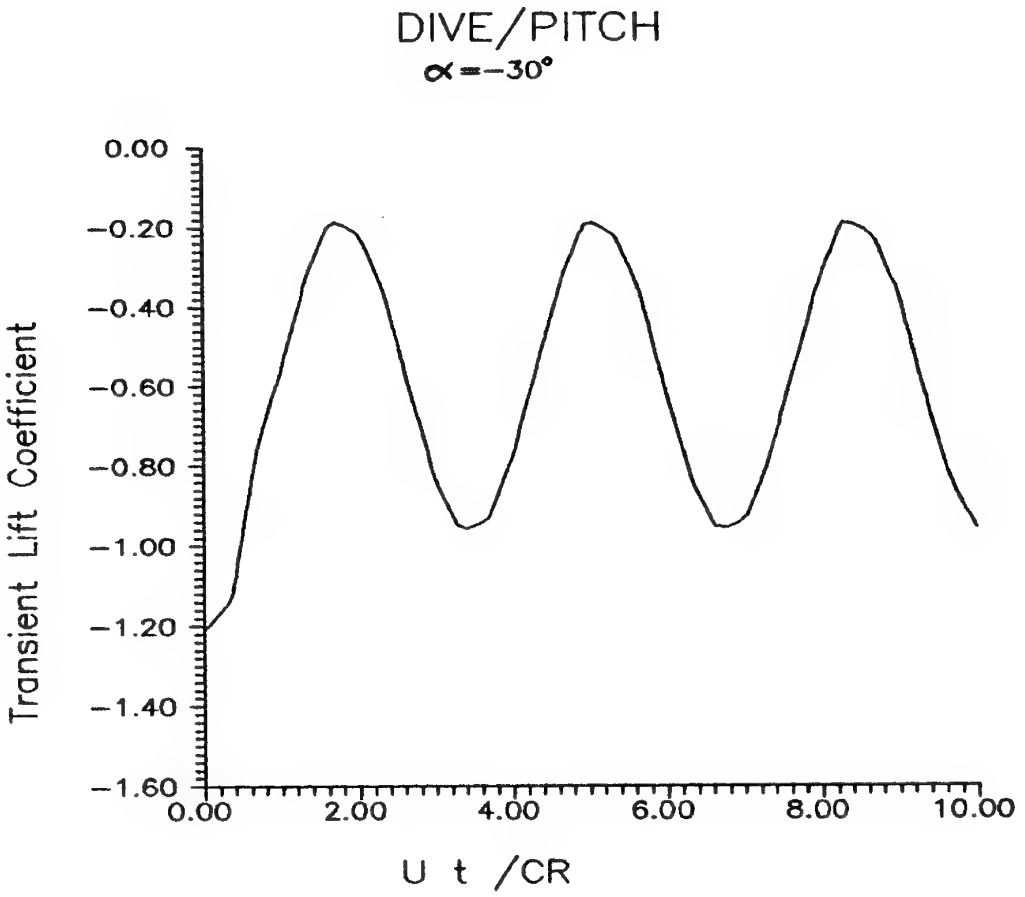

Figure 7.40 Time-dependent lift of a wing performing sinusoidal pitch motion during diving at -30° angle of attack.

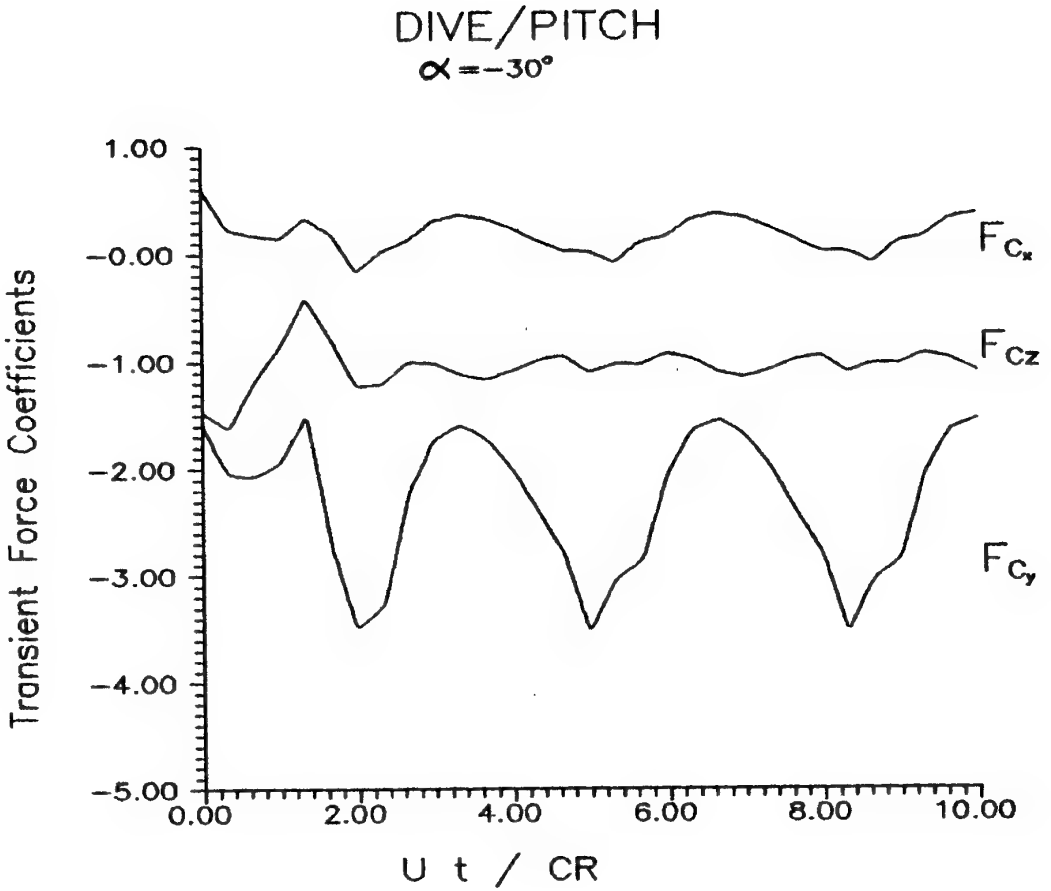

Figure 7.41 Time-dependent force components of an external store performing sinusoidal pitch motion during diving with the wing at -30° angle of attack.

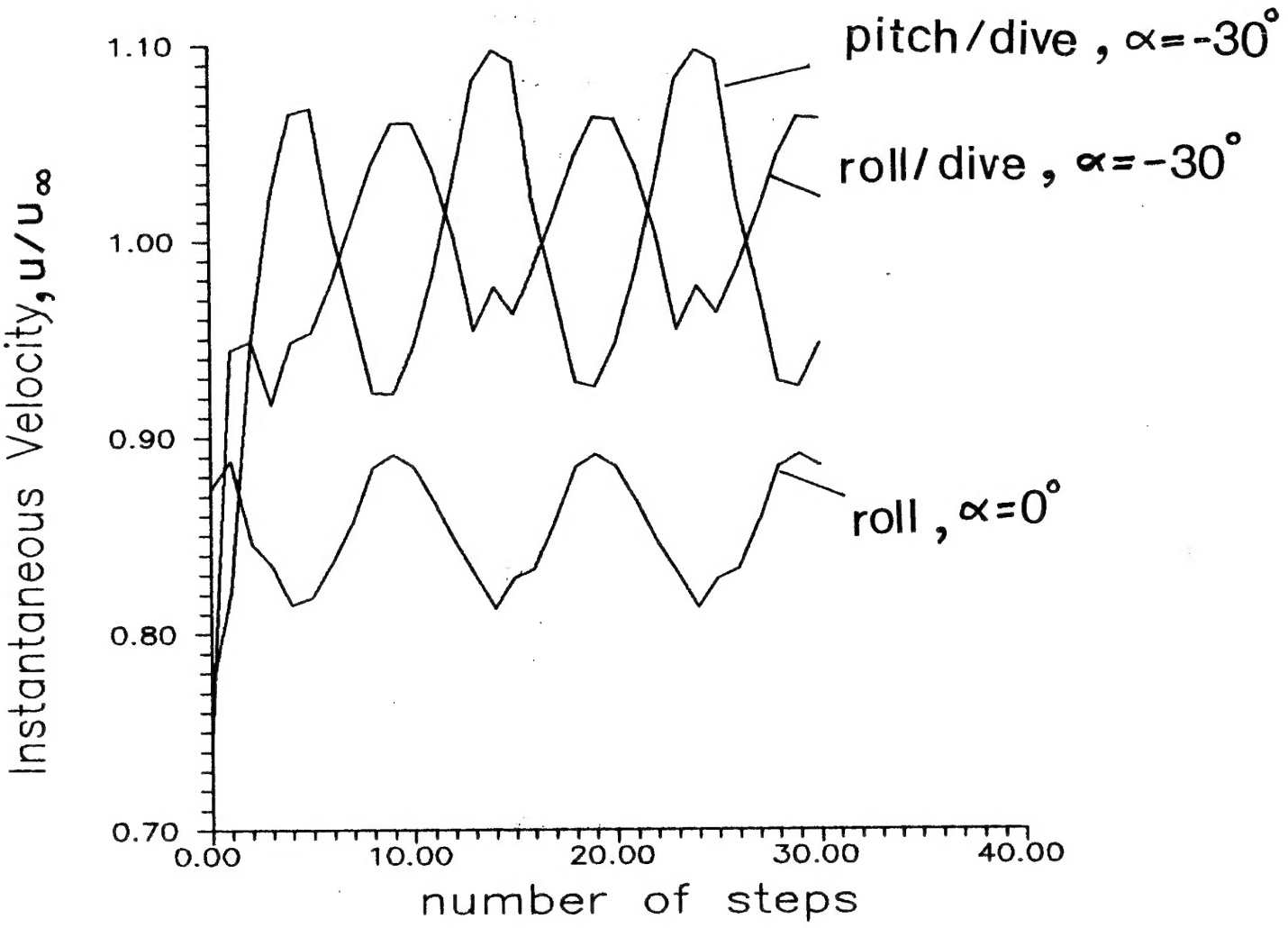

Figure 7.42 Time dependent streamwise velocity variation at the characteristic reference point near the external store trailing edge during unsteady maneuver.

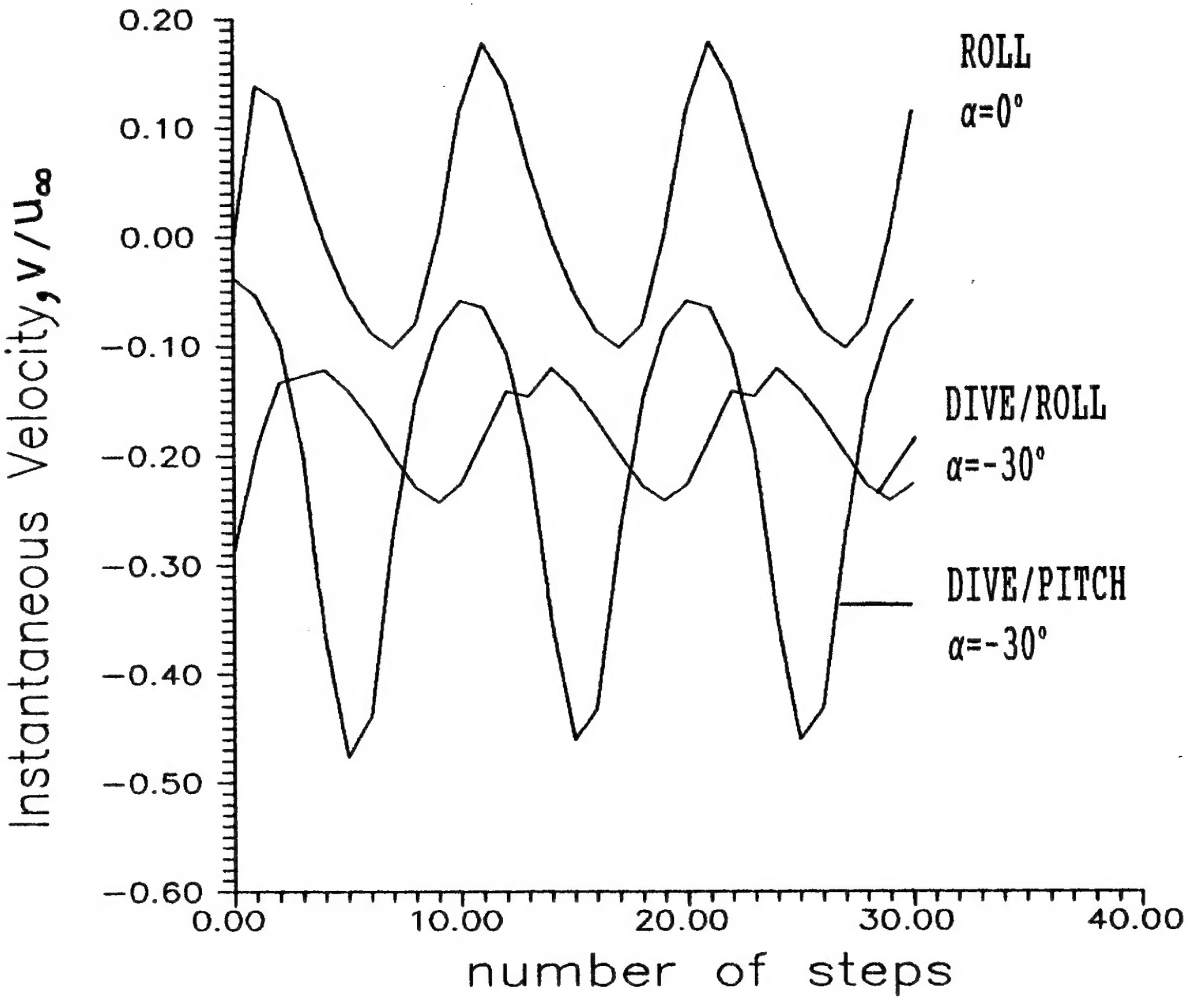

Figure 7.43 Time dependent spanwise velocity variation at the characteristic reference point near the external store trailing edge during unsteady maneuver.

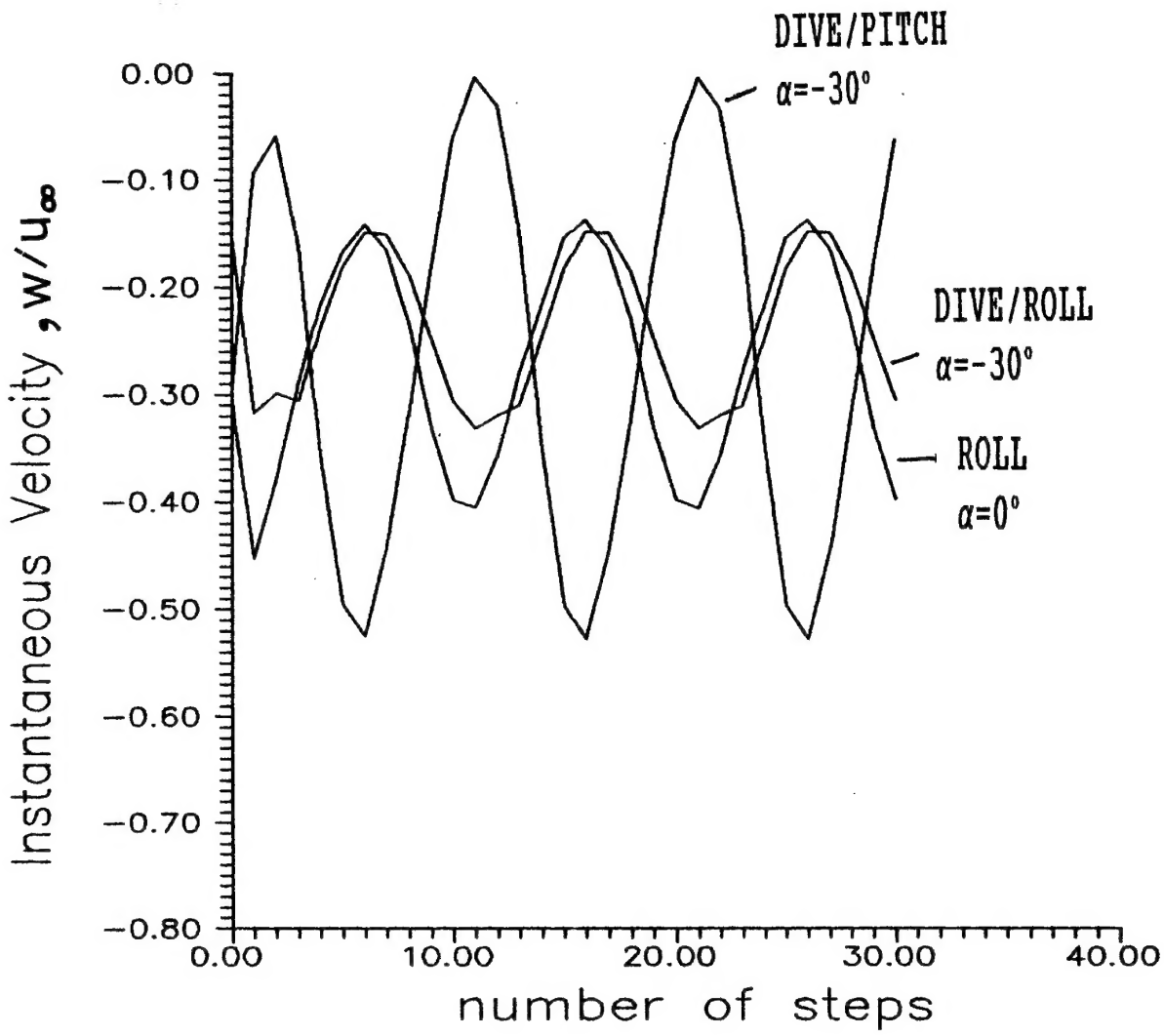

Figure 7.44 Time dependent vertical velocity variation at the characteristic reference point near the external store trailing edge during unsteady maneuver.

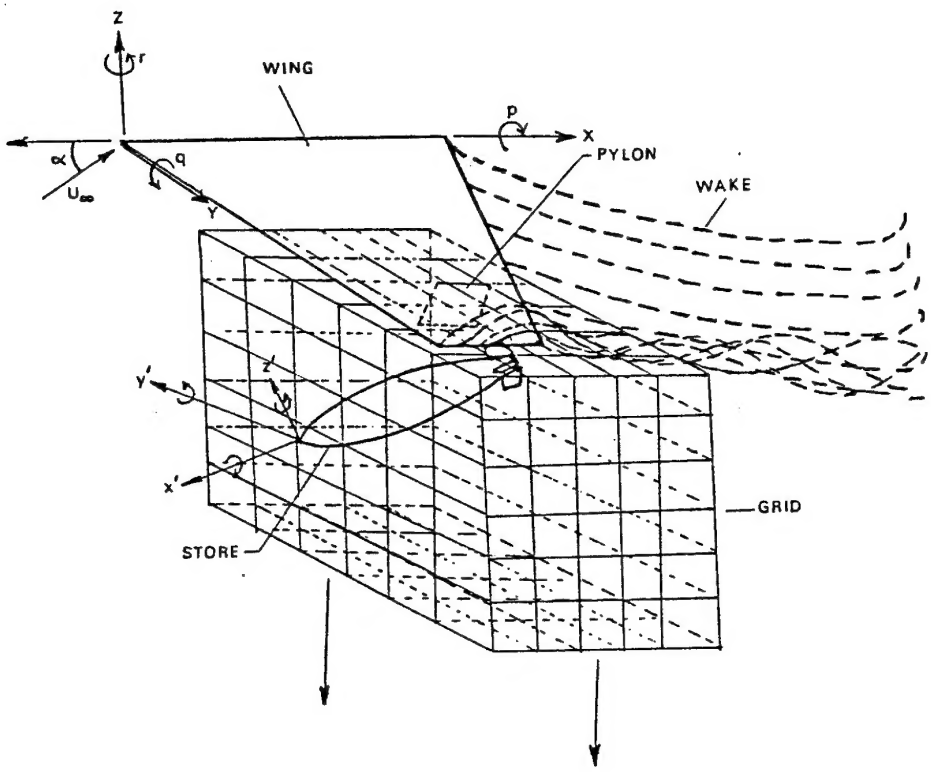

Figure 8.1 Details of external store separation including wake effect.